ARTICLE

A Scalable Bayesian Method for Integrating Functional Information in Genome-wide Association Studies

Jingjing Yang,[1] Lars G. Fritsche,[1,2] Xiang Zhou,[1,*] Gonçalo Abecasis,[1,*] and International Age-Related Macular Degeneration Genomics Consortium

Genome-wide association studies (GWASs) have identified many complex loci. However, most loci reside in noncoding regions and have unknown biological functions. Integrative analysis that incorporates known functional information into GWASs can help elucidate the underlying biological mechanisms and prioritize important functional variants. Hence, we develop a flexible Bayesian variable selection model with efficient computational techniques for such integrative analysis. Different from previous approaches, our method models the effect-size distribution and probability of causality for variants with different annotations and jointly models genome-wide variants to account for linkage disequilibrium (LD), thus prioritizing associations based on the quantification of the annotations and allowing for multiple associated variants per locus. Our method dramatically improves both computational speed and posterior sampling convergence by taking advantage of the block-wise LD structures in human genomes. In simulations, our method accurately quantifies the functional enrichment and performs more powerfully for prioritizing the true associations than alternative methods, where the power gain is especially apparent when multiple associated variants in LD reside in the same locus. We applied our method to an in-depth GWAS of age-related macular degeneration with 33,976 individuals and 9,857,286 variants. We find the strongest enrichment for causality among non-synonymous variants (54× more likely to be causal, 1.4× larger effect sizes) and variants in transcription, repressed Polycomb, and enhancer regions, as well as identify five additional candidate loci beyond the 32 known AMD risk loci. In conclusion, our method is shown to efficiently integrate functional information in GWASs, helping identify functional associated-variants and underlying biology.

Introduction

Genome-wide association studies (GWASs) have identified thousands of genetic loci for complex traits and diseases, providing insights into the underlying genetic architecture.[1–5] Each associated locus typically contains hundreds of variants in linkage disequilibrium (LD),[6,7] most of which are of unknown function and located outside protein-coding regions. Unsurprisingly, the biological mechanisms underlying the identified associations are often unclear[8] and pinpointing causal variants is difficult.[9]

Recent functional genomic studies help understand and pinpoint functional associations and mechanisms.[10–12] Genetic variants can be annotated based on the genomic location (e.g., coding, intronic, and intergenic), role in determining protein structure and function (e.g., Sorting Intolerant From Tolerant [SIFT][13] and Polymorphism Phenotyping [PolyPhen][14] scores), ability to regulate gene expression (e.g., expression quantitative trait loci [eQTL] and allelic specific expression [ASE] evidence[15,16]), biochemical function (e.g., DNase I hypersensitive sites [DHS], metabolomic QTL [mQTL] evidence,[17] and chromatin states[18–20]), evolutionary significance (e.g., Genomic Evolutionary Rate Profiling [GERP] annotations[21]), and a combination of different types of annotation (e.g., CADD[22]). Many statistical methods, including stratified LD score regression[23] and MQS,[24] can now evaluate the role of functional annotations in GWASs through heritability analysis. Preliminary studies also show higher proportions of associated variants in protein-coding exons, regulatory regions, and cell-type-specific DHSs.[25–27]

Integrating functional information into GWASs is expected to help identify and prioritize true associations. However, accomplishing this goal in practice requires methods to account for both LD and computational cost. Consider two recent methods, fGWAS[26] and PAINTOR,[27] as examples. fGWAS assumes that variants are independent and there is at most one association signal per locus, modeling no LD, which dramatically improves computational speed and allows fGWAS to be applied at genome-wide scale; PAINTOR accounts for LD, assuming the possibility of multiple association signals per locus, but is computationally slow and can be used to fine-map small regions only (~10 kb).

Here, we pair a flexible Bayesian method with an efficient computational algorithm. Together the two represent an attractive means to incorporate functional information into association mapping. Our model accounts for genotype correlation due to LD, allows for multiple signals per locus and, importantly, shares information genome-wide to increase association-mapping power. Our algorithm takes advantage of the local LD structure in the human

[1]Center for Statistical Genetics, Department of Biostatistics, University of Michigan School of Public Health, 1415 Washington Heights, Ann Arbor, MI 48109, USA; [2]K.G. Jebsen Center for Genetic Epidemiology, Department of Public Health and Nursing, NTNU, Norwegian University of Science and Technology, 7491 Trondheim, Norway
*Correspondence: xzhousph@umich.edu (X.Z.), goncalo@umich.edu (G.A.)
http://dx.doi.org/10.1016/j.ajhg.2017.08.002.

genome[28–30] and refines previous Markov chain Monte Carlo (MCMC) algorithms to greatly improve mixing, which is key when searching for independent signals among many associated variants in LD (but less important in other applications such as modeling total genomic heritability). We refer to our method as the Bayesian functional GWAS (bfGWAS). Below, we illustrate the benefits of our method with extensive simulations as well as real large-scale GWASs on age-related macular degeneration (AMD)[31] (33,976 individuals, 9,857,286 variants) and skin cancer (17,624 individuals, 8,626,534 variants).

Material and Methods

Bayesian Variable Selection Model

Our method is based on the standard Bayesian variable selection regression (BVSR) model[32] (Supplemental Note; Figure S1A),

$$\boldsymbol{y}_{\boldsymbol{n}\times\mathbf{1}} = \boldsymbol{X}_{\boldsymbol{n}\times\boldsymbol{p}}\,\boldsymbol{\beta}_{\boldsymbol{p}\times\mathbf{1}} + \boldsymbol{\epsilon}_{\boldsymbol{n}\times\mathbf{1}},$$
$$\beta_i \sim \pi_i N\left(0,\ \tau^{-1}\sigma_i^2\right) + (1-\pi_i)\delta_0(\beta_i),\ \epsilon_i \sim \mathrm{N}\left(0,\ \tau^{-1}\right),$$

where $\boldsymbol{y}_{\boldsymbol{n}\times\mathbf{1}}$ is the centered phenotype vector with n individuals, $\boldsymbol{X}_{\boldsymbol{n}\times\boldsymbol{p}}$ is the centered genotype matrix with p genetic variants, $\boldsymbol{\beta}_{\boldsymbol{p}\times\mathbf{1}}$ is a vector of genetic effect-sizes where each element β_i follows a "spike-and-slab" variable selection prior, $\beta_i \sim \pi_i N(0,\ \tau^{-1}\sigma_i^2) + (1-\pi_i)\delta_0(\beta_i)$. Different from the standard BVSR, however, our method considers functional annotations that classify variants into K non-overlapping categories. For example, all variants could be annotated based on their most important functions in a gene, such as non-synonymous, synonymous, intronic, intergenic, or other genomic, which classifies all variants into five non-overlapping categories.

Annotation-Specific Effect-Size Priors

We assume that variants in the same annotation category q share a prior[32,33] for effect sizes, $\beta_i \sim \pi_q N(0,\ \tau^{-1}\sigma_q^2) + (1-\pi_q)\delta_0(\beta_i)$, with the same category-specific parameters $(\pi_q,\ \sigma_q^2)$. This model implies that effect sizes are normally distributed as $\beta_i \sim N(0,\ \tau^{-1}\sigma_q^2)$ with probability π_q, or set to zero with probability $(1-\pi_q)$, with $\delta_0(\beta_i)$ denoting the point-mass function at 0. Here, π_q represents the (unknown) causal probability for variants in the qth category and σ_q^2 represents the (unknown) corresponding effect-size variance. An enhancement to previous Bayesian models[32,34,35] is that we model both the proportion of associated variants and their effect-size distribution in each annotation category. Note that our model is different from simply applying BVSR on variants of each annotation, because we model the LD among variants of different annotations.

We assume independent, conjugate, and non-informative priors for $(\pi_q,\ \sigma_q^2)$, e.g., $\pi_q \sim Beta(a_q,\ b_q)$ with mean 10^{-6} and $\sigma_q^2 \sim InverseGamma(k_1,\ k_2)$ with $k_1 = k_2 = 0.1$. Although independent and conjugate priors are assumed for the convenience of deriving closed-form expressions for the conditional posterior distributions (greatly saving computational cost), the posterior distributions of $(\pi_q,\ \sigma_q^2)$ depend on each other through effect sizes and the number of signals. Non-informative priors allow the Bayesian estimates to be mainly determined by the likelihood when there exist associations in the qth category (otherwise the Bayesian estimates will be determined by the respective prior modes; see derivation details in Supplemental Note). Particularly, assuming a conservative prior mean 10^{-6} for π_q (equivalent to assume one signal per 1M variants) enforces an initial sparse model, which helps control false positives and barely affects identifying real signals. Taking $k_1 = k_2 = 0.1$ makes the Inverse Gamma prior for σ_q^2 non-informative with mode at 0.09.

Our goal is to simultaneously make inference on the category-specific parameters $(\pi_q,\ \sigma_q^2)$ that represent the importance of each functional category, and on the variant-specific parameters—effect-size β_i and the probability of $\beta_i \neq 0$ (referred as posterior inclusion probability [PP_i], representing association evidence, i.e., the probability for the variant to be associated with the phenotype). Our model shares information genome-wide to estimate the category-specific parameters, which then inform the variant-specific parameters. As a result, variant associations will be prioritized based on the inferred importance of functional categories.

Scalable EM-MCMC Algorithm

Because standard MCMC algorithms suffer from heavy computational burden and poor mixing of posterior samples for large GWASs, we develop a scalable expectation-maximization MCMC (or EM-MCMC) algorithm. Our algorithm is based on the observation that LD decays exponentially with distance and displays local block-wise structure along the human genome.[28–30,36,37] This observation allows us to decompose the complex joint likelihood of our model into a product of block-wise likelihoods (Appendix A and Supplemental Note). Intuitively, conditional on a common set of category-specific parameters $(\pi_q,\ \sigma_q^2)$, we can infer $(\beta_i,\ PP_i)$ by running the MCMC algorithm per genome block. A diagram of this EM-MCMC algorithm is shown in Figure S1B.

Running MCMC per genome-block facilitates parallel computing and reduces the search space. Unlike previous MCMC algorithms for GWASs that use proposal distributions based only on marginal association evidence (such as implemented in GEMMA[38]), our MCMC algorithm uses a proposal distribution that favors variants near the "causal" variants being considered in each iteration and prioritizes among these neighboring variants based on their conditional association evidence (see Supplemental Note). Our strategy dramatically improves the MCMC mixing property, encouraging our method to explore different combinations of potentially associated variants in each locus (Figure S2). In addition, we implemented memory-reduction techniques that reduce memory usage up to 97%, effectively reducing the required physical memory from 120 Gb (usage by GEMMA[38]) to 3.6 Gb for a GWAS with ~33K individuals and ~400K genotyped variants (Appendix A and Supplemental Note).

In practice, we segment the whole genome into blocks of 5,000–10,000 variants, based on marginal association evidence, genomic distance, and LD. We always ensure variants in LD ($R^2 > 0.1$) with significant signals ($p < 5 \times 10^{-8}$) are in the same block (Appendix A). We first initialize the category-specific parameters $(\pi_q,\ \sigma_q^2)$, then run the MCMC algorithm per block (E-step), summarize the MCMC posterior estimates of $(\beta_i,\ PP_i)$ across all blocks to update $(\pi_q,\ \sigma_q^2)$ (M-step), and repeat the block-wise EM-MCMC steps until the estimates of $(\pi_q,\ \sigma_q^2)$ converge (Figure S1B).

In addition, we calculate the regional posterior inclusion probability (regional-PP) per block that is the proportion of MCMC iterations with at least one signal (see Supplemental Note). Because Bayesian PP might be split among multiple variants in high LD, the threshold of regional-PP > 0.95 (conservatively analogous to false discovery rate 0.05) is used for identifying loci.

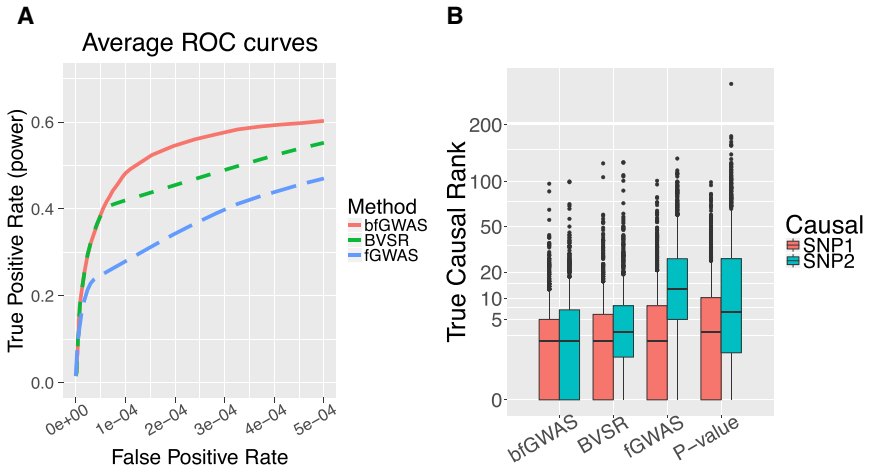

Figure 1. Power Comparison by Simulation Studies
Compare the power of bfGWAS, the standard Bayesian variable selection regression model (BVSR), fGWAS, p value of single variant test with conditional analysis, with 100 simulation replicates and complete sample size 33,976.
(A) Average ROC curves, larger area under curve suggests higher power.
(B) Boxplot of the ranks of the true causal SNP1 (with smaller p value) and SNP2, higher rank (smaller rank value) suggests higher power.

AMD and MGI GWAS Data

The GWAS data of age-related macular degeneration (AMD) consist of 33,976 unrelated European samples (16,144 advanced case subjects; 17,832 control subjects), and a total of 12,023,830 genotyped on a customized Exome-Chip and imputed against the 1000 Genomes Project phase I reference panel.[31,39] Advanced AMD case subjects include both subjects with choroidal neovascularization and subjects with geographic atrophy. Samples were aggregated across 26 studies and genotyped centrally.[31]

The Michigan Genomics Initiative (MGI) data are the institutional repository of DNA and electronic health records, collected from patients recruited on the day of their elective surgery or procedure at the University of Michigan Health System. DNA was extracted from blood and samples were genotyped on the Illumina HumanCoreExome v.12.1 array and then imputed against the HRC reference panel.[40] The MGI GWAS data studied in this paper contain 17,624 unrelated European individuals and ~8.7M genotyped or imputed variants with frequency > 0.5%. The phenotype of skin cancer was defined as the presence of ICD9 code 232 (carcinoma *in situ* of skin) on two or more visits (2,359 case subjects). The control phenotype was defined as the absence of ICD9 codes (172–173.99) on all visits (15,265 control subjects). For both MGI and the AMD genetic studies, all participants gave informed consent and the University of Michigan IRB approved our GWAS analyses.

Results

Simulation

We simulated phenotypes with the genotype data (chromosomes 18–22) from the AMD GWAS,[31] including 33,976 individuals and 52,549 variants with minor allele frequency (MAF) > 0.05. We segmented this small genome into 100 × 2.5 Mb blocks, each with ~5K variants. Within each block, we marked a 25 kb continuous region (starting 37.5 kb from the beginning of a block) as the potential locus. We randomly selected two causal SNPs per locus for ten randomly selected loci. We simulated two complementary annotations to classify variants into "coding" and "noncoding" groups, where the coding variants account for ~1% overall variants but ~10% variants within the causal loci (matching the pattern in the real AMD data). We simulated two scenarios: (1) coding variants ~53× enriched among causal variants (7 coding versus 13 noncoding) and (2) no enrichment (randomly selecting causal variants in risk loci with equally distributed annotations). A total of 15% of phenotypic variance was divided equally among causal variants. We compared bfGWAS with single variant likelihood-ratio test, conditional analysis, fGWAS, and the standard Bayesian variable selection regression model (BVSR, considering no functional information). The single-variant test (also referred to as p value), conditioned p value, fGWAS posterior association probability (PP, see Appendix A), BVSR PP, and bfGWAS PP were used as criteria to identify associations. The reason that we did not include PAINTOR into comparison is because PAINTOR costs >1,000 CPU hr to finish analyzing one 2.5 Mb genome-block with ~5K variants.

We first compared power of different methods using average ROC curves[27,32] across 100 simulation replicates. Because the p value is used differently from the other "fine-mapping" criteria (fGWAS PP, BVSR PP, bfGWAS PP), we compare only the average ROC curves of fGWAS, BVSR, and bfGWAS (Figure 1A). We found that bfGWAS (modeling LD and allowing multiple signals per locus) outperformed both fGWAS and BVSR. Specifically, with false positive rate (FPR) 2×10^{-4}, the power of identifying the true associations is 0.55 by bfGWAS, 0.45 by BVSR, and 0.34 by fGWAS. In addition, for identifying associated loci with regional-PP > 0.95, bfGWAS has power 0.98 and false discovery rate (FDR) 0.005, BVSR has power 0.97 and FDR 0.006, and fGWAS has power 0.97 and FDR 0.005.

In a typical GWAS, researchers identify a series of associated loci and then examine associated variants within each locus independently. We examined the ability of each method to prioritize the true associations in each locus. Since we simulated two causal SNPs per locus (SNP1 and SNP2), we examine the power for identifying each of these separately (Figure 1B). All methods have approximately the same median rank for causal SNP1 (typically, 2nd rank among 150 SNPs in the locus), suggesting that the strongest signal in a locus can often be identified without incorporating functional information and LD. The median rank

for the second causal SNP2 was the 2nd by bfGWAS, 3rd by BVSR, 13th by fGWAS, and 6th by conditioned p value—suggesting that incorporating functional information improves power to identify multiple signals in a locus and that fGWAS is limited by the assumption of at most one signal per locus. Stratified results based on the LD between two causal variants further demonstrate that bfGWAS has the highest power for identifying the weaker signal, especially when both SNPs are in high LD (Figure S3).

Both bfGWAS and fGWAS correctly identified enrichment in scenario 1 and properly controlled for the type I error of enrichment in scenario 2, despite some numerical issues for fGWAS (Figure S4). Moreover, bfGWAS estimated the effect-size variance per annotation. For all 100 simulation replicates under both scenarios, the 95% confidence intervals of the log-ratio of estimated effect-size variances between coding and noncoding overlapped with 0 (Figure S5), suggesting that effect-size variances were similar between two annotations (matching the simulated truth).

In summary, our simulation studies show that, in comparison with competing methods, bfGWAS has highest power, especially in loci with multiple associated variants. Further, bfGWAS produces enrichment parameter estimates that can help with interpretation of association results.

GWAS of AMD

Next, we applied our method to the AMD GWAS data with 33,976 unrelated European individuals (16,144 advanced case subjects; 17,832 control subjects). We analyzed 9,866,744 (~10M) low-frequency and common variants (MAF > 0.5%) with three types of genomic annotations: gene-based functional annotations by SeattleSeq, summarized regulatory annotations,[41] and the core 15 chromatin states profiled by ChromHMM[42,43] with respect to 127 consolidated epigenomes (ROADMAP, ENCODE).[44]

Coding Variation and AMD

We used SeattleSeq to classify variants according to their impact on coding sequences (Table S1) and then applied our method bfGWAS and fGWAS. bfGWAS identified 37 loci out of 1,063 considered genome blocks with regional-PP > 0.95 (Tables S2, S3, and S5), including 32 among the 34 known AMD loci[31] and 5 extra candidate loci. Using the threshold of Bayesian PP > 0.1068 (roughly equivalent to the p value 5×10^{-8} based on permutations of AMD data; Figure S6), we identified 150 associated variants (Figure S8A; Table S3), with 47 distributed among 42,005 non-synonymous variants, 4 among 67,165 synonymous coding variants, 54 among 3,679,235 intronic variants, 18 among 5,512,423 intergenic variants (including non-annotated variants), and 27 among 565,916 "other-genomic" variants (UTR, non-coding exons, upstream and downstream of genes). Very roughly, this corresponds to fraction of associated variants of ~1:1,000 among non-synonymous variants, 1:15,000 among synonymous variants, 1:100,000 among intronic variants, 1:300,000 among intergenic variants, and 1:20,000 among other-genomic variants.

Similarly, fGWAS identified 39 loci by regional-PP > 0.95, including all 34 known loci and the same 5 extra candidate loci identified by bfGWAS (Tables S2, S4, and S6; Figure S9B). A total of 94 associated variants were identified by fGWAS with fGWAS PP > 0.1068, including 22 non-synonymous, 6 coding-synonymous, 28 intronic, 15 intergenic, and 23 other-genomic signals. Compared with bfGWAS, the proportion of loci that contain at least one non-synonymous variant with PP > 0.1068 is smaller (31% by fGWAS versus 49% by bfGWAS). Similarly, the proportion of non-synonymous variants prioritized by fGWAS is also smaller (30% by fGWAS versus 46% by bfGWAS), indicating that bfGWAS places greater weight on non-synonymous variants—which, as a group, appears to have both a higher prior probability of association and larger effect sizes when associated.

Besides replicating the association results within known AMD loci,[31] bfGWAS identified five additional candidate loci (Table S5): missense *rs7562391/PPIL3*, *rs61751507/CPN1*, *rs2232613/LBP*, downstream *rs114318558/ZNRD1ASP*, and splice *rs6496562/ABHD2*. Among these five candidate loci, fGWAS identified three with the same top risk variants, a different top risk variant (coding-synonymous *rs61733667*) for *CPN1*, and a nearby locus (upstream *rs116803720/HLA-K*) of *ZNRD1ASP* (Table S6). Interestingly, there are several connections between these candidate loci and known AMD loci. Specifically, the protein encoded by *LBP* is part of the lipid transfer protein family (which also includes *CETP* among the known AMD risk loci) that promotes the exchange of neutral lipids and phospholipids between plasma lipoproteins.[45] *ZNRD1ASP* has been associated with lipid metabolisms[46] and *ABHD2* has been associated with coronary artery disease,[47] two other traits where the AMD loci encoding *CETP*, *APOE*, and *LIPC* are also involved. The gene *CPN1* has been associated with age-related disease (specifically, hearing impairment[48]).

Multiple Signals in a Single Locus

We use two examples to illustrate the importance of studying multiple signals in a single locus. Our first example focuses on a 1 Mb region around locus *C2/CFB/SKIV2L* on chromosome 6 where 1,862 variants have $p < 5 \times 10^{-8}$. There are an estimated 4 independent signals in the region by conditional analysis,[31] 1 variant with fGWAS PP > 0.1068, 11 with BVSR PP > 0.1068, and 8 with bfGWAS PP > 0.1068. Interestingly, the alternative methods (p value, fGWAS, and BVSR) identified intronic SNP *rs116503776/SKIV2L/NELFE* as the top candidates ($p = 2.1 \times 10^{-114}$; fGWAS PP = 0.912; BVSR PP = 1.0), while bfGWAS identified two missense SNPs, *rs4151667/C2/CFB* ($p = 1.4 \times 10^{-44}$; bfGWAS PP = 0.917) and *rs115270436/SKIV2L/NELFE* ($p = 2.8 \times 10^{-99}$; bfGWAS PP = 0.633), as the top functional candidates (Figure 2; Tables S2–S4).

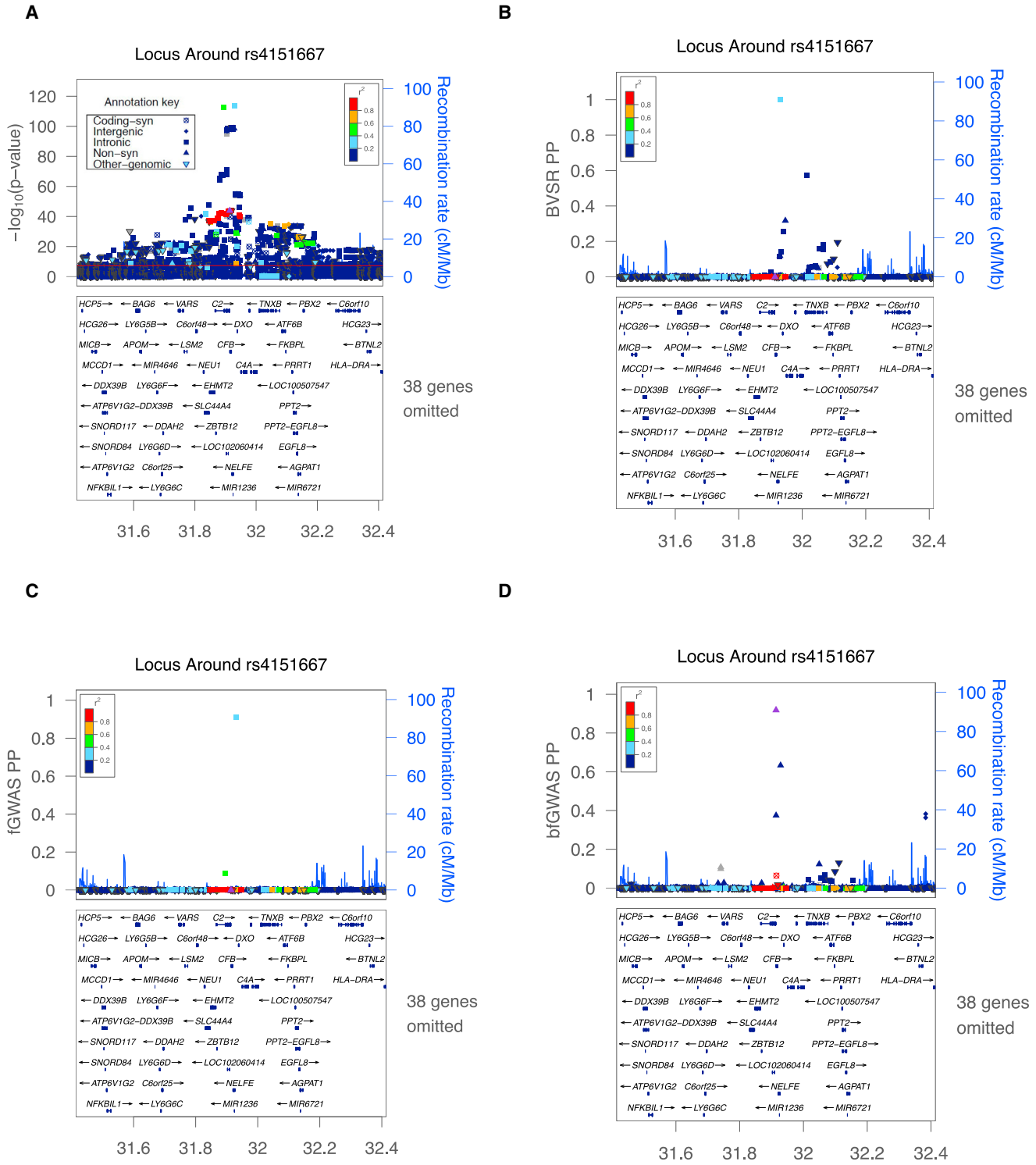

Figure 2. ZoomLocus Plots around *rs4151667* in the Locus *C2/CFB/SKIV2L*
(A) –log(p values) by single variant tests.
(B) Posterior inclusion probabilities (PP) by the standard Bayesian variable selection regression model (BVSR).
(C) Posterior association probabilities (PP) by fGWAS.
(D) Bayesian inclusion probabilities (PP) by bfGWAS.
The top cyan squares in (A)–(C) denote the intronic variant *rs116503776*; the purple triangle in (D) denotes the non-synonymous variant *rs4151667*.

A haplotype analysis describing the odds ratios (ORs) for all possible haplotypes for SNPs *rs116503776*, *rs4151667*, and *rs115270436* helps clarify the region. Intronic SNP *rs116503776* with the smallest p value appears to be associated with the phenotype by tagging the other two missense SNPs (Table S15). In particular, haplotypes with

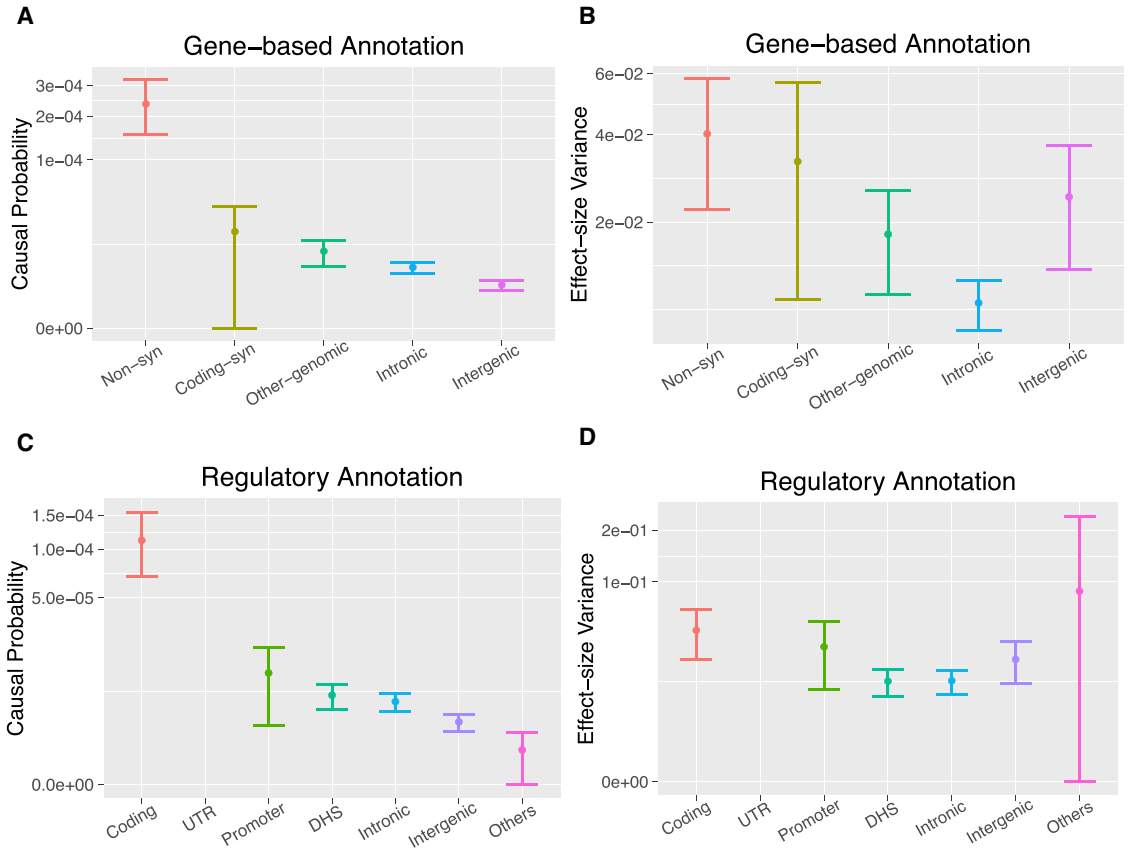

Figure 3. Category-Specific Parameter Estimates with 95% Error Bars by bfGWAS for Gene-Based Annotations and Regulatory Annotations

(A and C) Causal probabilities.

(B and D) Effect-size variances.

The estimates of UTR in (C) and (D) were estimated as their prior values due to no association was found for this annotation (hence not shown in the plots). The estimate of the effect-size variance for the "Others" category in (D) is also close to the prior because of low region-association evidence, hence it has a wide 95% error bar. The error bars denote the 95% confidence intervals for the category-specific parameter estimates.

rs116503776 can either increase or decrease risk, depending on alleles at the other two SNPs. To further confirm the importance of the missense SNPs *rs4151667* and *rs115270436*, we compared the AIC/BIC/loglikelihood between two models: one model with the top two independent signals (*rs116503776* and *rs114254831*) identified by single-variant conditional analysis,[31] versus the other model with the top two signals (*rs4151667* and *rs115270436*) identified by bfGWAS. As expected, the second model has smaller AIC/BIC and larger loglikelihood than the first one (Table S16). Thus, we can see that while alternative methods (p value, fGWAS, and BVSR) focus on the SNP with the smallest p value, our bfGWAS method finds an alternative pairing of missense signals that better accounts for all data.

Our second example focuses on a 1 Mb region around gene *C3* on chromosome 19 (Figure S9) with 112 genome-wide significant variants with $p < 5 \times 10^{-8}$. fGWAS discovered only a single missense signal, *rs2230199*, with the most significant $p = 1.7 \times 10^{-77}$ (top blue triangle in Figures S9A and S9C). However, both BVSR and bfGWAS identified two missense variants with PPs = 1.0 and five intronic variants with $0.11 < PPs < 0.18$. The top two missense signals, *rs2230199* and *rs147859257* (241 base pairs apart), were confirmed by conditional analysis,[31] where the second signal *rs147859257* has conditioned $p = 6.0 \times 10^{-33}$ (purple triangle in Figures S9B and S9D), overlapping with *rs2230199*. These two missense signals match the interpretation of previous studies.[49–51] Because five other intronic variants (*rs11569479*, *rs11569470*, *rs201063729*, *rs10408682*, and *rs11569466*) are in high LD with $R^2 > 0.98$ between each other, we believe this is the third independent signal whose Bayesian PP was split among five variants in high LD by bfGWAS.

Enrichment Analysis

bfGWAS estimated that non-synonymous variants are 10–100 times more likely to be causal than variants in other categories and that they also have larger effect sizes (Figures 3A and 3B). To better compare enrichment among multiple categories, we define two new sets of parameters (Supplemental Note). The first set of parameters (π_q/π_{avg}) is defined to contrast the posterior association probability

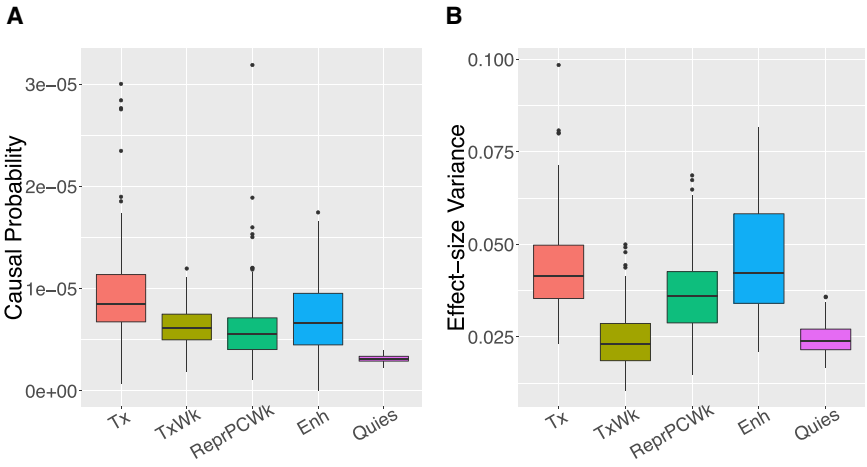

Figure 4. Top Five Enriched Chromatin States Identified by bfGWAS, using the AMD GWAS Data with Respect to 127 Epigenomes

(A) Boxplot of the category-specific causal probabilities for the top five enriched chromatin states.

(B) Boxplot of the effect-size variances for the top five enriched chromatin states.

estimate (π_q) for each category to the genome-wide average (π_{avg}). The second set of parameters ($\sigma_q^2/\sigma_{avg}^2$) is similarly defined to contrast the effect-size variance from each category to the genome-wide average. Moreover, the square root of the effect-size variance reflects the effect-size magnitude because of the prior assumption for the effect size in our model.

Compared to the genome-wide average probability of causality $\pi_{avg} = 4.3\times10^{-6}$ (Figure S12A), we found that non-synonymous category were 53× more likely to be causal ($p = 7.24 \times 10^{-84}$), that coding-synonymous and other variants were 4.3× and 2.2× more likely ($p = 0.005$, 0.003), and that intergenic variants were 0.7× less likely ($p = 4.9 \times 10^{-6}$), while the intronic variants matched the genome-wide average ($p = 0.659$). In addition, compared to the genome-wide average effect-size variance ($\sigma_{avg}^2 = 0.02$; Figure S12B), we found that the effect size variance of was 1.9× larger for non-synonymous variants ($p = 0.014$; i.e., 1.4× larger effect-size), and 0.4× smaller for variants in the intronic category ($p = 4.5 \times 10^{-6}$); remaining categories were not significantly different ($p > 0.2$). The estimated enrichment parameters by fGWAS show a similar pattern, although the contrast of the estimated enrichment for non-synonymous versus other annotations is not as pronounced as by bfGWAS (Figure S12A).

Analysis with Regulatory Annotations

In addition, we analyzed the GWAS data of AMD with the summarized regulatory annotations:[41] coding, UTR, promoter (defined as within 2 kb of a transcription starting site), DHS in any of 217 cell types, intronic, intergenic, and "others" (not annotated as any of the previous six categories). Overall GWAS results were similar as the ones described in previous context (Tables S7–S10). Compared to the genome-wide average association probability ($\pi_{avg} = 4.03\times10^{-6}$; Figure S12C), we found that the association probability of the coding category was 28× higher ($p < 2.2 \times 10^{-16}$), the promoter was 2.6× ($p = 0.028$) higher, and the intergenic and "others" were 0.5× and 0.9× less ($p = 5.3 \times 10^{-4}$, 0.033), while the DHS and intronic were not significantly different ($p > 0.1$). In addition, compared to the genome-wide average effect-size variance ($\sigma_{avg}^2 = 0.024$), we found that the effect-size variance of the coding category was 1.9× larger ($p = 0.019$; i.e., 1.4× larger effect size) and the DHS and intronic were 0.5× less ($p = 0.011$, 0.007), while the promoter, intergenic, and "others" were not significantly different ($p > 0.1$; Figure S12D). Here, fGWAS identified a slightly different enrichment pattern (Figure S12B), where UTR was identified as the second most enriched category. This is presumably because fGWAS assumes one signal per locus and tends to prioritize the variant with the smallest p value in each locus, e.g., UTR variants *rs1142/KMT2E/SPRK2* and *rs10422209/CNN2* have the highest fGWAS PP and the smallest p value in their respective locus (Tables S2 and S8).

Analysis with Chromatin States

Last, we considered the annotations of core 15 chromatin states profiled by ChromHMM[43] with respect to 127 consolidated epigenomes (ROADMAP, ENCODE):[44] active TSS (TssA), flanking active TSS (TssAFlnk), transcription at gene 5′ and 3′ (TxFlnk), strong transcription (Tx), weak transcription (TxWk), genic enhancers (EnhG), enhancers (Enh), ZNF genes & repeats (ZNF/Rpts), heterochromatin (Het), bivalent/poised TSS (TssBiv), flanking bivalent TSS/Enh (BivFlnk), bivalent enhancer (EnhBiv), repressed PolyComb (ReprPC), weak repressed PolyComb (ReprPCWk), and quiescent/low (Quies).

With each set of chromatin states profiled per epigenome, we applied bfGWAS on the GWAS data of AMD and then counted the frequency of the top 5 enriched chromatin states across all 127 epigenomes. We found that the associations are mostly enriched with strong transcription (Tx), weak transcription (TxWk), repressed PolyComb (ReprPC), enhancers (Enh), and Quies (Figure 4). Specifically, the highest estimates of the causal probabilities are 3.0×10^{-5} for strong transcription with respect to the fetal brain male tissue (E081), 1.2×10^{-5} for weak transcription with respect to the adipose nuclei (E063), 3.1×10^{-5} for repressed PolyComb with respect to the spleen tissue (E113), 1.7×10^{-5} for enhancers with respect to the ovary tissue (E097), and 3.9×10^{-6} for Quies with respect to the pancreatic islets.

We further examined the list of variants that contribute 95% posterior probabilities in the identified loci with regional-PP > 95%. We found that the results accounting

for the chromatin states that are profiled with respect to the epigenome of fetal thymus (E093) gave the shortest list (average 11 variants per locus, and we present the corresponding results as an example (Figures S12E, S12F, S13A, and S13B; Tables S11–S14). For this set of enrichment analysis, we found that the repressed PolyComb had the highest causal probability (3.8× higher than the genome-wide average $\pi_{avg} = 4.0\times10^{-6}$, $p = 6.7 \times 10^{-7}$; Figure S12E), and that all chromatin states have comparable effect-size variances (Figure S12F). Here, fGWAS identified transcription at gene 5′ and 3′ (TxFlnk) as the most enriched chromatin state (Figure S13C).

MGI GWAS of Skin Cancer

To illustrate the benefits of using bfGWAS for GWAS data that have relatively fewer loci, we further analyzed the MGI GWAS data with the phenotype of skin cancer, with 17,624 unrelated European samples (2,359 case subjects versus 15,265 control subjects) and ~8.7M variants with MAF > 0.5%. We corrected the phenotype of skin cancer with respect to age, sex, PC1-4, considered the same gene-based annotations (from SeattleSeq) as for the AMD GWAS, and compared the GWAS results by p value, BVSR, fGWAS, and bfGWAS.

For this GWAS data of skin cancer, all method identified the same four loci: *SLC45A2*, *IRF4*, *MC1R*, and *RALY* (Figures S14 and S15). Both bfGWAS and fGWAS identified that non-synonymous is the most enriched annotation (Figure S16). Although BVSR, fGWAS, and bfGWAS all produced the highest PP for the leading SNP with the smallest p value, our bfGWAS method outperformed BVSR for identifying the leading SNP at locus *SLC45A2*, as well as produced an additional and independent non-synonymous signal in locus *MC1R* (missed by fGWAS) for allowing multiple signals per locus as well as accounting for functional information and LD (Figure S17). In addition, our bfGWAS method avoids the false signal on chromosome 3 by BVSR for using annotation-specific priors. Specifically, by the threshold of PP > 0.1068, bfGWAS identified 9 associated variants (3 non-synonymous, 4 intronic, and 1 other genomic), and 9 by fGWAS (2 non-synoymous, 5 intronic, and 2 intergenic).

Therefore, this set of GWAS analyses further confirmed the advantages of using our bfGWAS method for integrating functional information and fine-mapping loci with multiple signals.

Discussion

Here, we describe a scalable Bayesian hierarchical method, bfGWAS, for integrating functional information in GWASs to help prioritize functional associations and understand underlying genetic architecture. bfGWAS models both association probability and effect-size distribution as a function of annotation categories for improving fine-mapping resolution. Unlike previous methods,[26,27] bfGWAS accounts for LD and allows for the possibility of multiple signals per locus while remaining capable of genome-wide inference. Further, bfGWAS employs an improved MCMC sampling strategy to greatly improve the mixing of MCMC samples, which ensures the capability of identifying a list of independent association candidates.

By simulation studies, we demonstrated that bfGWAS had higher power than the alternative methods for identifying multiple signals in a single locus by accounting for both functional information and LD. We also showed that bfGWAS accurately estimated the enrichment patterns under scenarios with or without enrichment for one annotation in simulations. In the real GWASs of AMD and skin cancer, we further confirmed the advantages of identifying multiple independent signals per locus and prioritizing important functional associations by bfGWAS. Further, we gave two fine-mapped AMD loci, *C2/CFB/SKIV2L* and *C3*, by bfGWAS as examples with justifications by haplotype analysis, model comparison, and previous findings. Thus, we believe our method is useful for understanding the underlying genetic architecture of complex traits and diseases for efficiently integrating functional information into GWASs.

Extending bfGWAS to deal with overlapping or quantitative annotations might seem trivial in theory, by assuming a logistic model with multiple functional covariates (both categorical and quantitative) for π_i in the BVSR model. However, the posterior estimates for the coefficients in the logistic model of π_i no longer have analytical formulas in the M-step of the EM-MCMC algorithm (Supplemental Note). Specifically, overestimated π_i will inflate the number of false positives. In preliminary analysis, we encountered computational challenges of controlling the false positive rate, which requires further studies.

Here, bfGWAS makes a key assumption that the variant correlation matrix has a block-wise structure, which allows us to segment the genome into approximately independent blocks, analyze variants per block by MCMC, and summarize genome-wide information by an EM algorithm. In parallel to our study, many recent studies have also explored the benefits of dividing the human genome into approximately independent LD blocks to facilitate genome-wide analyses.[26,52] Although the standard segmentation methods (e.g., based on genomic location[52] as we adopted here, or the number of variants per block[26]) are often sufficient in practice, we expect that a better segmentation method[30] based on LD blocks will further increase the association mapping power.

The biggest limitation of bfGWAS is probably computational cost, as we perform MCMC using the complete genotype data. Specifically, bfGWAS took 5,000 CPU hr (~5 hr with parallel computations on 1,000 CPUs for the 1,063 genome blocks) to analyze the AMD GWAS data with 33,976 individuals and 9,857,286 variants. Implementing bfGWAS with summary statistics is expected to reduce the computation cost significantly, which

is part of our continuing research. In addition, the variational approximation[53,54] and other approximations[55,56] of MCMC may provide an efficient alternative for posterior inference in large GWASs.

Appendix A

Bayesian Hierarchical Model Accounting for Functional Information

Recall the standard Bayesian variable selection regression (BVSR) model as described in the Material and Methods,

$$\boldsymbol{y}_{\boldsymbol{n}\times\mathbf{1}} = \boldsymbol{X}_{\boldsymbol{n}\times\boldsymbol{p}}\,\boldsymbol{\beta}_{\boldsymbol{p}\times\mathbf{1}} + \epsilon_{\boldsymbol{n}\times\mathbf{1}}\,,$$
$$\beta_i \sim \pi_i N\left(0,\ \tau^{-1}\sigma_i^2\right) + (1-\pi_i)\delta_0(\beta_i),\ \epsilon_i\ \sim \mathrm{N}\left(0,\ \tau^{-1}\right).$$

We assume that variants in the same functional category have the same spike-and-slab prior, $\beta_i \sim \pi_i N(0,\ \tau^{-1}\sigma_i^2) + (1-\pi_i)\delta_0(\beta_i)$, for the effect sizes. That is, $\pi_i = \pi_q,\ \sigma_i^2 = \sigma_q^2$ for variants of the qth functional annotation category. Consequently, π_q denotes the category-specific causal probability and σ_q^2 denotes the category-specific effect-size variance (the square root of σ_q^2 reflects the magnitude of effect size).

We further assume the following independent hyper priors:[34]

$$\pi_q \sim Beta\left(a_q,\ b_q\right),\ \sigma_q^2 \sim IG(k_1,\ k_2),\ \pi_q \perp \sigma_q^2,$$

where π_q follows a Beta distribution with positive shape parameters a_q and b_q and σ_q^2 follows an Inverse-Gamma distribution with shape parameter k_1 and scale parameter k_2. In order to adjust for the unbalanced distribution of functional annotations among all variants and enforce a sparse model in our analysis, we choose values for a_q and b_q such that the Beta distribution has mean $a_q/(a_q+b_q) = 10^{-6}$ with (a_q+b_q) equal to the number of variants in category q. We set $k_1 = k_2 = 0.1$ in our analysis to induce non-informative prior for σ_q^2. Note that τ is fixed as the phenotype variance value in our Bayesian inferences (Supplemental Note).

Bayesian Inference

We introduce a latent indicator vector $\boldsymbol{\gamma}_{\boldsymbol{p}\times\mathbf{1}}$ to facilitate computation, where each element γ_i is a binary variable and indicates whether $\beta_i = 0$ by $\gamma_i = 0$ or $\beta_i \sim N(0,\ \tau^{-1}\sigma_i^2)$ by $\gamma_i = 1$ (γ_i corresponds to the ith variant with genetic effect-size β_i). Equivalently,

$$\gamma_i \sim \mathrm{Bernoulli}(\pi_i),\ \boldsymbol{\beta}_{-\boldsymbol{\gamma}} \sim \boldsymbol{\delta}_0,\ \boldsymbol{\beta}_{\boldsymbol{\gamma}} \sim \boldsymbol{MVN}_{|\boldsymbol{\gamma}|}\left(0,\ \tau^{-1}\boldsymbol{V}_{\boldsymbol{\gamma}}\right),$$

where $|\boldsymbol{\gamma}|$ denotes the number of 1s in $\boldsymbol{\gamma}$; $\boldsymbol{\beta}_{-\boldsymbol{\gamma}}$ denotes the zero effect-size vector with $\gamma_i = 0$; $\boldsymbol{\beta}_{\boldsymbol{\gamma}}$ denotes the non-zero effect-size vector with $(\gamma_j = 1; j = 1,\ \ldots,\ |\boldsymbol{\gamma}|)$; and $\boldsymbol{V}_{\boldsymbol{\gamma}}$ denotes the diagonal covariance matrix, $diag(\sigma_1^2,\ \ldots,\ \sigma_{|\boldsymbol{\gamma}|}^2)$, corresponding to non-zero effect-sizes. Consequently, the expectation of γ_i is an estimate of the posterior inclusion probability (PP) for the ith variant, $E[\gamma_i] = Prob(\gamma_i = 1) = PP_i$.

The posterior joint distribution of our proposed Bayesian hierarchical model is proportional to

$$P\left(\boldsymbol{\beta},\ \boldsymbol{\gamma},\ \boldsymbol{\pi}, \boldsymbol{\sigma}^2,\ \tau \mid\ \boldsymbol{y},\ \boldsymbol{X},\ \boldsymbol{A}\right) \propto P(\boldsymbol{y} \mid \boldsymbol{X}, \boldsymbol{\beta}, \boldsymbol{\gamma},\ \tau) \times$$
$$P\left(\boldsymbol{\beta},\ |\boldsymbol{A},\ \boldsymbol{\pi}, \boldsymbol{\sigma}^2,\ \boldsymbol{\gamma}, \tau\right) P(\boldsymbol{\gamma} \mid \boldsymbol{\pi}) P(\boldsymbol{\pi}) P\left(\boldsymbol{\sigma}^2\right) P(\tau),$$

where $\boldsymbol{\pi} = (\pi_1,\ \ldots,\ \pi_Q)^T$, $\boldsymbol{\sigma}^2 = (\sigma_1^2,\ \ldots,\ \sigma_Q^2)^T$, $\boldsymbol{A}$ is the $p \times Q$ matrix of binary annotations, and Q is the total number of annotations. The goal is to estimate the category-specific parameters $(\boldsymbol{\pi},\ \boldsymbol{\sigma}^2)$ and the variant-specific parameters $(\boldsymbol{\beta},\ E[\boldsymbol{\gamma}])$ from their posterior distributions, conditioning on the data $(\boldsymbol{y},\ \boldsymbol{X},\ \boldsymbol{A})$. Here, the category-specific parameters denote the shared characteristics among all variants with the same annotation, which are also called enrichment parameters.

EM-MCMC Algorithm

The basic idea of the EM-MCMC algorithm is to segment the whole genome into approximately independent blocks each with 5,000–10,000 variants, run MCMC algorithm per block with fixed category-specific parameter values $(\boldsymbol{\pi},\ \boldsymbol{\sigma}^2)$ to obtain posterior estimates of $(\boldsymbol{\beta},\ E[\boldsymbol{\gamma}])$ (E-step), then summarize the genome-wide posterior estimates of $(\boldsymbol{\beta},\ E[\boldsymbol{\gamma}])$ and update values of $(\boldsymbol{\pi},\ \boldsymbol{\sigma}^2)$ by maximizing their posterior likelihoods (M-step). Repeat such EM-MCMC iterations for a few times until the estimates of $(\boldsymbol{\pi},\ \boldsymbol{\sigma}^2)$ (maximum *a posteriori* estimates, i.e., MAPs) converge (Figure S1).

We derive the log-posterior-likelihood functions for $(\boldsymbol{\pi},\ \boldsymbol{\sigma}^2)$ and the analytical formulas for their MAPs. In addition, we construct their confidence intervals using Fisher information, whose analytical forms are derived for our Bayesian hierarchical model (Supplemental Note). In our practical analyses, we find that, in general, with about 5 EM iterations and 50K MCMC iterations per block, the estimates for $(\boldsymbol{\pi},\ \boldsymbol{\sigma}^2)$ would achieve convergence. Our method of integrating functional information into GWAS by using the above Bayesian hierarchical model and EM-MCMC algorithm is referred as "Bayesian Functional GWAS" (bfGWAS).

Convergence Diagnosis

The MCMC algorithm implemented in bfGWAS is essentially a random walk over all possible linear regression models with combinations of variants, which can start with either a model containing multiple significant variants by sequential conditional analysis or the most significant variant by p value. In each MCMC iteration, a new model is proposed by including an additional variant, by deleting one variant from the current model, or by switching one variant within the current model with one outside; and then up to acceptation or rejection by the Metropolis-Hastings algorithm (Supplemental Note). Importantly, we refine the standard proposal strategy for the switching step by prioritizing variants in the neighborhood of the switch candidate according to their conditional association evidence (e.g., p values conditioning on variants,

except the switch candidate, in the current model). As a result, this MCMC algorithm encourages our method to explore different combinations of potential signals in each locus and significantly improves the mixing property.

We used the potential scale reduction factor (PSRF)[57] to quantitatively diagnose the MCMC mixing property. PSRF is essentially a ratio between the average within-chain variance of the posterior samples and the overall-chain variance with multiple MCMC chains. From the example plots of the PSRFs of Bayesian PPs (Figure S2), for 58 top marginally significant SNPs (with $p < 5 \times 10^{-8}$) in the WTCCC GWAS of Crohn disease,[1] we can see that about half of the PSRF values by the standard MCMC algorithm (used in GEMMA[35]) exceed 1.2, suggesting that the standard MCMC algorithm has poor mixing property. In contrast, the PSRF values by our MCMC algorithm are within the range of (0.9, 1.2), suggesting that our MCMC algorithm has greatly improved mixing property.

Key Implementation Details

We employ two computational techniques to save memory in the bfGWAS software. One is to save all genotype data as unsigned characters in memory, because unsigned characters are equivalent to unsigned integers in (0, 256) that can be easily converted to genotype values within the range of (0.0, 2.0) by multiplying with 0.01. This technique saves up to 90% memory compared to saving genotypes in double type. Second, with an option of in-memory compression, bfGWAS will further save additional 70% memory. As a result, we can decrease the memory usage from ~120 GB (usage by GEMMA[35]) to ~3.6 GB for a typical GWAS dataset with ~33K individuals and ~400K variants.

The bfGWAS software wraps a C++ executable file for the E-step (MCMC algorithm) and an R script for the M-step together by a Makefile, which is generated by a Perl script and enables parallel computation through submitting jobs. Generally, 50K MCMC iterations with ~5K variants and ~33K individuals require about 300 MB memory and 1 hr CPU time on a 1.6 GHz core, where the computation cost is of order $O(nm^2)$ with the sample size (n) and number of variants (m) considered in the linear models during MCMC iterations (usually $m < 10$). The computation cost for M-step is almost negligible due to the analytical formulas of the MAPs.

fGWAS

In this paper, the fGWAS results were generated by using summary statistics from single variant likelihood-ratio tests and the same annotation information used by bfGWAS. fGWAS[26] produces variant-specific posterior association probabilities (PPs), segment-specific PPs, and enrichment estimates for all annotations. We used the same genome segmentation as used by bfGWAS for fGWAS in both simulations and real data analyses, to produce comparable results. The final fGWAS PP is given by the product of the variant-specific PP and the corresponding segment-specific PP, and the fGWAS regional-PP is given by the highest segment-specific PP in a region or genome block.

Simulation Studies

We used genotype data on chromosomes 18–22 from the AMD GWAS (33,976 individuals and 241,500 variants with MAF > 0.05) to simulate quantitative phenotypes from the standard linear regression model $y_i = \boldsymbol{X}_i^T \boldsymbol{\beta} + \epsilon_i,\ \ i = 1, \ldots, 33976$, where $\boldsymbol{X}_i$ is the genotype vector of the ith individual and ϵ_i is the noise term generated from $N(0, \sigma_\epsilon^2)$. We segmented the genotype data into 100× 2.5 Mb blocks each with ~5,000 variants. Within each block, we marked a ~25 kb continuous region (starting 37.5 kb from the beginning of a block) as the causal locus and randomly selected two causal SNPs if the genome block was selected as a risk locus. Two complementary annotations ("coding" versus "noncoding") were simulated, where the coding variants account for ~1% overall variants but ~10% variants within the causal loci (matching the pattern in the real AMD analysis). We selected positive effect-size vector $\boldsymbol{\beta}$ and noise variance σ_ϵ^2 such that a total of 15% phenotypic variance was equally explained by causal SNPs. We controlled the enrichment-fold of coding variants by varying the number of coding variants among the causal SNPs.

We compared bfGWAS with p value, conditioned p value, and fGWAS. In the simulation studies, p values were obtained from a series of likelihood-ratio tests based on the standard linear regression model. p values conditioning on the top significant variant per locus were used to identify the second signal by conditional analysis. fGWAS was implemented with summary statistics from single variant tests and the same genome segmentation as used by bfGWAS. We failed to include PAINTOR in the comparison, because PAINTOR cannot complete the analysis for one block in >1,000 CPU hr (on a 2.5 GHz, 64-bit CPU) and is thus expected to require >1 million CPU hr for a genome-wide analysis.

GWAS of AMD

In the GWAS data of AMD, all genotypes were generated by a customized chip that contains (1) the usual genome-wide variant content, (2) exome content comparable to the Exome chip (protein-altering variants across all exons), (3) variants in known AMD risk loci (protein-altering variants and previously associated variants), and (4) previously observed and predicted variation in *TIMP3* and *ABCA4* (two genes implicated in monogenic retinal dystrophies). The genotyped variants (439,350) were then imputed to the 1000 Genomes reference panel (phase I),[58] resulting a total of 12,023,830 variants.

The software bfGWAS used dosage genotype data and standardized phenotypes. Phenotypes were first coded quantitatively with 1 for case subjects and 0 for control subjects; then corrected for the first and second principle components, age, gender, and source of DNA samples;

and then standardized to have mean 0 and standard deviation 1. In order to make the Bayesian inferences scalable to the AMD GWAS data (33,976 individuals, 9,866,744 variants with MAF > 0.5%), we segmented the whole genome into 1,063 non-overlapped blocks, such that each block has length ~2.5 Mb (containing ~10,000 variants) and all previously identified loci along with variants in LD ($R^2 > 0.1$) were not split. Then we applied the EM-MCMC algorithm with 5 EM steps and 50,000 MCMC iterations per block (including 50,000 extra burn-ins).

For comparison, p values were obtained by a series of likelihood-ratio tests, using the same "quantitative" phenotype vector as used by bfGWAS; fGWAS was implemented with the summary statistics from single variant tests and the same genome segmentation as used by bfGWAS; and a standard Bayesian variable selection regression (BVSR) method that models no functional information was also applied.

Three types of genomic annotations were considered for analyzing the AMD data: gene-based functional annotations of SNPs and small indels from SeattleSeq, summarized regulatory annotations,[41] and the chromatin states profiled respectively for 127 epigenomes by ChromHMM.[19,42,43] For variants annotated with multiple functions, we used the most severe function in the analysis: non-synonymous > coding-synonymous > other-genomic > intronic > intergenic for the gene-based annotations; coding > UTR > promoter > DHS > intronic > intergenic > "others" for the summarized regulatory annotations.

We further did sensitivity analysis using varying prior means as well as starting values (10^{-6}, 5×10^{-6}, 10^{-5}) for π_q, and varying starting values (10, 5, 1) for σ_q^2 in bfGWAS with gene-based functional annotations. As expected, the results showed that the posterior inference results were not affected by various practical prior assumptions and starting values of the category-specific parameters. Specifically, all three sets of results identified the same 37 risk loci, comparable number of associated variants with Bayesian PP > 0.1068, as well as the same enrichment pattern (Figure S10).

Accession Numbers

The accession number for the AMD genotype data analyzed in this paper is dbGaP: phs001039.v1.p1.

Supplemental Data

Supplemental Data include 17 figures, 16 tables, and a detailed technical note and can be found with this article online at http://dx.doi.org/10.1016/j.ajhg.2017.08.002.

Acknowledgments

X.Z. is supported by NIH grants R01HG009124 and R01GM126553 and the National Science Foundation (NSF) grant DMS1712933. J.Y. and G.A. are supported by NIH grants R01HG007022 and R01EY022005. The authors would like to thank the Michigan Genomics Initiative (MGI) for allowing us to use the GWAS data about the skin cancer phenotype.

Received: February 14, 2017
Accepted: August 3, 2017
Published: August 24, 2017

Web Resources

bfGWAS, https://github.com/yjingj/bfGWAS
ChromHMM, http://compbio.mit.edu/ChromHMM/
fGWAS, https://github.com/joepickrell/fgwas
GEMMA, https://github.com/genetics-statistics/GEMMA
Profiled chromatin states with respect to 127 epigenomes, http://egg2.wustl.edu/roadmap/web_portal/chr_state_learning.html#core_15state
SeattleSeq, http://snp.gs.washington.edu/SeattleSeqAnnotation138/

References

1. Wellcome Trust Case Control, C.; and Wellcome Trust Case Control Consortium (2007). Genome-wide association study of 14,000 cases of seven common diseases and 3,000 shared controls. Nature *447*, 661–678.
2. McCarthy, M.I., Abecasis, G.R., Cardon, L.R., Goldstein, D.B., Little, J., Ioannidis, J.P., and Hirschhorn, J.N. (2008). Genome-wide association studies for complex traits: consensus, uncertainty and challenges. Nat. Rev. Genet. *9*, 356–369.
3. Voight, B.F., Scott, L.J., Steinthorsdottir, V., Morris, A.P., Dina, C., Welch, R.P., Zeggini, E., Huth, C., Aulchenko, Y.S., Thorleifsson, G., et al.; MAGIC investigators; and GIANT Consortium (2010). Twelve type 2 diabetes susceptibility loci identified through large-scale association analysis. Nat. Genet. *42*, 579–589.
4. Visscher, P.M., Brown, M.A., McCarthy, M.I., and Yang, J. (2012). Five years of GWAS discovery. Am. J. Hum. Genet. *90*, 7–24.
5. Willer, C.J., Schmidt, E.M., Sengupta, S., Peloso, G.M., Gustafsson, S., Kanoni, S., Ganna, A., Chen, J., Buchkovich, M.L., Mora, S., et al.; Global Lipids Genetics Consortium (2013). Discovery and refinement of loci associated with lipid levels. Nat. Genet. *45*, 1274–1283.
6. Hirschhorn, J.N., and Daly, M.J. (2005). Genome-wide association studies for common diseases and complex traits. Nat. Rev. Genet. *6*, 95–108.
7. Yu, J., Pressoir, G., Briggs, W.H., Vroh Bi, I., Yamasaki, M., Doebley, J.F., McMullen, M.D., Gaut, B.S., Nielsen, D.M., Holland, J.B., et al. (2006). A unified mixed-model method for association mapping that accounts for multiple levels of relatedness. Nat. Genet. *38*, 203–208.
8. Hindorff, L.A., Sethupathy, P., Junkins, H.A., Ramos, E.M., Mehta, J.P., Collins, F.S., and Manolio, T.A. (2009). Potential etiologic and functional implications of genome-wide association loci for human diseases and traits. Proc. Natl. Acad. Sci. USA *106*, 9362–9367.
9. Yang, J., Ferreira, T., Morris, A.P., Medland, S.E., Madden, P.A., Heath, A.C., Martin, N.G., Montgomery, G.W., Weedon, M.N., Loos, R.J., et al.; Genetic Investigation of ANthropometric Traits (GIANT) Consortium; and DIAbetes Genetics Replication And Meta-analysis (DIAGRAM) Consortium (2012). Conditional and joint multiple-SNP analysis of GWAS summary

statistics identifies additional variants influencing complex traits. Nat. Genet. *44*, 369–375, S1–S3.
10. Carithers, L.J., and Moore, H.M. (2015). The Genotype-Tissue Expression (GTEx) Project. Biopreserv. Biobank. *13*, 307–308.
11. Dixon, J.R., Jung, I., Selvaraj, S., Shen, Y., Antosiewicz-Bourget, J.E., Lee, A.Y., Ye, Z., Kim, A., Rajagopal, N., Xie, W., et al. (2015). Chromatin architecture reorganization during stem cell differentiation. Nature *518*, 331–336.
12. Kellis, M., Wold, B., Snyder, M.P., Bernstein, B.E., Kundaje, A., Marinov, G.K., Ward, L.D., Birney, E., Crawford, G.E., Dekker, J., et al. (2014). Defining functional DNA elements in the human genome. Proc. Natl. Acad. Sci. USA *111*, 6131–6138.
13. Kumar, P., Henikoff, S., and Ng, P.C. (2009). Predicting the effects of coding non-synonymous variants on protein function using the SIFT algorithm. Nat. Protoc. *4*, 1073–1081.
14. Adzhubei, I., Jordan, D.M., and Sunyaev, S.R. (2013). Predicting functional effect of human missense mutations using PolyPhen-2. Curr. Protoc. Hum. Genet. *Chapter 7*, 20.
15. Pickrell, J.K., Marioni, J.C., Pai, A.A., Degner, J.F., Engelhardt, B.E., Nkadori, E., Veyrieras, J.B., Stephens, M., Gilad, Y., and Pritchard, J.K. (2010). Understanding mechanisms underlying human gene expression variation with RNA sequencing. Nature *464*, 768–772.
16. Tung, J., Zhou, X., Alberts, S.C., Stephens, M., and Gilad, Y. (2015). The genetic architecture of gene expression levels in wild baboons. eLife *4*, 4.
17. Lea, A.J., Tung, J., and Zhou, X. (2015). A Flexible, Efficient Binomial Mixed Model for Identifying Differential DNA Methylation in Bisulfite Sequencing Data. PLoS Genet. *11*, e1005650.
18. Pique-Regi, R., Degner, J.F., Pai, A.A., Gaffney, D.J., Gilad, Y., and Pritchard, J.K. (2011). Accurate inference of transcription factor binding from DNA sequence and chromatin accessibility data. Genome Res. *21*, 447–455.
19. Ernst, J., and Kellis, M. (2012). ChromHMM: automating chromatin-state discovery and characterization. Nat. Methods *9*, 215–216.
20. McVicker, G., van de Geijn, B., Degner, J.F., Cain, C.E., Banovich, N.E., Raj, A., Lewellen, N., Myrthil, M., Gilad, Y., and Pritchard, J.K. (2013). Identification of genetic variants that affect histone modifications in human cells. Science *342*, 747–749.
21. Cooper, G.M., Stone, E.A., Asimenos, G., Green, E.D., Batzoglou, S., Sidow, A.; and NISC Comparative Sequencing Program (2005). Distribution and intensity of constraint in mammalian genomic sequence. Genome Res. *15*, 901–913.
22. Kircher, M., Witten, D.M., Jain, P., O'Roak, B.J., Cooper, G.M., and Shendure, J. (2014). A general framework for estimating the relative pathogenicity of human genetic variants. Nat. Genet. *46*, 310–315.
23. Finucane, H.K., Bulik-Sullivan, B., Gusev, A., Trynka, G., Reshef, Y., Loh, P.R., Anttila, V., Xu, H., Zang, C., Farh, K., et al.; ReproGen Consortium; Schizophrenia Working Group of the Psychiatric Genomics Consortium; and RACI Consortium (2015). Partitioning heritability by functional annotation using genome-wide association summary statistics. Nat. Genet. *47*, 1228–1235.
24. Zhou, X. (2017). A unified framework for variance component estimation with summary statistics in genome-wide association studies. bioaRxiv. http://dx.doi.org/10.1101/042846.
25. Schork, A.J., Thompson, W.K., Pham, P., Torkamani, A., Roddey, J.C., Sullivan, P.F., Kelsoe, J.R., O'Donovan, M.C., Furberg, H., Schork, N.J., et al.; Tobacco and Genetics Consortium; Bipolar Disorder Psychiatric Genomics Consortium; and Schizophrenia Psychiatric Genomics Consortium (2013). All SNPs are not created equal: genome-wide association studies reveal a consistent pattern of enrichment among functionally annotated SNPs. PLoS Genet. *9*, e1003449.
26. Pickrell, J.K. (2014). Joint analysis of functional genomic data and genome-wide association studies of 18 human traits. Am. J. Hum. Genet. *94*, 559–573.
27. Kichaev, G., Yang, W.Y., Lindstrom, S., Hormozdiari, F., Eskin, E., Price, A.L., Kraft, P., and Pasaniuc, B. (2014). Integrating functional data to prioritize causal variants in statistical fine-mapping studies. PLoS Genet. *10*, e1004722.
28. Gabriel, S.B., Schaffner, S.F., Nguyen, H., Moore, J.M., Roy, J., Blumenstiel, B., Higgins, J., DeFelice, M., Lochner, A., Faggart, M., et al. (2002). The structure of haplotype blocks in the human genome. Science *296*, 2225–2229.
29. Wall, J.D., and Pritchard, J.K. (2003). Haplotype blocks and linkage disequilibrium in the human genome. Nat. Rev. Genet. *4*, 587–597.
30. Berisa, T., and Pickrell, J.K. (2016). Approximately independent linkage disequilibrium blocks in human populations. Bioinformatics *32*, 283–285.
31. Fritsche, L.G., Igl, W., Bailey, J.N., Grassmann, F., Sengupta, S., Bragg-Gresham, J.L., Burdon, K.P., Hebbring, S.J., Wen, C., Gorski, M., et al. (2015). A large genome-wide association study of age-related macular degeneration highlights contributions of rare and common variants. Nat. Genet. *48*, 134–143.
32. Guan, Y., and Stephens, M. (2011). Bayesian variable selection regression for genome-wide association studies and other large-scale problems. Ann. Appl. Stat. *5*, 1780–1815.
33. Chipman, H., George, E.I., and McCulloch, R.E. (2001). The Practical Implementation of Bayesian Model Selection. In Model selection, P. Lahiri, ed. (Beachwood, OH: Institute of Mathematical Statistics), pp. 65–116.
34. Carbonetto, P., and Stephens, M. (2013). Integrated enrichment analysis of variants and pathways in genome-wide association studies indicates central role for IL-2 signaling genes in type 1 diabetes, and cytokine signaling genes in Crohn's disease. PLoS Genet. *9*, e1003770.
35. Zhou, X., Carbonetto, P., and Stephens, M. (2013). Polygenic modeling with bayesian sparse linear mixed models. PLoS Genet. *9*, e1003264.
36. Marchini, J., Howie, B., Myers, S., McVean, G., and Donnelly, P. (2007). A new multipoint method for genome-wide association studies by imputation of genotypes. Nat. Genet. *39*, 906–913.
37. Wen, X., and Stephens, M. (2014). Bayesian Methods for Genetic Association Analysis with Heterogeneous Subgroups: From Meta-Analyses to Gene-Environment Interactions. Ann. Appl. Stat. *8*, 176–203.
38. Zhou, X., and Stephens, M. (2012). Genome-wide efficient mixed-model analysis for association studies. Nat. Genet. *44*, 821–824.
39. Abecasis, G.R., Auton, A., Brooks, L.D., DePristo, M.A., Durbin, R.M., Handsaker, R.E., Kang, H.M., Marth, G.T., McVean, G.A.; and 1000 Genomes Project Consortium (2012). An integrated map of genetic variation from 1,092 human genomes. Nature *491*, 56–65.
40. McCarthy, S., Das, S., Kretzschmar, W., Delaneau, O., Wood, A.R., Teumer, A., Kang, H.M., Fuchsberger, C., Danecek, P.,

Sharp, K., et al.; Haplotype Reference Consortium (2016). A reference panel of 64,976 haplotypes for genotype imputation. Nat. Genet. *48*, 1279–1283.
41. Gusev, A., Lee, S.H., Trynka, G., Finucane, H., Vilhjálmsson, B.J., Xu, H., Zang, C., Ripke, S., Bulik-Sullivan, B., Stahl, E., et al.; Schizophrenia Working Group of the Psychiatric Genomics Consortium; SWE-SCZ Consortium; Schizophrenia Working Group of the Psychiatric Genomics Consortium; and SWE-SCZ Consortium (2014). Partitioning heritability of regulatory and cell-type-specific variants across 11 common diseases. Am. J. Hum. Genet. *95*, 535–552.
42. Ernst, J., and Kellis, M. (2010). Discovery and characterization of chromatin states for systematic annotation of the human genome. Nat. Biotechnol. *28*, 817–825.
43. Ernst, J., Kheradpour, P., Mikkelsen, T.S., Shoresh, N., Ward, L.D., Epstein, C.B., Zhang, X., Wang, L., Issner, R., Coyne, M., et al. (2011). Mapping and analysis of chromatin state dynamics in nine human cell types. Nature *473*, 43–49.
44. Kundaje, A., Meuleman, W., Ernst, J., Bilenky, M., Yen, A., Heravi-Moussavi, A., Kheradpour, P., Zhang, Z., Wang, J., Ziller, M.J., et al.; Roadmap Epigenomics Consortium (2015). Integrative analysis of 111 reference human epigenomes. Nature *518*, 317–330.
45. Masson, D., Jiang, X.C., Lagrost, L., and Tall, A.R. (2009). The role of plasma lipid transfer proteins in lipoprotein metabolism and atherogenesis. J. Lipid Res. *50* (*Suppl*), S201–S206.
46. Kettunen, J., Tukiainen, T., Sarin, A.P., Ortega-Alonso, A., Tikkanen, E., Lyytikäinen, L.P., Kangas, A.J., Soininen, P., Würtz, P., Silander, K., et al. (2012). Genome-wide association study identifies multiple loci influencing human serum metabolite levels. Nat. Genet. *44*, 269–276.
47. Nikpay, M., Goel, A., Won, H.H., Hall, L.M., Willenborg, C., Kanoni, S., Saleheen, D., Kyriakou, T., Nelson, C.P., Hopewell, J.C., et al. (2015). A comprehensive 1,000 Genomes-based genome-wide association meta-analysis of coronary artery disease. Nat. Genet. *47*, 1121–1130.
48. Fransen, E., Bonneux, S., Corneveaux, J.J., Schrauwen, I., Di Berardino, F., White, C.H., Ohmen, J.D., Van de Heyning, P., Ambrosetti, U., Huentelman, M.J., et al. (2015). Genome-wide association analysis demonstrates the highly polygenic character of age-related hearing impairment. Eur. J. Hum. Genet. *23*, 110–115.
49. Helgason, H., Sulem, P., Duvvari, M.R., Luo, H., Thorleifsson, G., Stefansson, H., Jonsdottir, I., Masson, G., Gudbjartsson, D.F., Walters, G.B., et al. (2013). A rare nonsynonymous sequence variant in C3 is associated with high risk of age-related macular degeneration. Nat. Genet. *45*, 1371–1374.
50. Seddon, J.M., Yu, Y., Miller, E.C., Reynolds, R., Tan, P.L., Gowrisankar, S., Goldstein, J.I., Triebwasser, M., Anderson, H.E., Zerbib, J., et al. (2013). Rare variants in CFI, C3 and C9 are associated with high risk of advanced age-related macular degeneration. Nat. Genet. *45*, 1366–1370.
51. Zhan, X., Larson, D.E., Wang, C., Koboldt, D.C., Sergeev, Y.V., Fulton, R.S., Fulton, L.L., Fronick, C.C., Branham, K.E., Bragg-Gresham, J., et al. (2013). Identification of a rare coding variant in complement 3 associated with age-related macular degeneration. Nat. Genet. *45*, 1375–1379.
52. Loh, P.R., Bhatia, G., Gusev, A., Finucane, H.K., Bulik-Sullivan, B.K., Pollack, S.J., de Candia, T.R., Lee, S.H., Wray, N.R., Kendler, K.S., et al.; Schizophrenia Working Group of Psychiatric Genomics Consortium (2015). Contrasting genetic architectures of schizophrenia and other complex diseases using fast variance-components analysis. Nat. Genet. *47*, 1385–1392.
53. Jordan, M.I., Ghahramani, Z., Jaakkola, T.S., and Saul, L.K. (1999). An introduction to variational methods for graphical models. Mach. Learn. *37*, 183–233.
54. Carbonetto, P., and Stephens, M. (2012). Scalable variational inference for Bayesian variable selection in regression, and its accuracy in genetic association studies. Bayesian Analysis *7*, 73–108.
55. Rue, H., Martino, S., and Chopin, N. (2009). Approximate Bayesian inference for latent Gaussian models by using integrated nested Laplace approximations. J. R. Stat. Soc. Series B Stat. Methodol. *71*, 319–392.
56. Singh, S.W.M., and McCallum, A. (2012). Monte Carlo MCMC: efficient inference by approximate sampling. https://ciir-publications.cs.umass.edu/getpdf.php?id=1053.
57. Gelman, A., and Rubin, D.B. (1992). Inference from iterative simulation using multiple sequences. Stat. Sci. *7*, 457–472.
58. Auton, A., Brooks, L.D., Durbin, R.M., Garrison, E.P., Kang, H.M., Korbel, J.O., Marchini, J.L., McCarthy, S., McVean, G.A., Abecasis, G.R.; and 1000 Genomes Project Consortium (2015). A global reference for human genetic variation. Nature *526*, 68–74.

The American Journal of Human Genetics, Volume *101*

Supplemental Data

A Scalable Bayesian Method for Integrating Functional Information in Genome-wide Association Studies

Jingjing Yang, Lars G. Fritsche, Xiang Zhou, Gonçalo Abecasis, and International Age-Related Macular Degeneration Genomics Consortium

Supplemental Data

Supplemental Note

Technical Details about bfGWAS

Supplemental Figures

Figure S1: Flowcharts of bfGWAS.

Figure S2: Plots of the potential scale reduction factors (PSRF).

Figure S3: Prioritization ranks of the true causal SNP1 (pink) and SNP2 (cyan).

Figure S4: Estimates of the log-relative-risk $\ln(\pi_0/\pi_1)$ by bfGWAS and the enrich-parameter by fGWAS, along with 95% confidence intervals.

Figure S5: Estimates of the log-ratio of effect-size variances $\ln(\sigma_0^2/\sigma_1^2)$ by bfGWAS, along with 95% confidence intervals.

Figure S6: Sorted top bfGWAS PPs versus sorted top -log10(P-values) of single variant tests.

Figure S7: Manhattan plot highlighting AMD GWAS signals with BVSR PP >0.1068.

Figure S8: Manhattan plots highlighting AMD GWAS signals by accounting for gene-based annotations.

Figure S9: ZoomLocus plots of region *CHR19:6218146-7218146*.

Figure S10: Enrichment analysis results with varying prior means as well as starting values $(10^{-6}, 5\times10^{-6}, 10^{-5})$ for π_q, and varying starting values $(10, 5, 1)$ for σ_q^2.

Figure S11: fGWAS enrichment estimates with 95% error bars.

Figure S12: Ratios of enrich parameters versus the respective genome-wide averages, along with 95% confidence intervals.

Figure S13: Enrichment analysis results for the AMD GWAS data with chromatin states profiled with respect to the epigenome of fetal thymus (E093).

Figure S14: Manhattan plot highlighting MGI GWAS signals of skin cancer with BVSR PP >0.1068.

Figure S15: Manhattan plots highlighting MGI GWAS signals of skin cancer by accounting for gene-based annotations.

Figure S16: Enrichment analysis results of the MGI GWAS of skin cancer, accounting for gene-based annotations.

Figure S17: LocusZoom plots of region of *CHR16:89686117-90172696*.

Supplemental Tables

Table S1: Classification of gene-based functional annotations.

Table S2: Compare results by P-value, fGWAS, and bfGWAS in the 34 known AMD loci, accounting for gene-based functional annotations.

Table S3: AMD risk variants identified by bfGWAS in the 34 known loci, accounting for gene-based annotations.

Table S4: AMD risk variants by fGWAS in the 34 known loci, accounting for gene-based annotations.

Table S5: Candidate AMD loci identified by bfGWAS, accounting for gene-based annotations.

Table S6: Candidate AMD loci identified by fGWAS, accounting for gene-based annotations.

Table S7: AMD risk variants by bfGWAS in the 34 known loci, accounting for summarized regulatory annotations.

Table S8: AMD risk variants by fGWAS in the 34 known loci, accounting for summarized regulatory annotations.

Table S9: Candidate AMD loci identified by bfGWAS, accounting for summarized regulatory annotations.

Table S10: Candidate AMD loci identified by fGWAS, accounting for summarized regulatory annotations.

Table S11: AMD risk variants by bfGWAS in the 34 known loci, accounting for chromatin states profiled with the epigenome of fetal thymus.

Table S12: AMD risk variants by fGWAS in the 34 known loci, accounting for chromatin states profiled with the epigenome of fetal thymus.

Table S13: Candidate AMD loci identified by bfGWAS, accounting for chromatin states profiled with the epigenome of fetal thymus.

Table S14: Candidate AMD loci identified by fGWAS, accounting for chromatin states profiled with the epigenome of fetal thymus.

Table S15: Haplotype analysis in locus C2/CFB/SKIV2L.

Table S16: Model comparison.

Supplemental References

Supplemental Note

Technical Details about bfGWAS

1 Bayesian Hierarchical Model

1.1 Standard Bayesian Variable Selection Regression Model

Consider the following standard Bayesian variable selection regression (BVSR) model

$$\boldsymbol{y}_{n\times 1} = \boldsymbol{X}_{n\times p}\boldsymbol{\beta}_{p\times 1} + \boldsymbol{\epsilon}_{n\times 1},\ \beta_i \sim \pi_i N(0, \tau^{-1}\sigma_i^2) + (1-\pi_i)\delta_0(\beta_i),\ \epsilon_i \sim N(0, \tau^{-1}), \quad (1)$$

where $\boldsymbol{y}_{n\times 1}$ denotes the centered phenotype vector of n samples; $\boldsymbol{X}_{n\times p}$ denotes the centered genotype matrix of p genetic variants; ϵ_i denotes the residual error independently and identically distributed (i.i.d.) with normal distribution $N(0, \tau^{-1})$; and β_i follows a spike-and-slab prior distribution [5, 6, 7] — that is, β_i follows the normal distribution $N(0, \tau^{-1}\sigma_i^2)$ with probability π_i and the point-mass density function $\delta_0(\cdot)$ at 0 with probability $(1-\pi_i)$ ($\delta_0(\beta_i) = 1$ if $\beta_i = 0$, otherwise $\delta_0(\beta_i) = 0$).

Here, the genotype matrix contains either dosage data within range $[0, 2]$ or genotype data with values $\{0, 1, 2\}$ denoting the number of minor alleles. The assumption of the spike-and-slab prior for β_i enforces variable selection in the regression model (1). We drop the intercept term here for assuming both $\boldsymbol{y}_{n\times 1}$ and columns of $\boldsymbol{X}_{n\times p}$ are centered. Although this model is developed for quantitative trait, we can treat dichotomous traits (e.g., cases and controls) as quantitative with values of 1 and 0 (e.g., 1 for cases and 0 for controls), which was proven to be equivalent as using the logistic or probit model by previous approaches [6, 7].

1.2 Integrating Functional Information

In this paper, we only consider non-overlapped categorical annotations. Let $\boldsymbol{A_i} = (A_{i1}, \cdots, A_{iQ})^T$ denotes the vector of Q annotations for the ith variant, where A_{iq} takes binary values $(1/0)$ to denote whether the ith variant is of the qth annotation. In order to integrate functional annotations into the standard BVSR model (1), we assume all variants

of annotation q have the same spike-and-slab prior with parameters (π_q, σ_q^2). We further assume the following independent and conjugate hyper priors (Figure S 1(A)):

$$\pi_q \text{ i.i.d.} \sim Beta(a_q, b_q),\ \sigma_q^2 \text{ i.i.d.} \sim IG(k_1, k_2),\ \tau \sim G(k_3, k_4), \tag{2}$$

where $Beta(a_q, b_q)$ denotes a Beta distribution with positive shape parameters a_q and b_q, $IG(k_1, k_2)$ denotes an Inverse-Gamma distribution with shape parameter k_1 and scale parameter k_2, and $G(k_3, k_4)$ denotes a Gamma distribution with shape parameter k_3 and scale parameter k_4 (Figure S1(A)). Note that parameters (a_q, b_q) could be different with respect to different annotations. This hierarchical BVSR model is equivalent to the standard BVSR model when modeling no functional information (i.e., assuming the same π_q and σ_q^2 for all variants).

In order to adjust for the unbalance distribution of functional annotations among all variants and encourage for a sparse model, we choose values for a_q and b_q such that the mean of the Beta distribution $\frac{a_q}{a_q+b_q} = 10^{-6}$ with $(a_q + b_q) = m_q = \sum_{i=1,j=q}^{p} A_{ij}$ (the total number of variants of annotation q). Here, the mean 10^{-6} of $Beta(a_q, b_q)$ helps enforce a sparse initial model that is desired for controlling false positives (assuming one signal per1M variants). We take $k_1 = k_2 = k_3 = k_4 = 0.1$ to induce non-informative priors on σ_q^2 and τ. Thus, the posterior estimates of π_q and σ_q^2 will mainly depend on the data likelihood. However, when there are few association signals in the qth category, the posterior estimates of π_q and σ_q^2) will be set as their respective prior modes. Note that although the hyper priors are assumed to be independent, the posterior distributions of π_q and σ_q^2 are no longer independent.

1.3 Latent Indicator Variable

To facilitate computation, we introduce a latent indicator vector $\boldsymbol{\gamma}_{p\times 1}$ [5] into the model, where each element $\gamma_i \in \{0, 1\}$ indicates whether the corresponding ith effect β_i equals to 0 with $\gamma_i = 0$ or follows the $N(0, \tau^{-1}\sigma_i^2)$ distribution with $\gamma_i = 1$. Equivalently,

$$\gamma_i \sim Bernoulli(\pi_i),\ \boldsymbol{\beta}_{-\boldsymbol{\gamma}} \sim \delta_0(\cdot),\ \boldsymbol{\beta}_{\boldsymbol{\gamma}} \sim MVN_{|\boldsymbol{\gamma}|}(0, \tau^{-1}\boldsymbol{V}_{\boldsymbol{\gamma}}),$$

where $|\boldsymbol{\gamma}|$ denotes the number of non-zero entries in $\boldsymbol{\gamma}$; $\boldsymbol{\beta}_{-\boldsymbol{\gamma}}$ denotes the sub-vector of $\boldsymbol{\beta}_{p\times 1}$ corresponding to variants with $\gamma_i = 0$; $\boldsymbol{\beta}_{\boldsymbol{\gamma}}$ denotes the sub-vector of $\boldsymbol{\beta}_{p\times 1}$ corresponding to the variants with $\{\gamma_j = 1; j = 1, \cdots, |\boldsymbol{\gamma}|\}$; and $\boldsymbol{V}_{|\boldsymbol{\gamma}|}$ is the corresponding sub-matrix (with $\gamma_j = 1$) of $\boldsymbol{V}_{p\times p} = diag(\sigma_1^2, \cdots, \sigma_p^2)$.

1.4 Bayesian Inference

With the above Bayesian hierarchical model, the posterior joint distribution of $(\boldsymbol{\beta}, \boldsymbol{\gamma}, \boldsymbol{\sigma^2}, \boldsymbol{\pi}, \tau)$ is proportional to the product of likelihood and prior density functions,

$$P(\boldsymbol{\beta}, \boldsymbol{\gamma}, \boldsymbol{\sigma^2}, \boldsymbol{\pi}, \tau | \boldsymbol{y}, \boldsymbol{X}, \boldsymbol{A}) \propto P(\boldsymbol{y}|\boldsymbol{X}, \boldsymbol{\beta}, \boldsymbol{\gamma}, \tau) P(\boldsymbol{\beta}|\boldsymbol{A}, \boldsymbol{\pi}, \boldsymbol{\sigma^2}, \tau) P(\boldsymbol{\gamma}|\boldsymbol{\pi}) P(\boldsymbol{\pi}) P(\boldsymbol{\sigma^2}) P(\tau), \quad (3)$$

where $\boldsymbol{\pi} = (\pi_1, \ldots, \pi_Q)$, $\boldsymbol{\sigma^2} = (\sigma_1^2, \ldots, \sigma_Q^2)$, and $\boldsymbol{A}$ is the $p \times Q$ annotation matrix with binary values.

Now our goal is to make inference on the category-specific parameters $(\boldsymbol{\pi}, \boldsymbol{\sigma^2})$ and the variable-specific parameters $(\boldsymbol{\beta}, E[\boldsymbol{\gamma}])$ from their respective marginal posterior distributions, conditioning on the data $(\boldsymbol{y}, \boldsymbol{X}, \boldsymbol{A})$. The category-specific parameters $(\boldsymbol{\pi}, \boldsymbol{\sigma^2})$ denote the shared characteristics of variants with the same annotation, which are also referred as enrichment parameters in this paper. Specifically, π_q denotes the causality for variants of annotation q, and σ_q^2 denotes the effect-size variance for associated variants (with nonzero β_j) of annotation q.

To make the Bayesian inference of our model applicable for genome-wide analysis, we pair it with a novel Expectation-Maximization Markov chain Monte Carlo (EM-MCMC) algorithm. Because of the block-wise linkage disequilibrium (LD) structure of human genome, we can segment the genotype data $\boldsymbol{X}$ into K approximately independent blocks, i.e., $\boldsymbol{X} = \{\boldsymbol{X}_1, \boldsymbol{X}_2, \cdots, \boldsymbol{X}_K\}$, where each submatrix $\boldsymbol{X}_k$ has dimension $n \times p_k$ (genotypes of p_k variants for n samples). Thus, we can write the likelihood function in (3) as a product of a series likelihood functions for $\boldsymbol{X_k}$,

$$P(\boldsymbol{y}|\boldsymbol{X}, \boldsymbol{\beta}, \boldsymbol{\gamma}, \tau) = \prod_{k=1}^{K} P_k(\boldsymbol{y}|\boldsymbol{X}_k, \boldsymbol{\beta}_k, \boldsymbol{\gamma}_k, \tau), \quad (4)$$

where $(\boldsymbol{y}|\boldsymbol{X}_k, \boldsymbol{\beta}_k, \boldsymbol{\gamma}_k, \tau) \sim MVN_{|\boldsymbol{\gamma_k}|}(\boldsymbol{X}_k\boldsymbol{\beta}_k, \tau^{-1}\boldsymbol{I}_{|\boldsymbol{\gamma_k}|})$.

To avoid adjusting for the residual variance with respect to each genome-block, we fix τ^{-1} as the phenotype variance. This assumption is reasonable because most genome-blocks explain little phenotype variance in practice. Although fixing τ^{-1} as the phenotype variance seems conservative for genome-blocks with true signals, our analysis showed that it barely affect identifying true signals.

In the Expectation step (E-step), $(\boldsymbol{\beta_k}, E[\boldsymbol{\gamma_k}])$ are estimated by implementing MCMC per block, conditioning on the given values of $(\boldsymbol{\pi}, \boldsymbol{\sigma})$; in the Maximization step (M-step), $(\boldsymbol{\pi}, \boldsymbol{\sigma})$ are updated, conditioning on genome-wide estimates of $(\boldsymbol{\beta}, E[\boldsymbol{\gamma}])$ from the E-step. In general, $\sim$5 EM iterations will lead to convergent estimates of $(\boldsymbol{\pi}, \boldsymbol{\sigma})$, and the estimates of $(\boldsymbol{\beta_k}, E[\boldsymbol{\gamma_k}])$ from the last E-step will be used to identify association signals (details are provided in Section 2; Figure S 1(B)).

1.4.1 Conditional Posterior Distribution for $\boldsymbol{\beta_k}$

Conditioning on the values of $(\boldsymbol{\pi}, \boldsymbol{\sigma^2}, \tau)$, the posterior distribution for the variant-specific parameters $(\boldsymbol{\beta}_k, \boldsymbol{\gamma}_k)$ of block k is

$$P(\boldsymbol{\beta}_k, \boldsymbol{\gamma}_k | \boldsymbol{X}_k, \boldsymbol{y}, \boldsymbol{\pi}, \boldsymbol{\sigma^2}, \tau) \propto P(\boldsymbol{y} | \boldsymbol{X}_k, \boldsymbol{\beta}_k, \boldsymbol{\gamma}_k, \tau) P(\boldsymbol{\beta}_k | \boldsymbol{\gamma}_k, \boldsymbol{\sigma^2}, \tau) P(\boldsymbol{\gamma}_k | \boldsymbol{\pi}). \tag{5}$$

Conditioning on the indicator vector $\boldsymbol{\gamma_k}$, the effect-sizes associated with zero indicator variables are 0, while the posterior distribution for $\boldsymbol{\beta}_{|\boldsymbol{\gamma_k}|}$ is given by

$$\begin{aligned}
&P(\boldsymbol{\beta}_{|\boldsymbol{\gamma_k}|} | \boldsymbol{X}_{|\boldsymbol{\gamma_k}|}, \boldsymbol{y}, \boldsymbol{\gamma}_k, \boldsymbol{\sigma^2}, \tau) \propto P_k(\boldsymbol{y} | \boldsymbol{X}_{|\boldsymbol{\gamma_k}|}, \boldsymbol{\beta}_{|\boldsymbol{\gamma_k}|}, \boldsymbol{\gamma}_k, \tau) P(\boldsymbol{\beta}_{|\boldsymbol{\gamma_k}|} | \boldsymbol{\gamma}_k, \boldsymbol{\sigma^2}, \tau) \\
&\propto \exp\left\{-\tfrac{\tau}{2}(\boldsymbol{y} - \boldsymbol{X}_{|\boldsymbol{\gamma_k}|}\boldsymbol{\beta}_{|\boldsymbol{\gamma_k}|})^T(\boldsymbol{y} - \boldsymbol{X}_{|\boldsymbol{\gamma_k}|}\boldsymbol{\beta}_{|\boldsymbol{\gamma_k}|})\right\} \exp\left\{-\tfrac{\tau}{2}\boldsymbol{\beta}_{|\boldsymbol{\gamma_k}|}^T \boldsymbol{V}_{|\boldsymbol{\gamma_k}|}^{-1} \boldsymbol{\beta}_{|\boldsymbol{\gamma_k}|}\right\} \\
&\propto \exp\left\{-\tfrac{\tau}{2}\left(\boldsymbol{\beta}_{|\boldsymbol{\gamma_k}|}^T \boldsymbol{X}_{|\boldsymbol{\gamma_k}|}^T \boldsymbol{X}_{|\boldsymbol{\gamma_k}|} \boldsymbol{\beta}_{|\boldsymbol{\gamma_k}|} - 2\boldsymbol{\beta}_{|\boldsymbol{\gamma_k}|}^T \boldsymbol{X}_{|\boldsymbol{\gamma_k}|} \boldsymbol{y} + \boldsymbol{\beta}_{|\boldsymbol{\gamma_k}|}^T \boldsymbol{V}_{|\boldsymbol{\gamma_k}|}^{-1} \boldsymbol{\beta}_{|\boldsymbol{\gamma_k}|}\right)\right\} \\
&\propto \exp\left\{-\tfrac{\tau}{2}\left(\boldsymbol{\beta}_{|\boldsymbol{\gamma_k}|}^T (\boldsymbol{X}_{|\boldsymbol{\gamma_k}|}^T \boldsymbol{X}_{|\boldsymbol{\gamma_k}|} + \boldsymbol{V}_{|\boldsymbol{\gamma_k}|}^{-1}) \boldsymbol{\beta}_{|\boldsymbol{\gamma_k}|} - 2\boldsymbol{\beta}_{|\boldsymbol{\gamma_k}|}^T \boldsymbol{X}_{|\boldsymbol{\gamma_k}|}^T \boldsymbol{y}\right)\right\}.
\end{aligned} \tag{6}$$

From (6), it is easy to see that

$$\begin{aligned}
&(\boldsymbol{\beta}_{|\boldsymbol{\gamma_k}|} | \boldsymbol{X}_{|\boldsymbol{\gamma_k}|}, \boldsymbol{y}, \boldsymbol{\gamma}_k, \boldsymbol{\sigma^2}, \tau) \sim \\
&MVN_{|\boldsymbol{\gamma_k}|}\left((\boldsymbol{X}_{|\boldsymbol{\gamma_k}|}^T \boldsymbol{X}_{|\boldsymbol{\gamma_k}|} + \boldsymbol{V}_{|\boldsymbol{\gamma_k}|}^{-1})^{-1} \boldsymbol{X}_{|\boldsymbol{\gamma_k}|}^T \boldsymbol{y},\ \tau^{-1}(\boldsymbol{X}_{|\boldsymbol{\gamma_k}|}^T \boldsymbol{X}_{|\boldsymbol{\gamma_k}|} + \boldsymbol{V}_{|\boldsymbol{\gamma_k}|}^{-1})^{-1}\right).
\end{aligned} \tag{7}$$

Here, the subscript $|\gamma_k|$ indicates sub-matrices or sub-vectors corresponding to variants with nonzero indicator variables, and $\boldsymbol{V}_{|\boldsymbol{\gamma_k}|}$ is a diagonal matrix with $(\boldsymbol{V}_{|\boldsymbol{\gamma_k}|})_{jj} = \sigma_q^2$ if the jth variant is of annotation q.

1.4.2 Conditional Posterior Distribution for $\boldsymbol{\gamma_k}$

Because of the conditional conjugate prior for $\boldsymbol{\beta_k}$, we can easily integrate $\boldsymbol{\beta}_k$ out from the joint conditional posterior distribution (5) to obtain the marginal conditional posterior distribution for $\boldsymbol{\gamma}_k$,

$$\begin{aligned}
P(\boldsymbol{\gamma}_k | \boldsymbol{X}_k, \boldsymbol{y}, \boldsymbol{\pi}, \boldsymbol{\sigma^2}, \tau) &\propto \int_{\boldsymbol{\beta}_k} P_k(\boldsymbol{y} | \boldsymbol{X}_k, \boldsymbol{\beta}_k, \boldsymbol{\gamma}_k, \tau) P(\boldsymbol{\beta}_k | \boldsymbol{\gamma}_k, \boldsymbol{\sigma^2}, \tau) P(\boldsymbol{\gamma}_k | \boldsymbol{\pi}) d\boldsymbol{\beta}_k \\
&\propto |\boldsymbol{\Omega}_{|\boldsymbol{\gamma_k}|}|^{-1/2} \exp\left\{\frac{\tau}{2} \boldsymbol{y}^T \boldsymbol{X}_{|\boldsymbol{\gamma_k}|} \boldsymbol{V}_{|\boldsymbol{\gamma_k}|} \boldsymbol{\Omega}_{|\boldsymbol{\gamma_k}|}^{-1} \boldsymbol{X}_{|\boldsymbol{\gamma_k}|}^T \boldsymbol{y}\right\} P(\boldsymbol{\gamma}_k | \boldsymbol{\pi}),
\end{aligned} \tag{8}$$

where $\boldsymbol{\Omega}_{|\boldsymbol{\gamma_k}|} = \boldsymbol{V}_{|\boldsymbol{\gamma_k}|} \boldsymbol{X}_{|\boldsymbol{\gamma_k}|}^T \boldsymbol{X}_{|\boldsymbol{\gamma_k}|} + \boldsymbol{I}_{|\boldsymbol{\gamma_k}|}$.

2 EM-MCMC Algorithm

The steps of the EM-MCMC algorithm are as follows:

(i) Fix τ at the value of phenotype variance;

(ii) Set initial values for the category-specific parameters $(\boldsymbol{\pi}, \boldsymbol{\sigma^2})$;

(iii) E-step: Conditioning on the most recent values of $(\boldsymbol{\pi}, \boldsymbol{\sigma^2})$, estimate variant-specific parameters $(\boldsymbol{\beta}, E[\boldsymbol{\gamma}])$ by implementing MCMC per block;

(iv) M-step: Conditioning on the genome-wide estimates of $(\boldsymbol{\beta}, E[\boldsymbol{\gamma}])$ from the previous E-step, update $(\boldsymbol{\pi}, \boldsymbol{\sigma^2})$ by their MAPs (maximum a posteriori estimates), maximizing the expected log-posterior-likelihood functions [2];

(v) Repeat the EM-steps (iii) and (iv) for a few times until the MAPs of $(\boldsymbol{\pi}, \boldsymbol{\sigma^2})$ converge.

2.1 Setup Initial Values

In this paper, we fix τ at the value of phenotype variance, equivalent to assuming no phenotype variance explained by the genetic variants. This assumption is true for most blocks and slightly conservative for blocks with true signals. However, our analysis showed that this assumption barely affects identifying true signals. We take initial values $\pi_q = 1 \times 10^{-6}$ to initial a sparse and conservative model, and $\sigma_q^2 = 10$ to start with a large effect-size variance for all associated variants.

2.2 MCMC Sampling Scheme

The MCMC sampling is implemented per block for estimating $(\boldsymbol{\beta_k}, E[\boldsymbol{\gamma_k}])$, conditioning on category-specific parameters $(\boldsymbol{\pi}, \boldsymbol{\sigma^2})$:

(i) First, sort all variants in the block by their base positions, perform single variant tests, and rank variants based on their marginal association evidence (e.g., P-values) from strong to weak.

(ii) Second, select an initial model with independent significant signals. We first include the variant with the smallest P-value into the model (i.e., set the corresponding indicator value as 1). Then, conditioning on the currently selected variant(s), select the next most significant variant with P-value $< 5 \times 10^{-8}$. Stop selection when no other independent genome-wide signal exists. Generally, most of the blocks with $\sim$10K variants will start with only one variant.

(iii) Third, repeat the MCMC sampling for a large number of iterations (e.g., 50K iterations with 50K burnins), in which the Metropolis-Hastings algorithm is used

to draw posterior samples for $\boldsymbol{\gamma_k}$ based on (8). With indicator vector $\boldsymbol{\gamma'_k}$ and corresponding effect-size vector $\boldsymbol{\beta}_{|\boldsymbol{\gamma'_k}|}$ from previous iteration, each MCMC iteration is as follows:

(a) Randomly propose a new indicator vector $\boldsymbol{\gamma''_k}$ by:

- Including an extra variant into the model with probability $1/3$: generate a rank r from a proposal distribution P_{γ_k} such that the variant with rank r is not included in the current model (change the corresponding indicator variable from 0 to 1). Here, P_{γ_k} is constructed as the mixture distribution $0.9{*}U_{top}{+}0.1U_{rest}$, where U_{top} denotes the uniform distribution on top ranks $(1, \ldots, t_k)$ and U_{rest} denotes the uniform distribution on the remain ranks $(t_{k+1}, \cdots, p_k)$ (t_k is an arbitrary number). That is, we assume a variant whose P-value is ranked in the top association group will be proposed with probability $0.9/(t_k)$, while a variant in the remaining group will be proposed with probability $0.1/(p_k - t_k)$. A rank will keep being proposed from P_{γ_k} until the corresponding variant is absent in the current model. We take $t_k = min(p_k, 300)$ in our software.
- Deleting a variant from the current model with probability $1/3$: randomly delete a variant from the current model (change the corresponding indicator variable from 1 to 0), i.e., each variant in the current model has probability $1/|\boldsymbol{\gamma'_k}|$ to be deleted.
- Switching a variant in the current model with an un-included variant in the neighborhood of the switch candidate (switch the corresponding indicator variable values): randomly select a variant in the current model as a switch candidate; propose a variant within its neighborhood from the proposal distribution P_{neib}. In order to improve the MCMC mixing property, we calibrate P_{neib} based on the conditional association evidence of all un-included variants in the neighborhood, conditioning on all variants in the current model except the switch candidate. For example, if there are 20 un-included variants in the neighborhood with conditional likelihood ratio test (LRT) statistic values $\{s_1, \cdots, s_{20}\}$, we first subtract the largest statistic value s_{max} from all values, then take $P_{neib}(s_j) = \exp(s_j - s_{max}) / \sum_{b=1}^{20} \exp(s_b - s_{max})$ as the probability for the corresponding jth variant to be proposed. The neighborhood size can be tuned by users (we set the neighborhood window as 100 variants near the switch candidate in our analyses).

(b) Conditioning on the indicator vector $\boldsymbol{\gamma}_{\boldsymbol{k}}''$, the effect-size vector $\boldsymbol{\beta}_{|\boldsymbol{\gamma}_{\boldsymbol{k}}''|}$ is estimated by its conditional posterior mean in (7).

(c) Calculate the Metropolis-Hastings acceptance ratio, and then decide whether to accept or reject $\boldsymbol{\gamma}_{\boldsymbol{k}}''$ by the Metropolis-Hastings algorithm.

(iv) Finally, $E[\gamma_{kj}]$ is estimated by u_{kj}/M, where u_{kj} is the number of times when the jth variant in block k is included into the model and M is the total MCMC iterations. Note that $E[\gamma_{kj}]$ is also referred as the Bayesian posterior inclusion probability (PP), evidence for the ith variant in block k to be an association signal. The Bayesian estimate of the corresponding β_{kj} is given by the posterior mean $\sum_{l=1}^{u_{kj}} \beta_{kjl}/u_{kj}$, where β_{kjl} is the effect-size estimate for the jth variant (in block k) when it is included into the model for the lth time.

Within the MCMC sampling, we also record the number of iterations M_{active} when the linear regression model includes at least one variant by the Metropolis-Hastings algorithm. Then the proportion of such MCMC iterations M_{active}/M gives us the regional posterior inclusion probability (regional-PP) of the study block, which is the probability of existing at least one signal in the block. Because variants in high LD and the same annotation category have the same chance to be included into the linear model (splitting the posterior probability for a single signal), the regional-PP is more appropriate than the single variant Bayesian PP for claiming a risk locus.

2.3 EM Algorithm

In the EM algorithm, values of $(\boldsymbol{\pi}, \boldsymbol{\sigma^2})$ are updated by their respective maximum a posteriori estimates (MAPs), maximizing expected log-posterior-likelihood functions. With the Bayesian estimates of $(\boldsymbol{\beta}, E[\boldsymbol{\gamma}])$ from the E-step, the expected log-posterior-likelihood functions and MAPs can be derived with closed-form expressions.

2.3.1 MAP for $\boldsymbol{\sigma^2}$

From the joint posterior distribution (3), the conditional posterior density function (posterior likelihood) of $\boldsymbol{\sigma^2}$ becomes

$$P(\boldsymbol{\sigma^2}|\boldsymbol{\beta}, \boldsymbol{\gamma}, \tau) \propto P(\boldsymbol{\beta}|\boldsymbol{\gamma}, \boldsymbol{\sigma^2}, \tau) P(\boldsymbol{\sigma^2}), \tag{9}$$

where $P(\boldsymbol{\sigma^2}) = \prod_{q=1}^{Q} P(\sigma_q^2)$ with $\sigma_q^2 \sim IG(k_1, k_2)$, i.e. $P(\sigma_q^2) \propto \left(\sigma_q^2\right)^{-(k_1+1)} \exp\left(-\frac{k_2}{\sigma_q^2}\right)$; $P(\boldsymbol{\beta}|\boldsymbol{\gamma}, \boldsymbol{\sigma^2}, \tau) = \prod_{i=1}^{p} P(\beta_i|\sigma_i^2, \gamma_i, \tau)$ with $P(\beta_i|\sigma_i^2, \gamma_i, \tau) =$

$(\gamma_i N(\beta_i; 0, \tau^{-1}\sigma_i^2) + (1-\gamma_i)\delta_0(\beta_i))$; and $\sigma_i^2 = \sigma_q^2$ if the ith variant is of annotation q.

The expected log-posterior-likelihood of $\boldsymbol{\sigma^2}$ is given by

$$\begin{aligned}
& l(\boldsymbol{\sigma^2}) = E_{\boldsymbol{\gamma}}\left[ln(P(\boldsymbol{\sigma^2}|\boldsymbol{\beta},\boldsymbol{\gamma},\tau))\right] \\
= \;& E_{\boldsymbol{\gamma}}\left[\sum_{i=1}^{p} ln\left(P(\beta_i|\sigma_i^2,\gamma_i,\tau)\right)\right] + \sum_{q=1}^{Q} ln\left(P(\sigma_q^2)\right) + C \\
= \;& \sum_{i=1}^{p} E_{\boldsymbol{\gamma}}\left[ln\left(P(\beta_i|\sigma_i^2,\gamma_i,\tau)\right)\right] + \sum_{q=1}^{Q} ln\left(P(\sigma_q^2)\right) + C \\
\approx \;& \sum_{i=1}^{p}\left[\widehat{\gamma_i} ln\left(P(\beta_i|\gamma_i=1,\sigma_i^2)\right) + (1-\widehat{\gamma_i}) ln\left(P(\beta_i|\gamma_i=0)\right)\right] + \\
& \sum_{q=1}^{Q}\left[(k_1+1)ln\left(\frac{1}{\sigma_q^2}\right) - k_2\frac{1}{\sigma_q^2}\right] + C \\
= \;& \sum_{i=1}^{p}\left[\widehat{\gamma_i}\left(\frac{1}{2}ln\left(\frac{\tau}{\sigma_i^2}\right) - \frac{\tau\widehat{\beta_i}^2}{2\sigma_i^2}\right)\right] + \sum_{q=1}^{Q}\left[(k_1+1)ln\left(\frac{1}{\sigma_q^2}\right) - k_2\frac{1}{\sigma_q^2}\right] + C, \qquad (10)
\end{aligned}$$

where $\{\widehat{\gamma_i} = E[\gamma_i]\}, \{\widehat{\beta_i}\}$ are Bayesian estimates by MCMC in the E-step, and C is a constant free of $\boldsymbol{\sigma^2}$.

From (10), we can see that the posterior distributions of $\{\sigma_q^2;\, q = 1, \ldots, Q\}$ are disjoint, because of independent priors and non-overlapped annotations. Thus, the expected log-posterior-likelihood function for each σ_q^2 is

$$l_{\sigma_q^2} = \sum_{j_q=1}^{m_q}\left[\widehat{\gamma_{j_q}}\left(\frac{1}{2}ln\left(\frac{\tau}{\sigma_q^2}\right) - \frac{\tau\widehat{\beta_{j_q}}^2}{2\sigma_q^2}\right)\right] + (k_1+1)ln\left(\frac{1}{\sigma_q^2}\right) - \frac{k_2}{\sigma_q^2} + C, \qquad (11)$$

where $\{\widehat{\gamma_{j_q}}, \widehat{\beta_{j_q}};\, j_q = 1, \ldots, n_q\}$ are the Bayesian estimates for variants of annotation q, and m_q is the total number of variants with annotation q. The MAP of σ_q^2 can be solved from

$$\frac{dl_{\sigma_q^2}}{d(1/\sigma_q^2)} = \sum_{j_q=1}^{m_q}\left[\widehat{\gamma_{j_q}}\frac{\sigma_q^2}{2} - \widehat{\gamma_{j_q}}\frac{\tau\beta_{j_q}^2}{2}\right] + (k_1+1)\sigma_q^2 - k_2 = 0,$$

which is

$$\widehat{\sigma_q^2} = \frac{\tau\sum_{j_q=1}^{m_q}(\widehat{\gamma_{j_q}}\widehat{\beta_{j_q}^2}) + 2k_2}{\sum_{j_q=1}^{m_q}\widehat{\gamma_{j_q}} + 2(k_1+1)}.$$

2.3.2 MAP for $\boldsymbol{\pi}$

From the joint posterior distribution (3), the conditional posterior density function (posterior likelihood) of $\boldsymbol{\pi}$ becomes

$$P(\boldsymbol{\pi}|\boldsymbol{\gamma}) \propto P(\boldsymbol{\gamma}|\boldsymbol{\pi})P(\boldsymbol{\pi}), \tag{12}$$

where $P(\boldsymbol{\gamma}|\boldsymbol{\pi}) = \prod_{i=1}^{p} P(\gamma_i|\pi_i) \propto \prod_{i=1}^{p} \pi_i^{\gamma_i}(1-\pi_i)^{1-\gamma_i}$; $\pi_i = \pi_q$ if the ith variant is of annotation q; and $P(\boldsymbol{\pi}) = \prod_{q=1}^{Q} P(\pi_q)$ with π_q i.i.d. $\sim Beta(a_q, b_q)$.

The expected log-posterior-likelihood of $\boldsymbol{\pi}$ can be derived as

$$\begin{aligned}
& l(\boldsymbol{\pi}) = E_{\boldsymbol{\gamma}}\left[ln(P(\boldsymbol{\pi}|\boldsymbol{\gamma}))\right] \\
= \;& E_{\boldsymbol{\gamma}}\left[\sum_{i=1}^{p} ln(P(\gamma_i|\pi_i))\right] + ln\left(P(\boldsymbol{\pi})\right) + C \\
= \;& \sum_{i=1}^{p} E_{\boldsymbol{\gamma}}\left[ln(P(\gamma_i|\pi_i))\right] + ln\left(P(\boldsymbol{\pi})\right) + C \\
= \;& \sum_{i=1}^{p} \left(Prob(\gamma_i = 1)ln(\pi_i) + Prob(\gamma_i = 0)ln(1-\pi_i)\right) + \\
& \sum_{q=1}^{Q} \left((a_q - 1)ln(\pi_q) + (b_q - 1)ln(1-\pi_q)\right) + C \\
\approx \;& \sum_{i=1}^{p} \left(\widehat{\gamma_i} ln(\pi_i)) + (1-\widehat{\gamma_i})ln(1-\pi_i)\right) + \sum_{q=1}^{Q} \left((a_q - 1)ln(\pi_q) + (b_q - 1)ln(1-\pi_q)\right) + C,
\end{aligned} \tag{13}$$

where $\{\widehat{\gamma_i} = E[\gamma_i]\}$ are estimated by MCMC, and C is a constant free of $\boldsymbol{\pi}$.

Similarly, because the posterior distributions of $\{\pi_q;\, q = 1, \ldots, Q\}$ are also disjoint, the expected log-posterior-likelihood function for π_q is given by

$$l_{\pi_q} = \sum_{j_q=1}^{m_q} \left[\widehat{\gamma_{j_q}} ln(\pi_q) + (1 - \widehat{\gamma_{j_q}})ln(1-\pi_q)\right] + (a_q - 1)ln(\pi_q) + (b_q - 1)ln(1-\pi_q) + C, \tag{14}$$

and the MAP for π_q is solved as

$$\widehat{\pi_q} = \frac{\sum_{j_q=1}^{m_q} \widehat{\gamma_{j_q}} + a_q - 1}{m_q + a_q + b_q - 2}.$$

3 Construct Confidence Intervals by Fisher Information

Fisher information of $(\boldsymbol{\pi}, \boldsymbol{\sigma^2})$ can be derived from the second derivatives of the respective expected log-posterior-likelihood functions as in (11) and (13). By the asymptotic-normality of MAP, as $n \to \infty$, the distribution of a MAP estimate $\widehat{\boldsymbol{\theta}}$ converges to a multivariate normal (MVN) distribution with mean equal to the true parameter value $\boldsymbol{\theta_0}$ and covariance matrix equal to the inverse of the Fisher information.

Therefore, the MAPs $\widehat{\boldsymbol{\sigma^2}}$ and $\widehat{\boldsymbol{\pi}}$ are converging to the following MVN distributions as $n \to \infty$,

$$\widehat{\boldsymbol{\sigma^2}} \longrightarrow MVN(\boldsymbol{\sigma^2_*}, \boldsymbol{I_{\sigma^2}}(\widehat{\boldsymbol{\sigma^2}})^{-1}),\ \widehat{\boldsymbol{\pi}} \longrightarrow MVN(\boldsymbol{\pi_*}, \boldsymbol{I_{\pi}}(\widehat{\boldsymbol{\pi}})^{-1}), \tag{15}$$

where $\boldsymbol{\sigma^2_*}$ and $\boldsymbol{\pi}_*$ are the true parameter values; $\boldsymbol{I_{\sigma^2}}(\widehat{\boldsymbol{\sigma^2}}) \approx -\frac{\partial^2 l(\boldsymbol{\sigma^2})}{\partial \boldsymbol{\sigma^2} (\partial \boldsymbol{\sigma^2})^T}|_{\widehat{\boldsymbol{\sigma^2}}}$; and $\boldsymbol{I_{\pi}}(\widehat{\boldsymbol{\pi}}) \approx -\frac{\partial^2 l(\boldsymbol{\pi})}{\partial \boldsymbol{\pi} \partial \boldsymbol{\pi}^T}|_{\widehat{\boldsymbol{\pi}}}$. Because of the mutual independence among $\{\sigma_q^2, \pi_q;\ q = 1, \ldots, Q\}$ (conditioning on the estimates of $\boldsymbol{\beta}$ and $E[\boldsymbol{\gamma}]$), the analytical forms for the second derivatives of $l_{\sigma_q^2}, l_{\pi_q}$ are

$$\frac{dl_{\sigma_q^2}}{d^2\sigma_q^2} = \sum_{j_q=1}^{m_q} \left(\frac{\widehat{\gamma_{j_q}}}{2(\sigma^2)^2} - \frac{\widehat{\gamma_{j_q}} \tau \widehat{\beta_{j_q}}^2}{(\sigma^2)^3} \right) + \frac{k_1 + 1}{(\sigma^2)^2} - \frac{2k_2}{(\sigma^2)^3},$$

$$\frac{dl_{\pi_q}}{d^2\pi_q} = -\frac{\sum_{j_q=1}^{m_q} \widehat{\gamma_{j_q}} + a_q - 1}{\pi_q^2} - \frac{n_q - \sum_{j_q=1}^{m_q} \widehat{\gamma_{j_q}} + b_q - 1}{(1 - \pi_q)^2}.$$

Then the Fisher informations of σ_q^2, π_q are given by

$$I(\sigma_q^2) = \frac{1}{(\sigma_q^2)^2} \left(\sum_{j_q=1}^{m_q} \widehat{\gamma_{j_q}} (\tau - 0.5) - (k_1 + 1) + \frac{2k_2}{\sigma_q^2} \right),$$

$$I(\pi_q) = \frac{\sum_{j_q=1}^{m_q} \widehat{\gamma_{j_q}} + a_q - 1}{\pi_q^2} + \frac{n_q - \sum_{j_q=1}^{m_q} \widehat{\gamma_{j_q}} + b_q - 1}{(1 - \pi_q)^2}.$$

The $(1 - \alpha)\%$ confidence intervals of σ_q^2, π_q can be constructed by

$$\widehat{\sigma_q^2} \pm Z_{\alpha/2} \sqrt{I(\widehat{\sigma_q^2})^{-1}},\ \widehat{\pi_q} \pm Z_{\alpha/2} \sqrt{I(\widehat{\pi_q})^{-1}}, \tag{16}$$

where $Z_{\alpha/2}$ is the upper $\alpha/2$ quantile of the standard normal distribution $N(0, 1)$.

4 Compare Enrichment among Multiple Groups

With the MAPs of (π_q, σ_q^2) and corresponding standard errors, we can easily compare the enrichment among multiple groups. Take the case with two annotation groups for an example, the 95% confidence intervals of the quantities $ln(\pi_1/\pi_2)$, $ln(\sigma_1^2/\sigma_2^2)$ can be easily approximated by Fieller's theorem [3] (if variables $a \sim N(a_0, \sigma_a^2)$, $b \sim N(b_0, \sigma_b^2)$, then $ln\left(a/b\right) \sim N\left(ln\left(a_0/b_0\right), \sigma_a^2/a_0^2 + \sigma_b^2/b_0^2\right)$), and then can be used to test whether or not the enrichment is significantly different between two groups (i.e. whether or not the 95% confidence intervals of $ln(\pi_1/\pi_2)$, $ln(\sigma_1^2/\sigma_2^2)$ overlap 0). Moreover, with the approximated variance of the log-ratio by Fieller's theorem, we can calculate a P-value for the null hypothesis that the log-ratio equals 0. For example, the P-value for testing the null hypothesis $ln(\pi_1/\pi_2) = 0$ vs. the alternative hypothesis $ln(\pi_1/\pi_2) \neq 0$ can be calculated by

$$2\left(1 - \Psi\left(\frac{|ln(\widehat{\pi_1}/\widehat{\pi_2})|}{sd(ln(\pi_1/\pi_2))}\right)\right),$$

where Ψ is the probability distribution function of $N(0,1)$, $(\widehat{\pi_1}, \widehat{\pi_2})$ are MAPs, and $sd(ln(\pi_1/\pi_2))$ is the standard deviation of $ln(\pi_1/\pi_2)$.

For the case with multiple annotation groups, we can calculate similar quantities to compare the estimates by each group vs. the genome-wide average. That is, for causal probability, $ln(\pi_q/\pi_{avg})$ is used to test whether or not the causal probability of group q is significantly different from the overall average, where $\pi_{avg} = \sum_{q=1}^{Q} w_q\pi_q$, $w_q = \frac{m_q}{\sum_{q=1}^{Q} m_q}$ (m_q is the number of variants of annotation q). For the effect-size variance, a similar quantity $ln(\sigma_q^2/\sigma_{avg}^2)$ is used, where $\sigma_{avg}^2 = \sum_{q=1}^{Q} f_q\sigma_q^2$ is the weighted average of effect-size variances with weights given by $f_q = \frac{m_q\pi_q}{\sum_{q=1}^{Q} m_q\pi_q}$ ($m_q\pi_q$ is the expected number of associations in annotation category q). Again, the hypothesis tests for comparing enrichment among multiple groups can be easily performed, because the approximated 95% confidence intervals of these log-ratios can be easily obtained by Fieller's theorem [3].

In addition, we can approximate the enrichment-fold π_1/π_2 by $\exp(ln(\pi_1/\pi_2))$, and σ_1^2/σ_2^2 by and $\exp(ln(\sigma_1^2/\sigma_2^2))$.

5 Convergence Diagnosis

We used the potential scale reduction factor (PSRF) [4] to quantify the mixing property of MCMC algorithms. With multiple MCMC chains, the PSRF for a parameter is basically the ratio between the overall estimated parameter variance and the within-chain variance. A PSRF value within $(0.9, 1.2)$ suggests that the MCMC algorithm has good mixing property

and posterior samples converge. For example, in Figure S2, we present the PSRFs for the $E[\gamma_i]$ of top 58 variants with P-values $< 5 \times 10^{-8}$ in the WTCCC GWAS of Chrohn's disease [1]. We can see that about half of the 58 variants had PSRFs > 1.2 by the standard MCMC algorithm as used in GEMMA [7], while all PSRFs by our MCMC algorithm all fall within $(0.9, 1.2)$, suggesting greatly improved mixing property due to the refined proposal distribution and relatively small block-sizes.

6 Challenges for Extending bfGWAS for Overlapped and Quantitative Annotations

Theoretically, this Bayesian hierarchical model can be easily extended for analyzing overlapped categorical and quantitative annotations, by assuming the following logistic model for the π_i in model (1),

$$logit(\pi_i) = \alpha_0 + \boldsymbol{A_i}^T \boldsymbol{\alpha}. \tag{17}$$

In the logistic model (17), $\boldsymbol{A_i}$ is the quantitative annotation vector (with binary values for categorical annotations) for the ith variant, and $\boldsymbol{\alpha} = (\alpha_1, \cdots, \alpha_Q)$ is the vector of log-odds for all considered annotations. Independent normal distributions can be assumed as the hyper priors for the category-specific (enrichment) parameters $(\alpha_0, \boldsymbol{\alpha})$. With a large number of annotations, variable selection of annotations might even be integrated by assuming independent point-normal priors for $\boldsymbol{\alpha}$.

Conditioning on values for $(\alpha_0, \boldsymbol{\alpha})$, the MCMC algorithm (Section 2.2) can be implemented similarly per block in the E-step. However, in the M-step, analytical formulas are no longer available for the posterior MAPs of $(\alpha_0, \boldsymbol{\alpha})$. In preliminary analysis, we found that the false positive rate was inflated due to over estimated π_i, which is due to the difficulties of estimating $(\alpha_0, \boldsymbol{\alpha})$. We are still exploring an appropriate approach to effectively control the false positive rate for this extension.

7 Software

Software implementing this Bayesian hierarchical model with the EM-MCMC algorithm, referred as Bayesian Functional Genome-wide Association Study (bfGWAS), is now available at GitHub (`https://github.com/yjingj/bfGWAS`). Within the software, the E-step (MCMC algorithm) is written in C++ language; the M-step is written in an R script; and both steps are wrapped together (enabling parallel computation) through submitting jobs by a Makefile that is generated by a Perl script.

Supplemental Figures

Figure S 1: Flowcharts of bfGWAS.

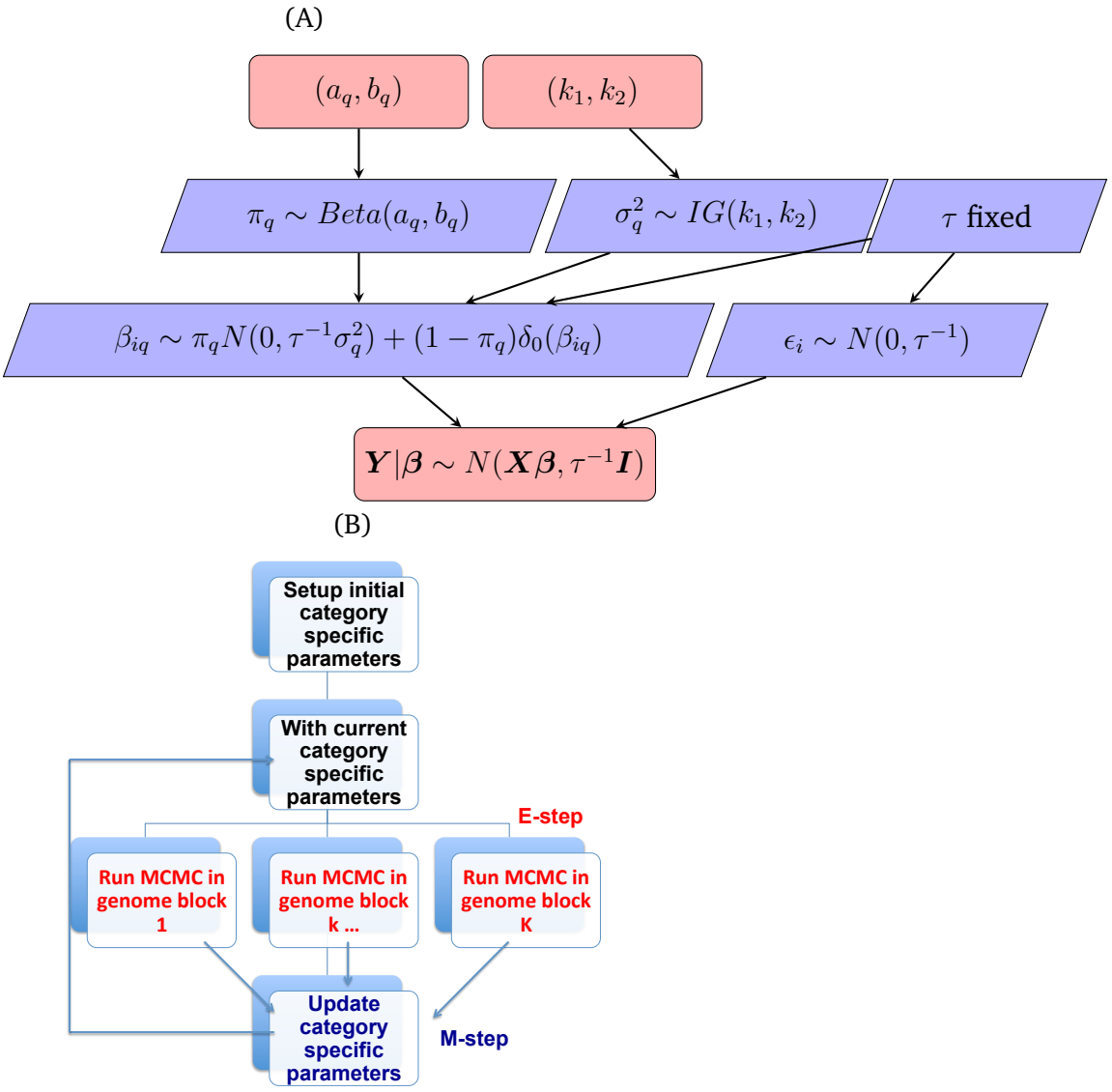

(A) Hierarchical Bayesian variable selection model; (B) EM-MCMC algorithm.

Figure S 2: Plots of the potential scale reduction factors (PSRF).

(A) (B)

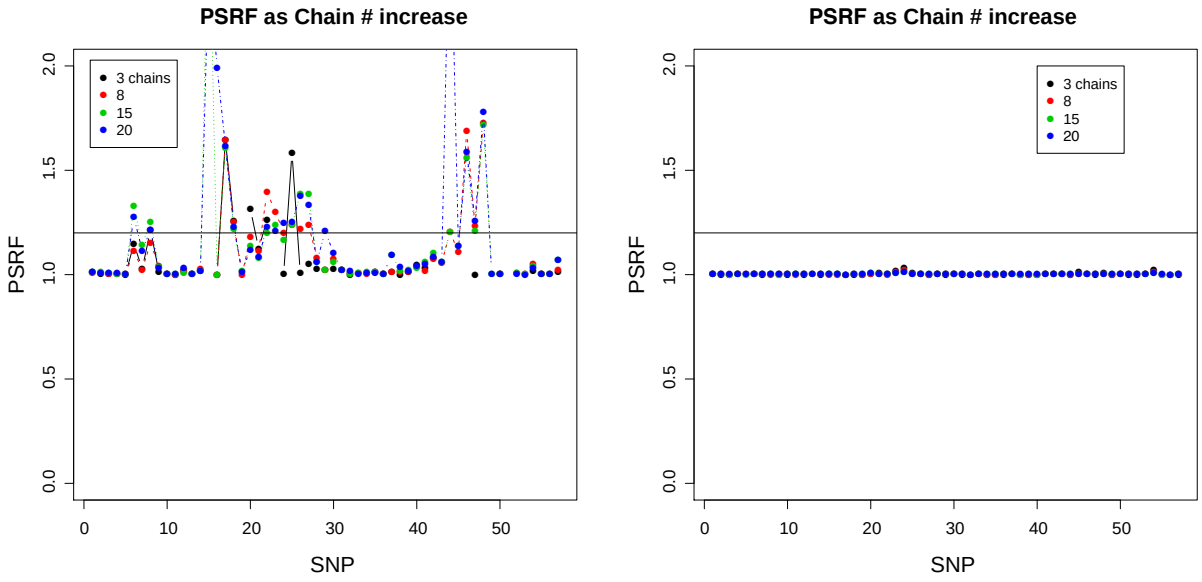

Potential scale reduction factors (PSRF) of the Bayesian posterior inclusion probabilities of 58 top marginally significant SNPs (WTCCC GWAS of Crohn's disease) with 3, 8, 15, and 20 MCMC chains, where PSRF within $(0.9, 1.2)$ suggests good mixing property. (A) Standard MCMC algorithm as used in GEMMA; (B) Our MCMC algorithm.

Figure S 3: Prioritization ranks of the true causal SNP1 (pink) and SNP2 (cyan).

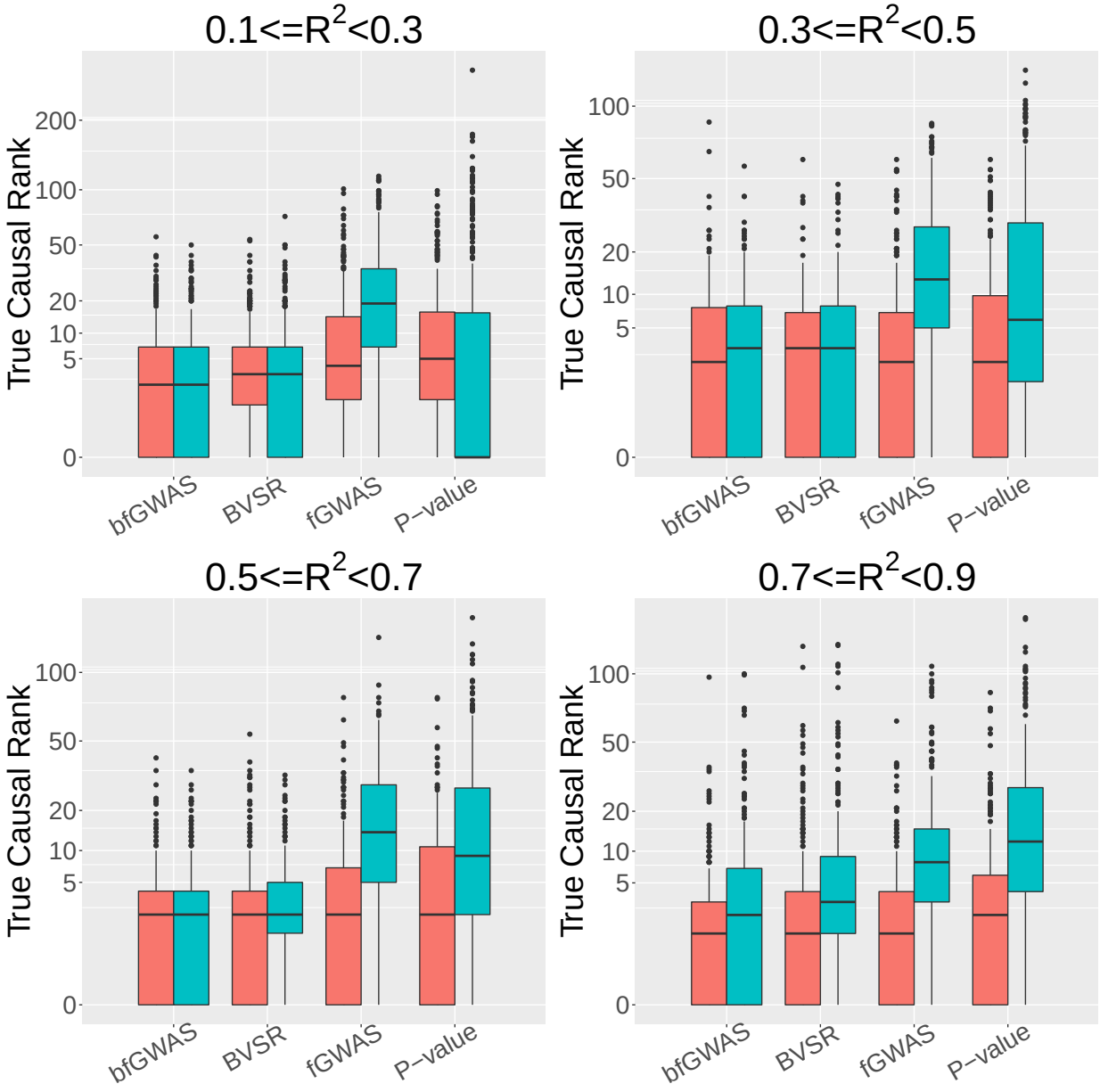

Ranks prioritized by bfGWAS, the standard Bayesian variable selection regression model (BVSR), fGWAS, P-value (single variant test for SNP1 and conditional analysis for SNP2), stratified by the R2 (LD) between SNP1 and SNP2. Here higher ranks (smaller numeric values) suggest higher power.

Figure S 4: Estimates of the log-relative-risk $ln(\pi_0/\pi_1)$ by bfGWAS and the enrich-parameter by fGWAS, along with 95% confidence intervals.

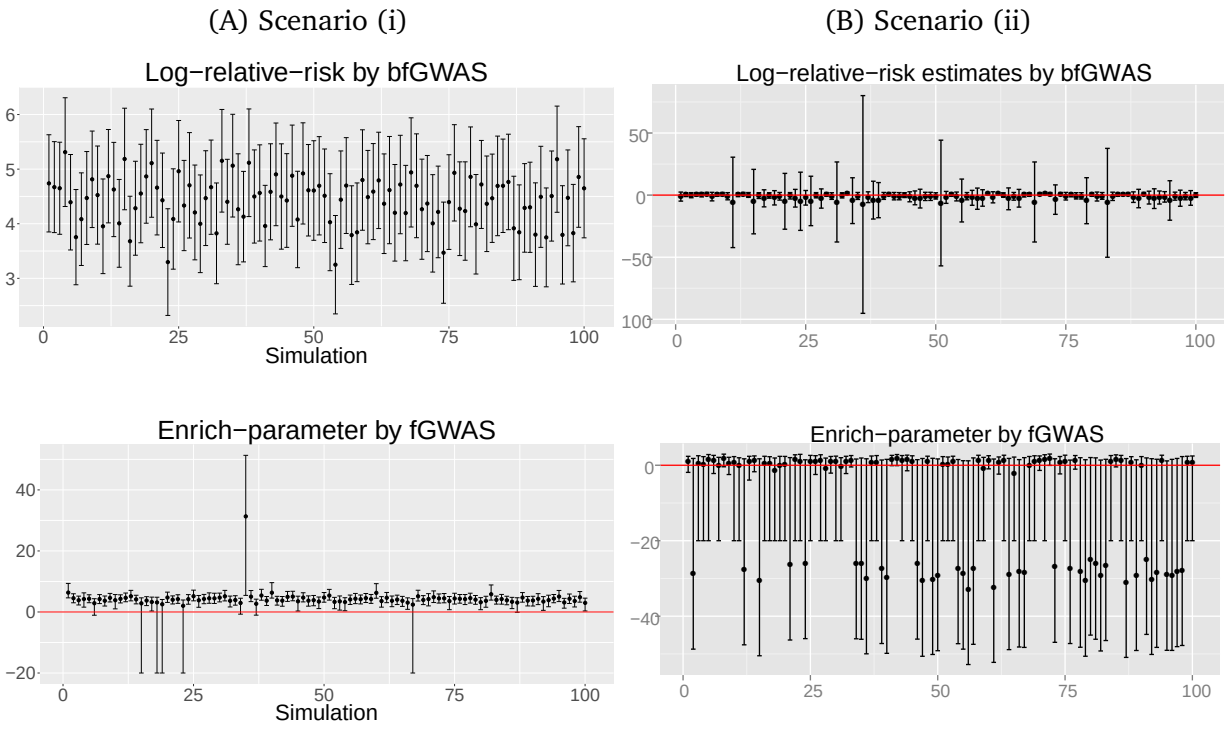

(A) Simulation scenario (i) with enrichment in coding and Scenario; (B) Simulation scenario (ii) with no enrichment. No enrichment is estimated when the 95% confidence interval covers 0, while enrichment for coding is estimated with the 95% confidence interval above 0.

Figure S 5: Estimates of the log-ratio of effect-size variances $ln(\sigma_0^2/\sigma_1^2)$ by bfGWAS, along with 95% confidence intervals.

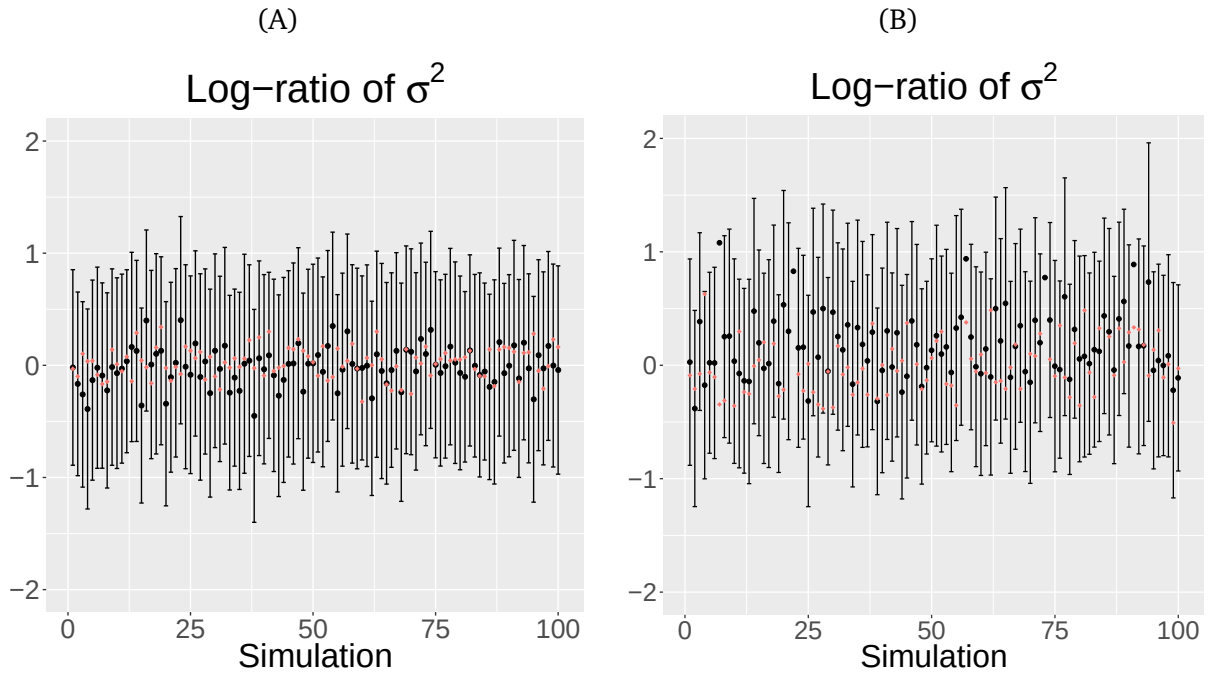

(A) Simulation scenario (i) with enrichment in coding; (B) Simulation scenario (ii) with no enrichment. Note that the effect-sizes of both groups in scenarios (i) and (ii) were simulated from the same normal distribution, thus the 95% confidence intervals covering 0 suggest that bfGWAS estimates similar effect-size variances between two categories.

Figure S 6: Sorted top bfGWAS PPs versus sorted top $-log10$(P-values) of single variant tests.

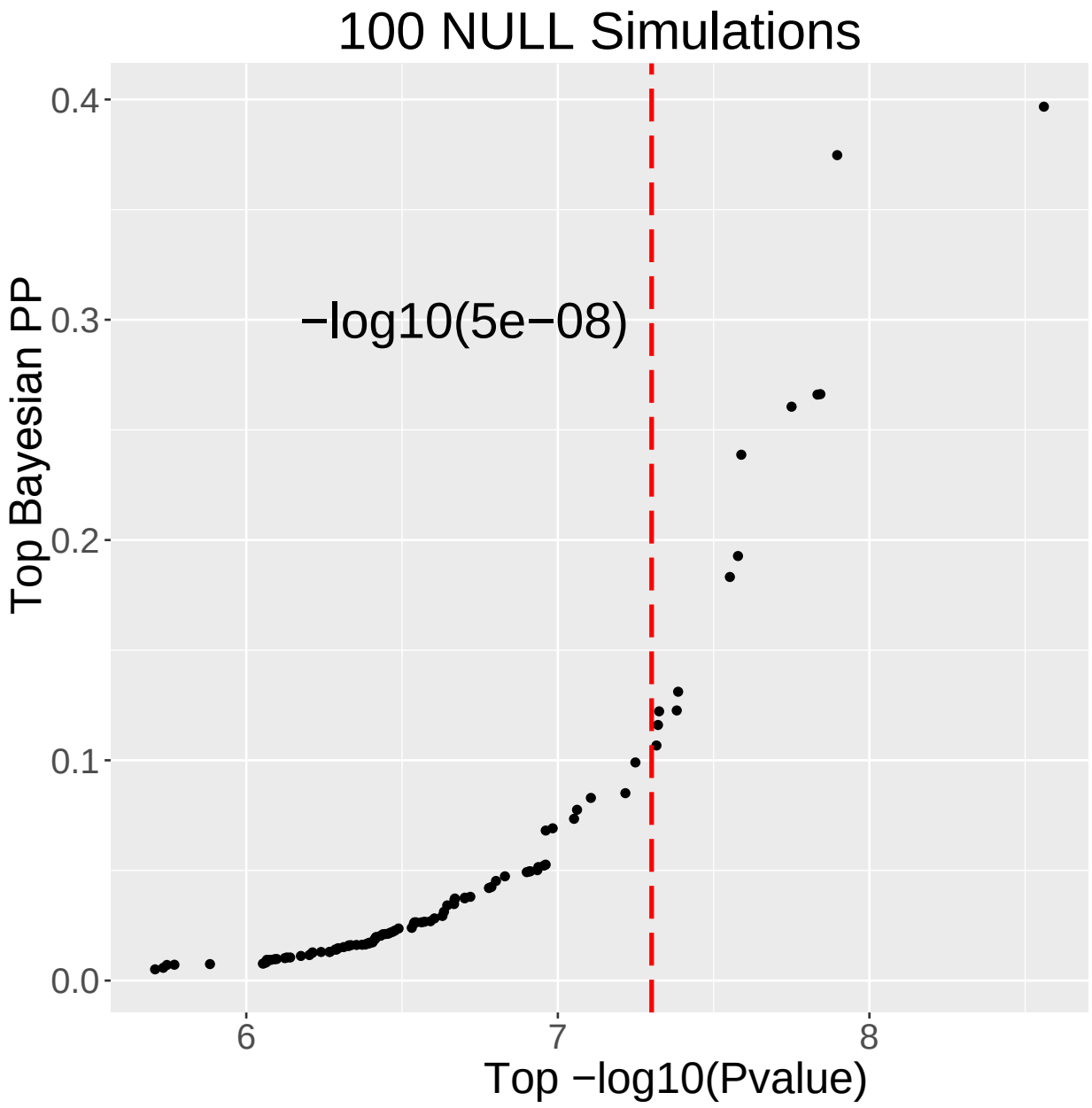

Results of 100 GWASs with AMD genotype data and permuted phenotypes. Note that the P-value 5×10^{-8} roughly corresponds to bfGWAS posterior inclusion probability (PP) 0.1068.

Figure S 7: Manhattan plot highlighting AMD GWAS signals with BVSR $PP > 0.1068$.

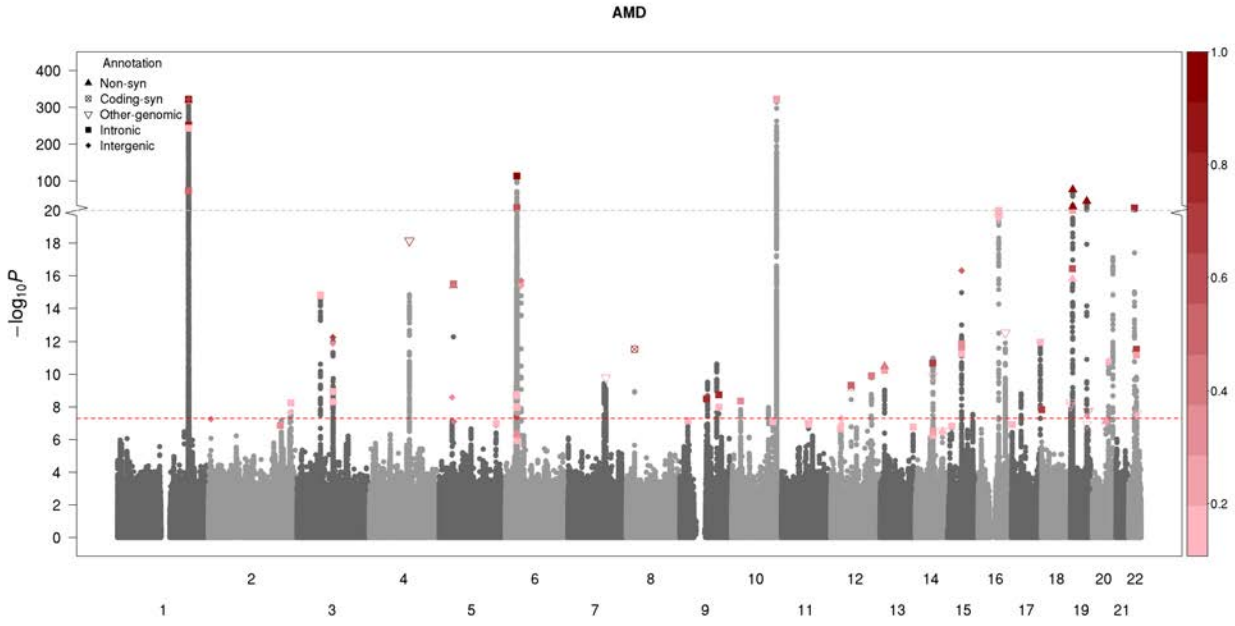

Figure S 8: Manhattan plots highlighting AMD GWAS signals by accounting for gene-based annotations.

(A)

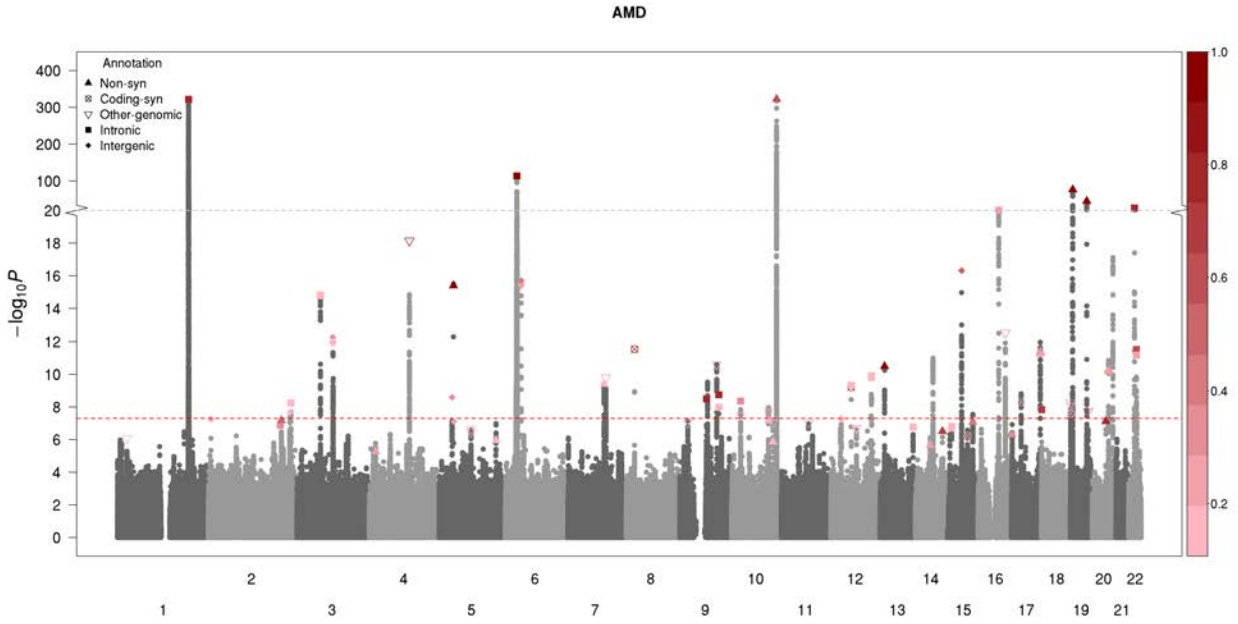

(B)

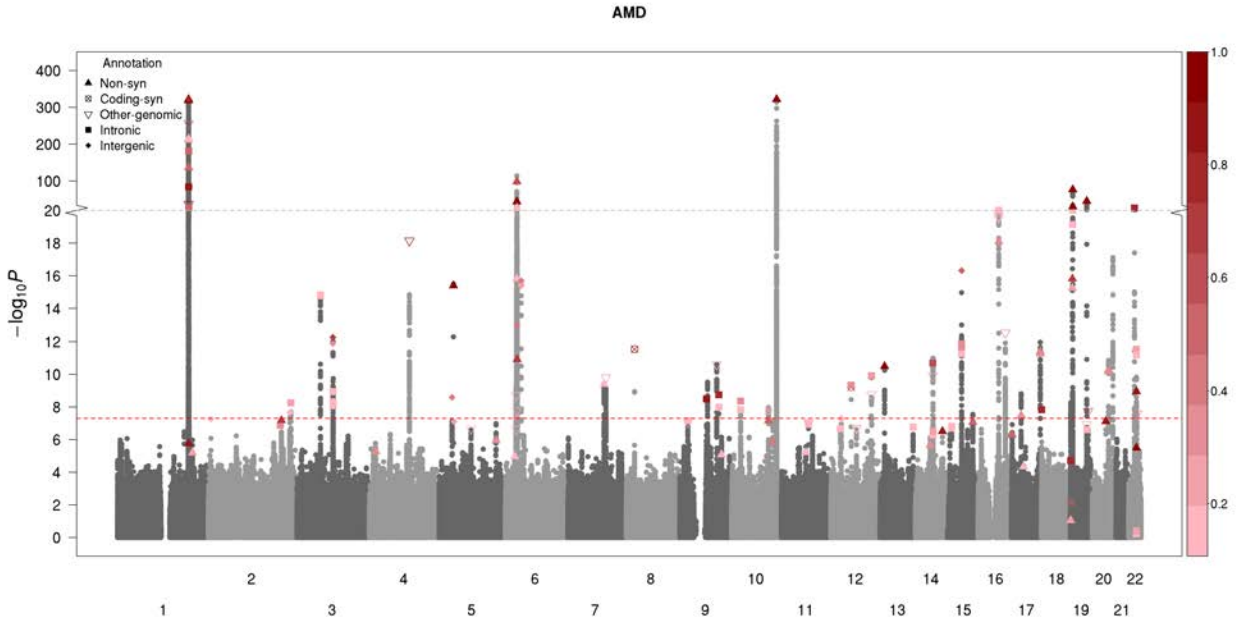

(A) Highlighting signals with fGWAS posterior association probability (PP) > 0.1068 are colored; (B) Highlighting signals with bfGWAS PP > 0.1068.

Figure S 9: LocusZoom plots of region *CHR19:6218146-7218146*.

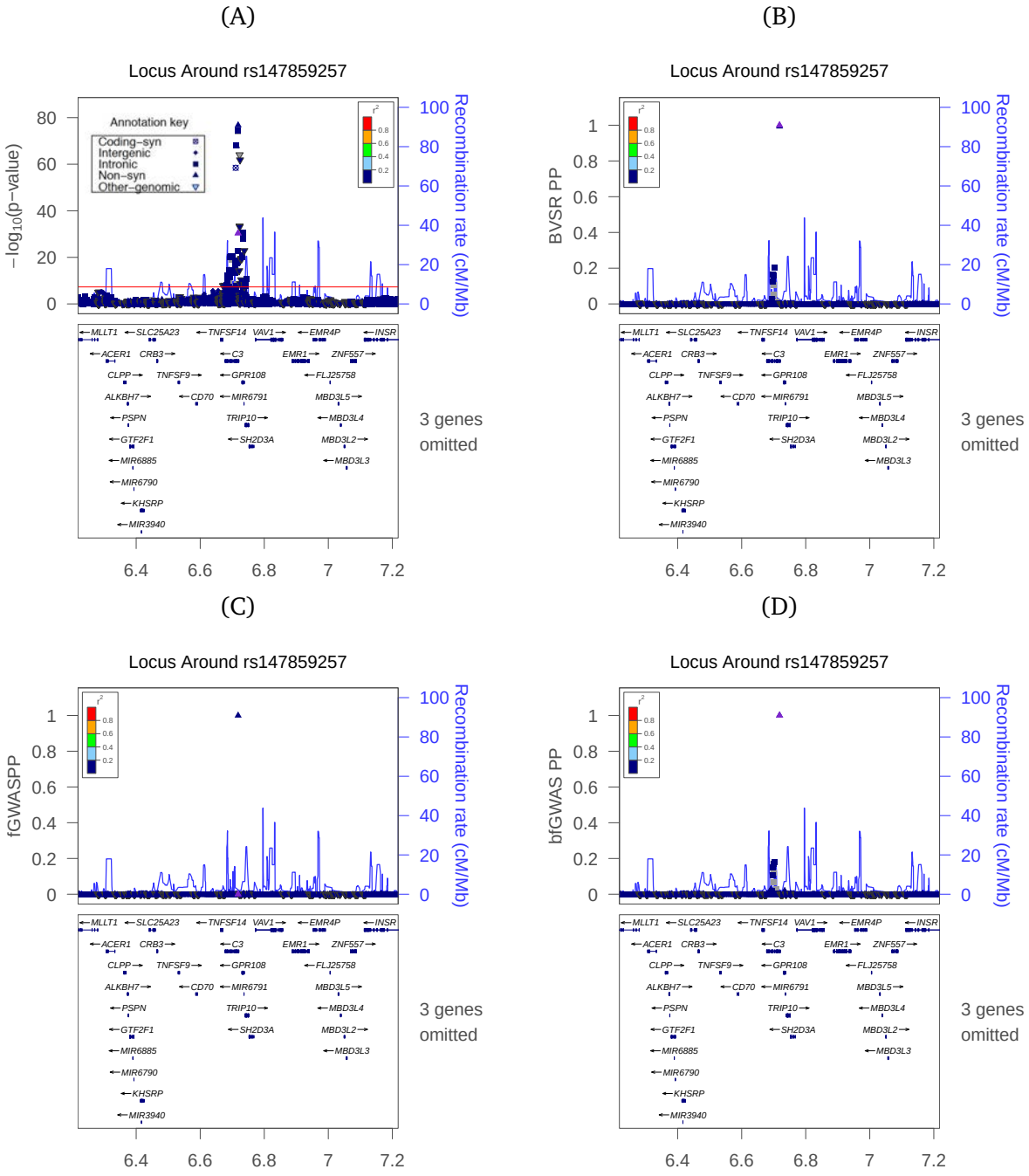

(A) P-values by single variant tests; (B) BVSR PPs; (C) fGWAS PPs; (D) bfGWAS PPs. The purple triangle in (B, D) denotes the variant *rs147859257*; the blue triangle in (A, C) denotes the top significant variant by single variant tests *rs2230199*.

Figure S 10: Enrichment analysis results with varying prior means as well as starting values $(10^{-6}, 5 \times 10^{-6}, 10^{-5})$ for π_q, and varying starting values $(10, 5, 1)$ for σ_q^2.

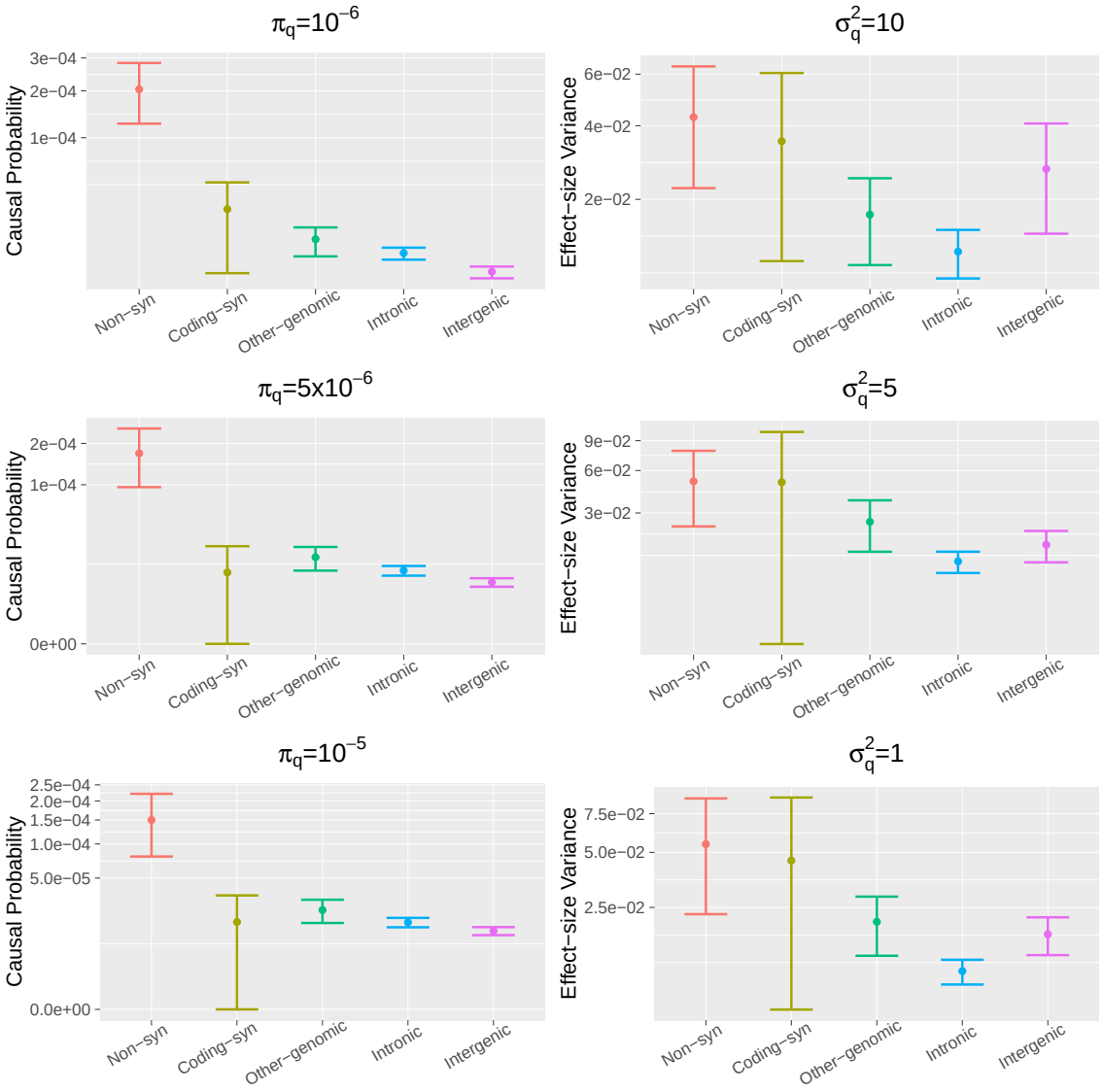

Figure S 11: fGWAS enrichment estimates with 95% error bars.

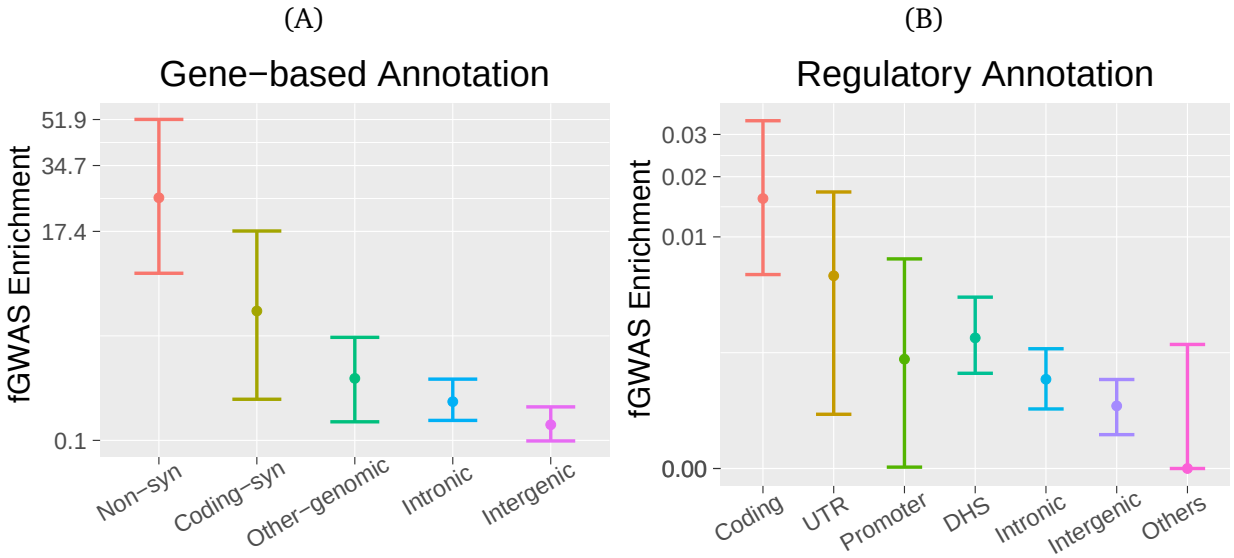

Figure S 12: Ratios of enrich parameters versus the respective genome-wide averages, along with 95% confidence intervals.

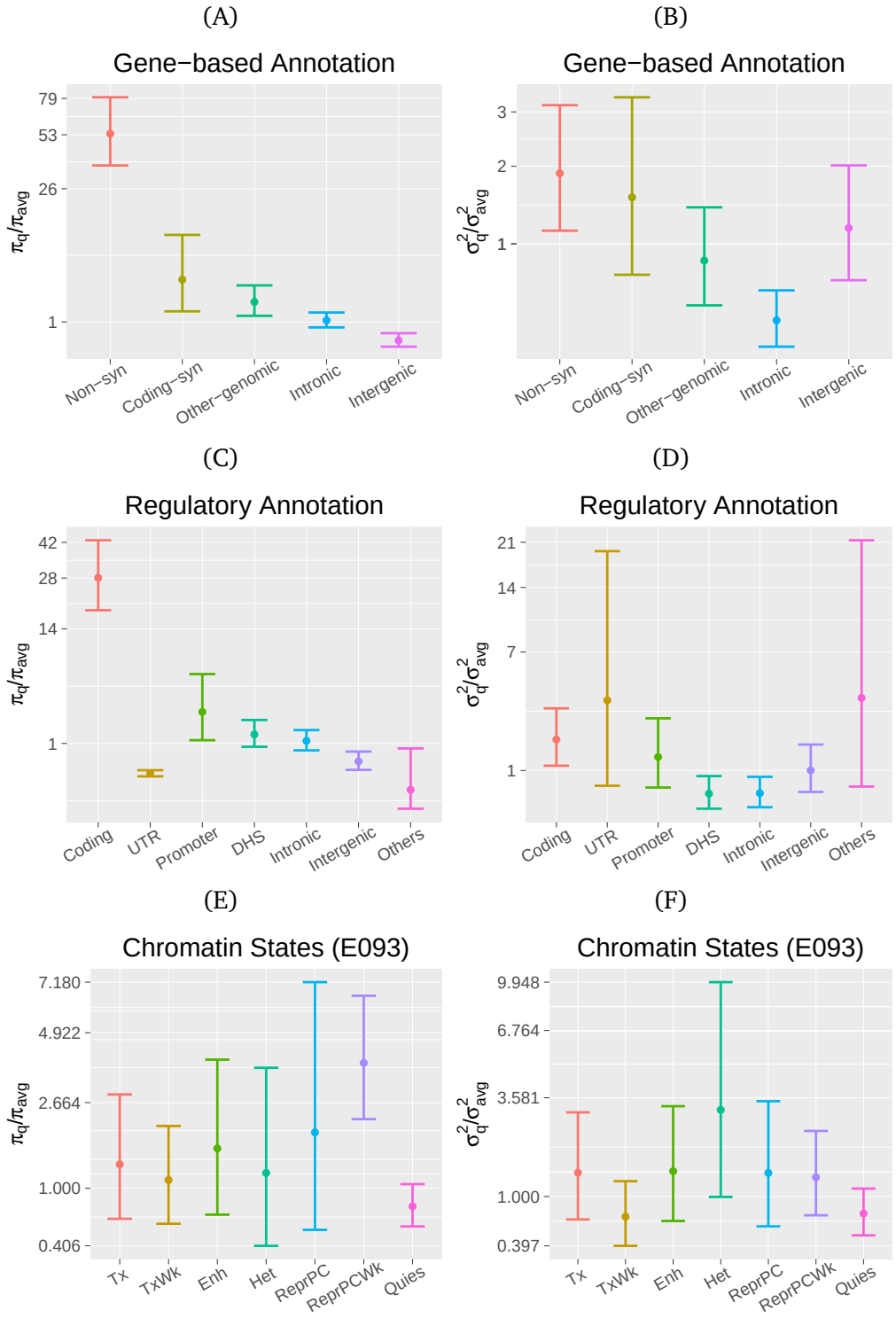

(A, C, E) Causal probability ratios (π_q/π_{avg}); (B, D, F) Effect-size variance ratios ($\sigma^2_q/\sigma^2_{avg}$).

Figure S 13: Enrichment analysis results for the AMD GWAS data with chromatin states profiled with respect to the epigenome of fetal thymus (E093).

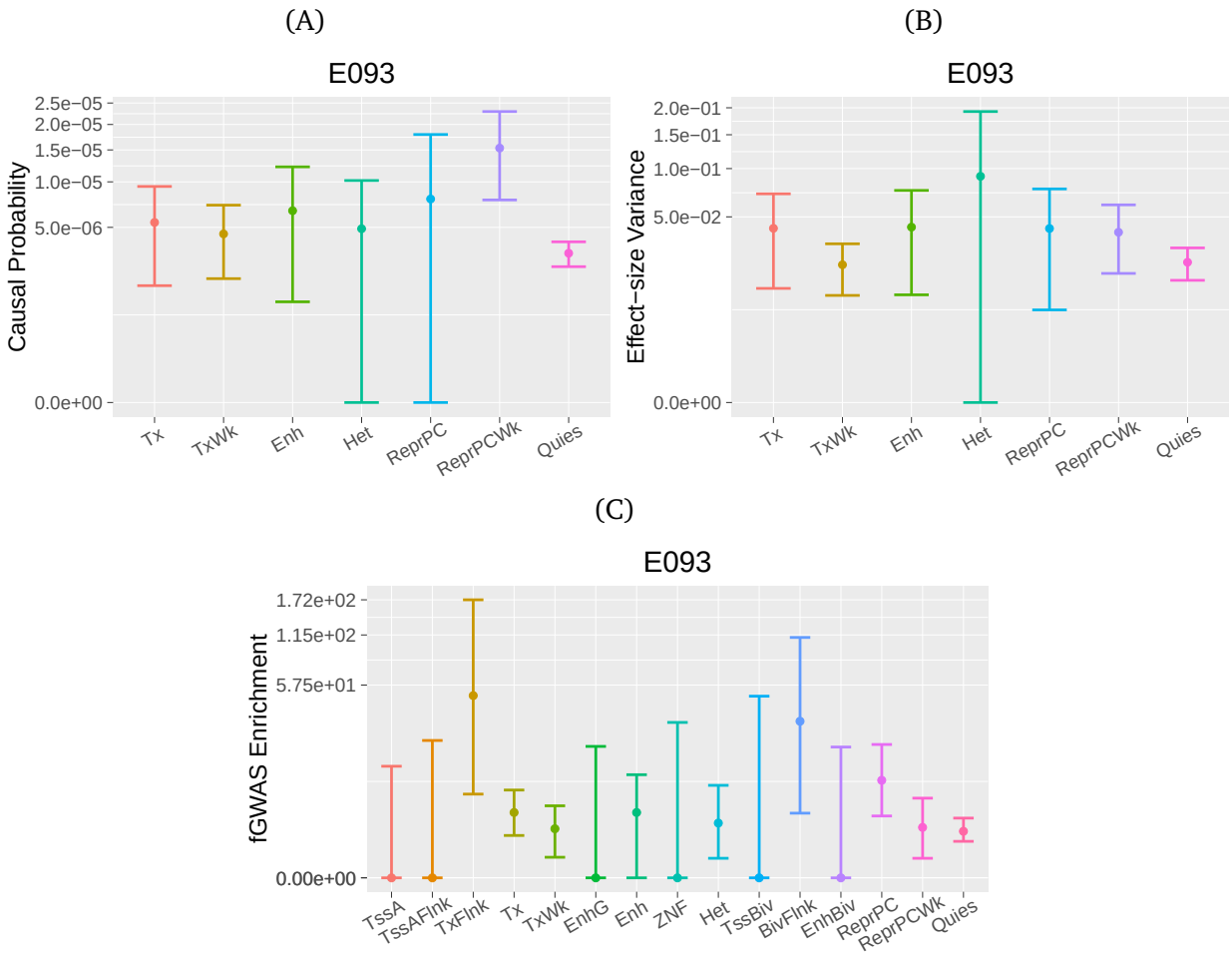

Figure S 14: Manhattan plot highlighting MGI GWAS signals of skin cancer with BVSR PP > 0.1068.

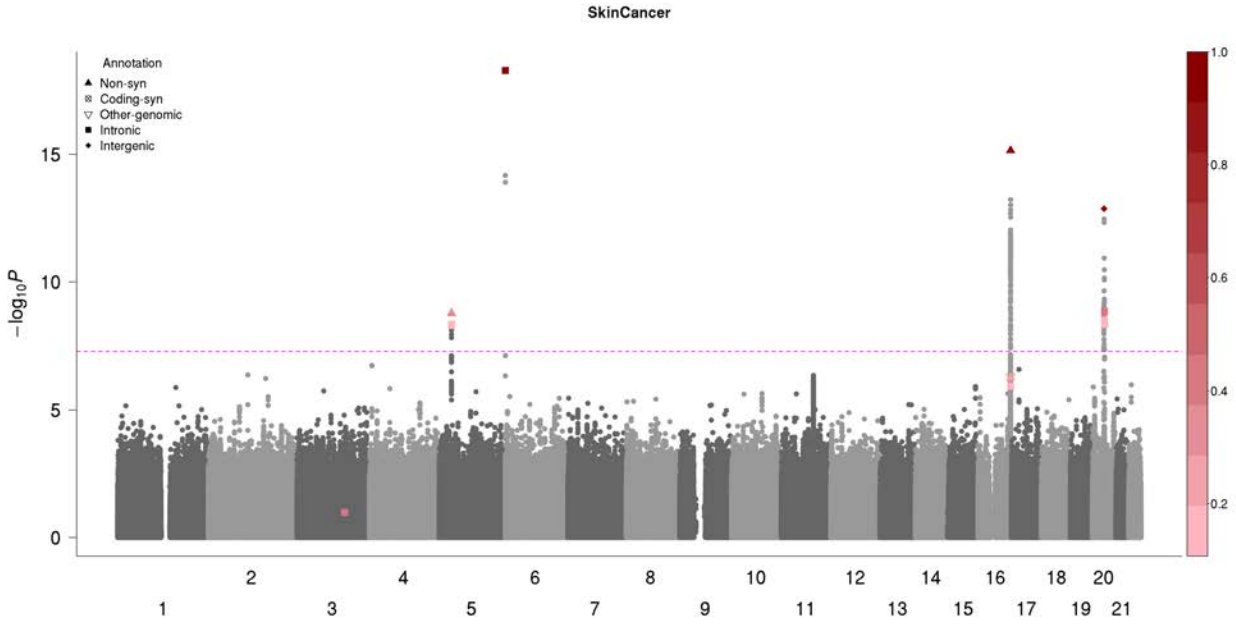

Figure S 15: Manhattan plots highlighting MGI GWAS signals of skin cancer by accounting for gene-based annotations.

(A)

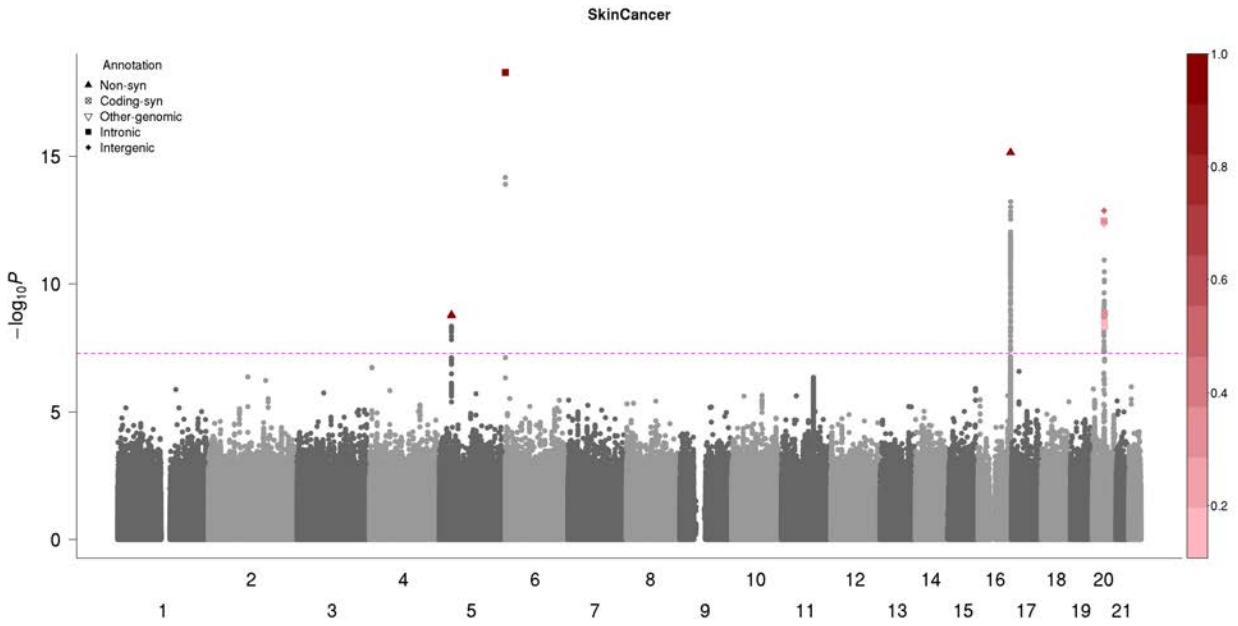

(B)

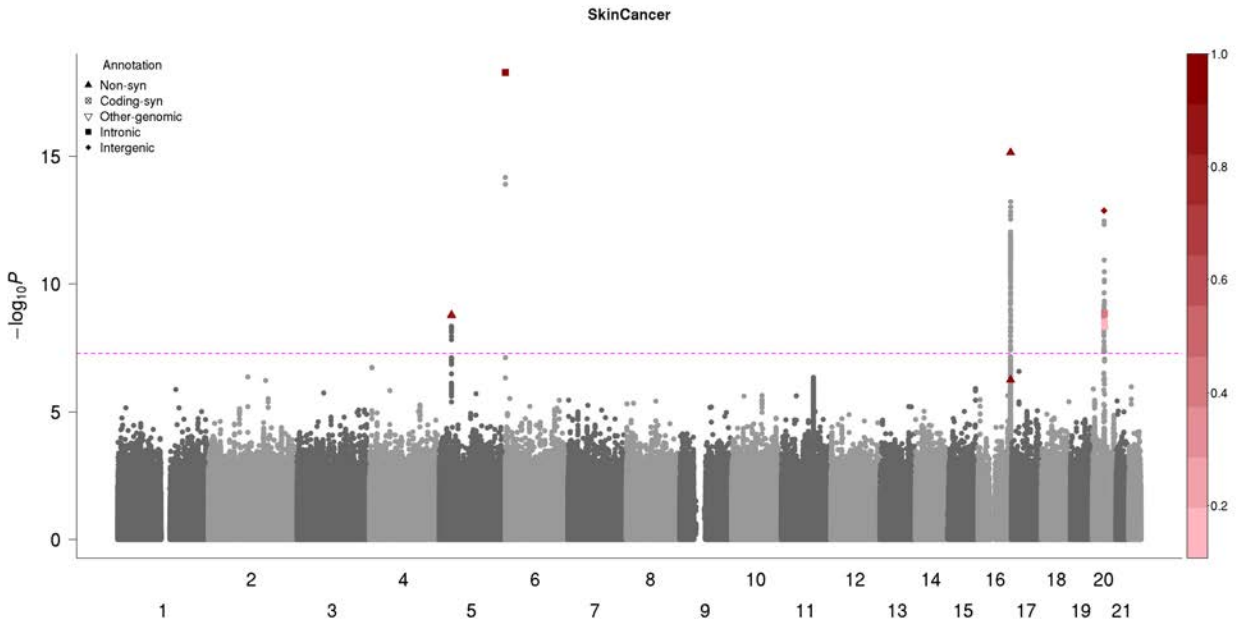

(A) Highlighting signals with with fGWAS PP > 0.1068; (B) Highlighting signals with bfGWAS PP > 0.1068. Variants with PP > 0.1068 are plotted in different shapes with respect to gene-based annotations.

Figure S 16: Enrichment analysis results of the MGI GWAS of skin cancer, accounting for gene-based annotations.

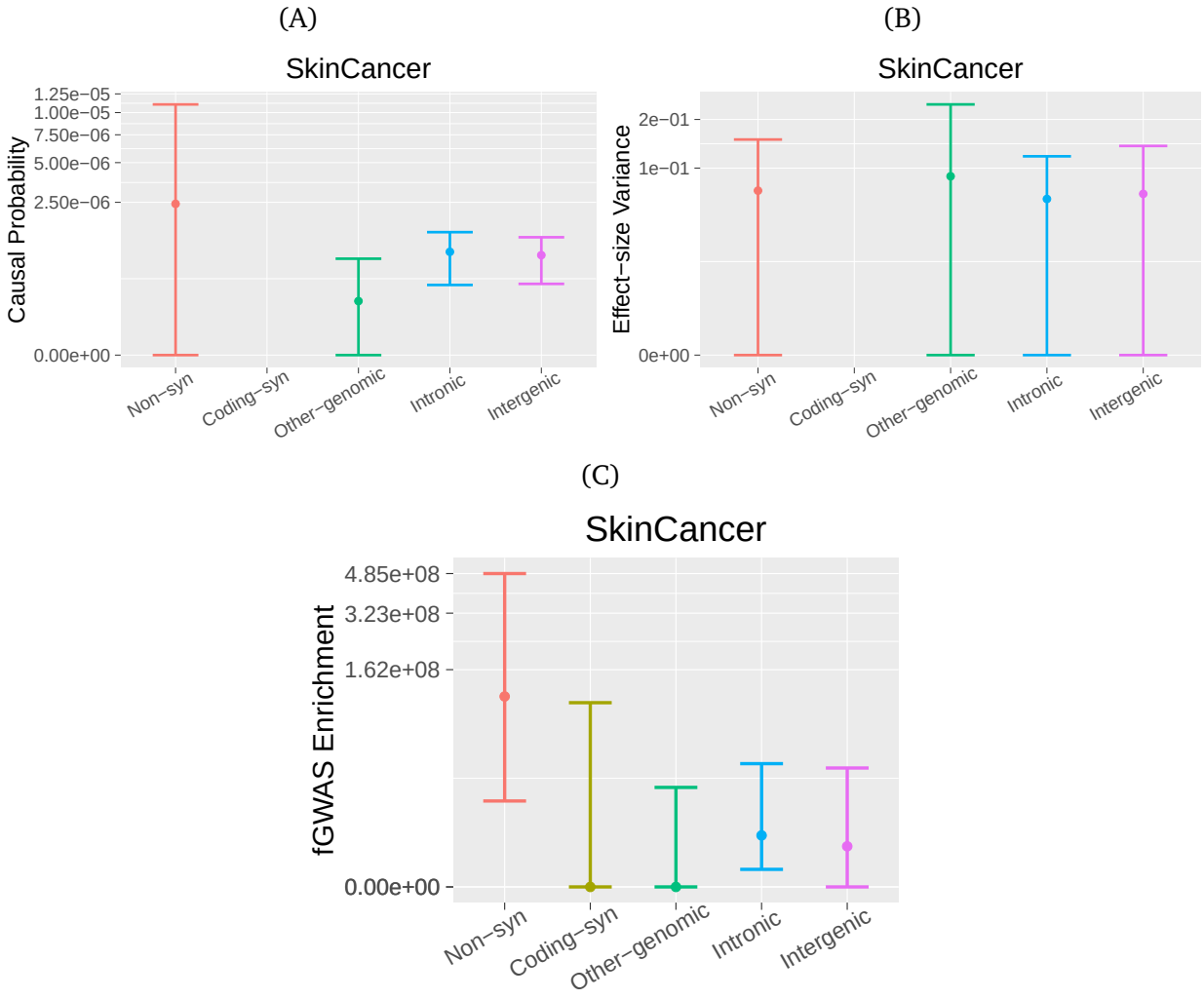

Figure S 17: LocusZoom plots in the region of *CHR16:89686117-90172696*.

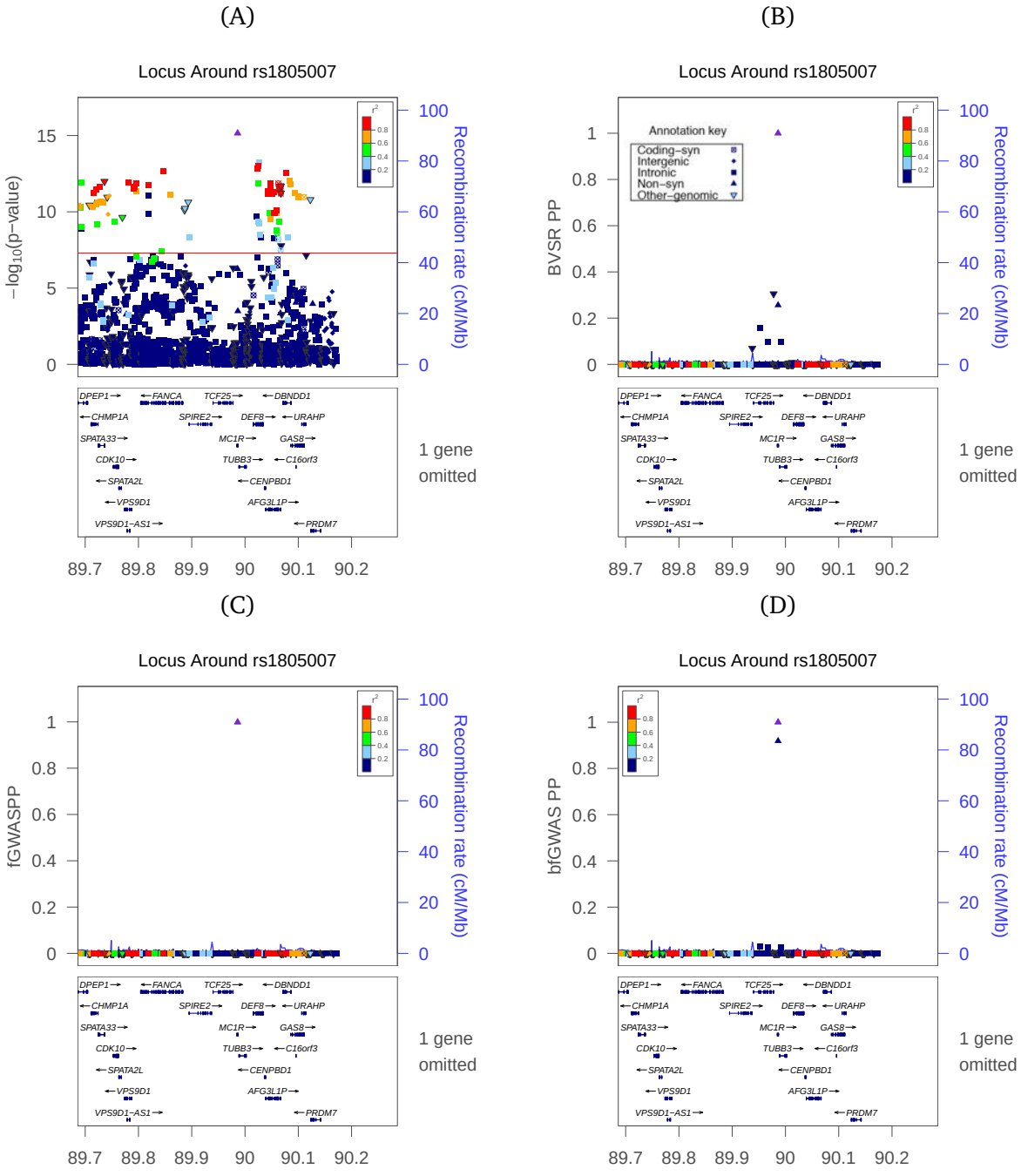

(A) P-values by single variant tests; (B) BVSR PPs; (C) fGWAS PPs; (D) bfGWAS PPs. The purple triangle denotes the variant *rs1805007*.

Supplemental Tables

Table S1: Classification of gene-based functional annotations.

Native gene-based functional annotations	Annotation categories considered in the analysis
frameshift, frameshift-near-splice	Non-synonymous
splice-acceptor, splice-donor,	
stop-gained, stop-gained-near-splice, stop-lost	
missense, missense-near-splice	
synonymous-near-splice, non-coding-exon-near-splice, coding-near-splice, coding-unknown-near-splice, intron-near-splice	
coding, coding-unknown, synonymous, nc-transcript-variant	Coding-synonymous
intronic	Intronic
intergenic, NAs	Intergenic
3-prime-UTR, 5-prime-UTR,	Other-genomic
downstream-gene, upstream-gene, non-coding-exon	

Table S2: Compare results by P-value, fGWAS, and bfGWAS in the 34 known AMD loci, accounting for gene-based annotations.

Known 34 Loci				Top significant variant by P-value					Bayesian Regional-PP	fGWAS Regional-PP
Locus name	Chr	Start	End	dbSNPID	Chr:Position	MAF	P-value	Anno		
CFH	1	195,679,832	197,768,053	rs10922109	1:196,704,632	0.329	$<9\times10^{-321}$	intronic	1.000	1.000
COL4A3	2	227,573,015	228,592,110	rs11884770	2:228,086,920	0.731	5.6×10^{-9}	intronic	0.984	0.986
ADAMTS9-AS	3	64,199,445	65,230,121	rs62247658	3:64,715,155	0.551	1.4×10^{-15}	intronic	0.978	1.000
COL8A1	3	98,551,114	100,381,567	rs140647181	3:99,180,668	0.019	5.4×10^{-13}	intergenic	1.000	0.999
CFI	4	110,126,506	111,185,820	rs10033900	4:110,659,067	0.506	7.1×10^{-19}	downstream	1.000	1.000
C9	5	38,699,134	39,831,894	rs62358361	5:39,327,888	0.012	3.1×10^{-16}	intronic	1.000	1.000
PRLR/SPEF2	5	34,769,332	36,493,378	rs114092250	5:35,494,448	0.018	2.5×10^{-9}	intergenic	0.961	0.987
C2/CFB/SKIV2L	6	30,505,490	33,238,589	rs116503776	6:31,930,462	0.120	2.1×10^{-114}	intronic	1.000	1.000
VEGFA	6	43,305,296	44,329,629	rs943080	6:43,826,627	0.518	2.0×10^{-16}	intergenic	1.000	1.000
KMT2E/SRPK2	7	104,081,402	105,563,372	rs1142	7:104,756,326	0.357	1.5×10^{-10}	downstream	0.999	0.999
PILRB/PILRA	7	99,394,940	100,611,776	rs7803454	7:99,991,548	0.199	3.6×10^{-10}	intronic	0.999	0.999
TNFRSF10B	8	22,582,971	23,588,984	rs79037040	8:23,080,971	0.534	2.9×10^{-12}	nc-transcript	1.000	0.999
MIR6130/RORB	9	75,935,160	77,189,752	rs10781180	9:76,615,662	0.683	3.0×10^{-10}	intergenic	0.997	0.999
TRPM3	9	72,938,605	73,946,180	rs7150714	9:73,438,605	0.584	3.2×10^{-9}	intronic	0.929	0.999
TGFBR1	9	101,358,102	102,431,769	rs1626340	9:101,923,372	0.199	2.3×10^{-11}	intergenic	1.000	0.999
ABCA1	9	107,139,414	108,167,147	rs2740488	9:107,661,742	0.265	1.7×10^{-9}	intronic	0.963	0.985
ARHGAP21	10	24,360,361	25,556,538	rs12357257	10:24,999,593	0.232	4.3×10^{-9}	intronic	0.962	0.986
ARMS2/HTRA1	10	123,702,126	124,735,355	rs3750846	10:124,215,565	0.316	$<9\times10^{-321}$	intronic	1.000	1.000
RDH5/CD63	12	55,615,585	56,713,297	rs3138141	12:56,115,778	0.214	4.7×10^{-10}	intronic	0.034	0.999
ACAD10	12	110,919,995	113,502,935	rs73205633	12:112,357,085	0.019	1.2×10^{-10}	intergenic	0.997	0.999

Known 34 Loci				Top significant variant by P-value					Bayesian Regional-PP	fGWAS Regional-PP
Locus name	Chr	Start	End	dbSNPID	Chr:Position	MAF	P-value	Anno		
B3GALTL	13	31,242,232	32,339,274	rs9564692	13:31,821,240	0.288	3.2×10^{-11}	splice	1.000	0.999
RAD51B	14	68,227,506	69,550,783	rs1956526	14:68,799,787	0.650	$1..0\times10^{-11}$	intronic	1.000	0.999
LIPC	15	58,171,721	59,242,418	rs2414577	15:58,680,638	0.365	4.8×10^{-17}	nc-transcript	1.000	1.000
CETP	16	56,485,514	57,506,829	rs5817082	16:56,997,349	0.248	1.7×10^{-21}	intronic	1.000	1.000
CTRB2/CTRB1	16	74,732,528	76,017,115	rs72802342	16:75,234,872	0.073	2.8×10^{-13}	downstream	1.000	1.000
TMEM97/VTN	17	26,092,946	27,240,139	rs11080055	17:26,649,724	0.524	1.5×10^{-9}	intronic	0.996	0.998
NPLOC4/TSPAN10	17	79,015,509	80,186,552	rs6565597	17:79,526,821	0.390	1.0×10^{-12}	intronic	1.000	0.999
C3	19	5,311,717	7,224,340	rs2230199	19:6,718,387	0.764	1.7×10^{-77}	missense	1.000	1.000
CNN2	19	523,867	1,533,360	rs10422209	19:1,026,318	0.132	5.5×10^{-9}	upstream	0.970	0.993
APOE	19	44,892,254	46,313,830	rs429358	19:45,411,941	0.118	3.3×10^{-46}	missense	1.000	1.000
MMP9	20	44,114,991	45,160,699	rs142450006	20:44,614,991	0.132	1.4×10^{-11}	intergenic	1.000	0.999
C20orf85	20	56,084,276	57,174,034	rs117739907	20:56,652,781	0.062	7.8×10^{-18}	intergenic	1.000	1.000
SYN3/TIMP3	22	32,546,536	33,613,375	rs5754227	22:33,105,817	0.123	2.0×10^{-27}	intronic	1.000	1.000
SLC16A8	22	37,795,271	39,003,972	rs8135665	22:38,476,276	0.205	2.9×10^{-12}	intronic	1.000	0.999

Table S3: AMD risk variants identified by bfGWAS in the 34 known loci, accounting for gene-based annotations.

Signal number	Reside/Nearby Gene	dbSNPID	Chr:Position	Anno	MAF	bfGWAS PP	Effect-size	P-value
1.1	*CFH*	rs800292	1:196,642,233	missense	0.183	0.997	-0.312	2.4×10^{-319}
1.2	*CFH*	rs10922094	1:196,661,505	intronic	0.530	1.000	-0.214	$< 9.0\times10^{-321}$
1.3	*CFHR1*	rs605082	1:196,801,917	downstream	0.353	0.518	-0.092	7.5×10^{-257}
1.4	*CFHR4*	rs58175074	1:196,820,080	intronic	0.158	0.792	-0.314	$< 9.0\times10^{-321}$
1.5	*CFHR4*	rs149032610	1:196,857,150	5'-UTR	0.015	1.000	0.195	6.6×10^{-38}
1.6	*CFHR4*	rs10494745	1:196,887,457	missense	0.134	0.526	0.092	7.4×10^{-137}
1.7	*CFHR2*	rs138579109	1:196,923,955	intronic	0.043	0.893	0.167	8.4×10^{-85}
1.8	*CFHR5*	rs35662416	1:196,967,354	missense	0.022	0.889	-0.122	5.8×10^{-6}
2	*COL4A3*	rs11884770	2:228,086,920	intronic	0.731	0.269	0.052	5.6×10^{-9}
3	*ADAMTS9-AS2*	rs7428936	3:64,710,850	intronic	0.448	0.167	-0.061	1.5×10^{-15}
4	*COL8A1*	rs140647181	3:99,180,668	intergenic	0.019	0.687	0.224	54×10^{-13}
5	*CFI*	rs10033900	4:110,659,067	downstream	0.506	0.999	-0.067	7.2×10^{-19}
6	*C9*	rs34882957	5:39,331,894	missense	0.012	0.998	0.278	4.0×10^{-16}
7	*PRLR/SPEF2*	rs114092250	5:35,494,448	intergenic	0.019	0.403	-0.174	2.5×10^{-9}
8.1	*C2/CFB*	rs4151667	6:31,914,024	missense	0.036	0.917	-0.279	1.4×10^{-44}
8.2	*SKIV2L/NELFE*	rs115270436	6:31,928,306	missense	0.071	0.633	-0.321	2.8×10^{-99}
8.3	*HLA-DQB1*	rs3891176	6:32,634,318	missense	0.159	0.726	0.153	1.2×10^{-11}
9	*VEGFA*	rs943080	6:43,826,627	intergenic	0.518	0.435	0.063	2.0×10^{-16}
10	*KMT2E/SRPK2*	rs1142	7:104,756,326	downstream	0.357	0.125	0.052	1.5×10^{-10}
11	*PILRB*	rs35986051	7:99,956,439	missense	0.139	0.193	0.075	4.0×10^{-10}
12	*TNFRSF10A*	rs79037040	8:23,082,971	nc-transcript	0.534	0.996	0.053	2.9×10^{-12}
13	*MIR6130/RORB*	rs10781182	9:76,617,720	intergenic	0.684	0.070	-0.052	3.0×10^{-10}
14	*TRPM3*	rs71507014	9:73,438,605	intronic	0.584	0.822	-0.046	3.2×10^{-9}
15	*TGFBR1*	rs10819635	9:101,864,510	upstream	0.186	0.137	-0.066	2.4×10^{-11}
16	*ABCA1*	rs2740488	9:107,661,742	intronic	0.266	0.756	-0.053	1.7×10^{-9}
17	*ARHGAP21*	rs12357257	10:24,999,593	intronic	0.232	0.318	0.053	4.3×10^{-9}
18	*ARMS2*	rs10490924	10:124,214,448	missense	0.316	0.996	0.474	$< 9.0\times10^{-321}$
19	*RDH5/CD63*	rs3138142	12:56,115,585	coding-syn	0.213	0.706	0.074	6.1×10^{-10}
20	*MAPKAPK5*	rs61941287	12:112,330,305	intronic	0.019	0.309	0.191	1.2×10^{-10}
21	*B3GLCT*	rs9564692	13:31,821,240	splice	0.288	0.942	-0.056	3.2×10^{-11}
22	*RAD51B*	rs2842339	14:68,986,999	intronic	0.899	0.243	-0.082	3.1×10^{-7}
23	*ALDH1A2*	rs2414577	15:58,680,638	intronic	0.366	0.501	-0.067	4.8×10^{-17}
24	*CETP*	rs1532625	16:57,005,301	splice	0.448	0.358	0.044	7.9×10^{-19}
25	*CTRB2*	rs72802342	16:75,234,872	downstream	0.360	0.297	-0.114	2.8×10^{-13}
26	*CTB-96E2.2/VTN*	rs704	17:26,694,861	missense	0.483	0.325	0.042	3.3×10^{-8}
27	*NPLOC4/TSPAN10*	rs6420484	17:79,612,397	missense	0.622	0.402	-0.055	4.0×10^{-12}
28.1	*FUT6/NRTN*	rs17855739	19:5,831,840	missense	0.044	0.681	-0.159	1.5×10^{-16}
28.2	*C3/CTD-3128G10.7*	rs147859257	19:6,718,146	missense	0.008	1.000	0.501	4.3×10^{-31}
28.3	*C3/CTD-3128G10.7*	rs2230199	19:6,718,387	missense	0.764	1.000	-0.172	1.7×10^{-77}

Signal number	Reside/Nearby Gene	dbSNPID	Chr:Position	Anno	MAF	bfGWAS PP	Effect-size	P-value
29.1	*ABCA7*	rs3752237	19:1,047,161	coding-syn	0.644	0.544	-0.065	6.7×10^{-3}
29.2	*ABCA7*	rs12151021	19:1,050,874	intronic	0.708	1.000	0.091	1.9×10^{-5}
30	*APOE/TOMM40/ CTB-129P6.7*	rs429358	19:45,411,941	missense	0.118	1.000	-0.173	3.3×10^{-46}
31	*MMP9/RP11-465L10.10*	rs2274755	20:44,639,692	splice	0.138	0.435	-0.073	5.4×10^{-11}
32	*C20orf85*	rs201459901	20:56,653,724	intergenic	0.063	0.078	-0.135	7.9×10^{-18}
33	*SYN3*	rs5754227	22:33,105,817	intronic	0.124	0.764	-0.128	2.0×10^{-27}
34.1	*SLC16A8/BAIAP2L2*	rs4289289	22:38,477,342	missense	0.485	0.824	0.056	1.1×10^{-09}
34.2	*SLC16A8/BAIAP2L2*	rs77968014	22:38,478,666	splice	0.009	0.973	0.212	3.1×10^{-6}

Variants with Bayesian PPs >0.5 or the highest bfGWAS PPs in the loci are listed. Shown are reside/nearby genes, dbSNPIDs, positions, functional annotations, MAFs (unfolded, corresponding to the direction of effect-sizes), P-values, and Bayesian PPs/effect-sizes.

Table S4: AMD risk variants identified by fGWAS in the 34 known loci, accounting for gene-based annotations.

Signal number	Reside/Nearby Gene	dbSNPID	Chr:Position	Anno	MAF	fGWAS PP	P-value
1	*CFH*	rs10922109	1:196,704,632	intronic	0.329	0.802	$< 9.0\times10^{-321}$
2	*COL4A3*	rs11884770	2:228,086,920	intronic	0.731	0.181	5.7×10^{-9}
3	*ADAMTS9-AS2*	rs62247658	3:64,715,155	intronic	0.551	0.167	1.5×10^{-15}
4	*COL8A1*	rs140647181	3:99,180,668	intergenic	0.019	0.999	5.4×10^{-13}
5	*CFI*	rs10033900	4:110,659,067	downstream	0.506	0.996	7.2×10^{-19}
6	*C9*	rs34882957	5:39,331,894	missense	0.012	0.900	4.0×10^{-16}
7	*PRLR/SPEF2*	rs114092250	5:35,494,448	intergenic	0.019	0.626	2.5×10^{-9}
8	*NELFE/SKIV2L*	rs116503776	6:31,930,462	intronic	0.120	0.912	2.1×10^{-114}
9	*VEGFA*	rs943080	6:43,826,627	intergenic	0.518	0.437	2.0×10^{-16}
10	*KMT2E/SRPK2*	rs1142	7:104,756,326	downstream	0.357	0.182	1.5×10^{-10}
11	*PILRB*	rs72615157	7:99,956,444	missense	0.139	0.118	4.0×10^{-10}
12	*TNFRSF10A*	rs79037040	8:23,082,971	nc-transcript	0.534	0.996	2.9×10^{-12}
13	*MIR6130/RORB*	rs10781180	9:76,615,662	intergenic	0.683	0.068	3.0×10^{-10}
14	*TRPM3*	rs71507014	9:73,438,605	intronic	0.584	0.860	3.2×10^{-9}
15	*TGFBR1*	rs10819635	9:101,864,510	upstream	0.186	0.188	2.4×10^{-11}
16	*ABCA1*	rs2740488	9:107,661,742	intronic	0.266	0.760	1.7×10^{-9}
17	*ARHGAP21*	rs12357257	10:24,999,593	intronic	0.232	0.280	4.3×10^{-9}
18	*ARMS2*	rs10490924	10:124,214,448	missense	0.316	0.626	$< 9.0\times10^{-321}$
19	*RDH5/CD63*	rs3138142	12:56,115,585	coding-syn	0.213	0.847	6.1×10^{-10}
20	*MAPKAPK5*	rs61941287	12:112,330,305	intronic	0.019	0.503	1.2×10^{-10}
21	*B3GALTL*	rs9564692	13:31,821,240	splice	0.288	0.889	3.2×10^{-11}
22	*RAD51B*	rs1956526	14:68,799,787	intronic	0.650	0.039	1.0×10^{-11}
23	*ALDH1A2*	rs2414577	15:58,680,638	intronic	0.366	0.495	4.8×10^{-17}
24	*CETP*	rs5817082	16:56,997,349	intronic	0.248	0.193	1.7×10^{-21}
25	*BCAR1*	rs72802395	16:75,286,484	intronic	0.068	0.605	2.1×10^{-11}
26	*POLDIP2/TNFAIP1*	rs13469	17:26,676,135	coding-syn	0.523	0.168	5.1×10^{-9}
27	*NPLOC4/TSPAN10*	rs6420484	17:79,612,397	missense	0.622	0.351	4.0×10^{-12}
28	*C3*	rs2230199	19:6,718,387	missense	0.764	0.999	1.7×10^{-77}
29	*CNN2*	rs10422209	19:1,026,318	upstream	0.132	0.229	5.2×10^{-9}
30	*APOE/TOMM40*	rs429358	19:45,411,941	missense	0.118	1.000	3.3×10^{-46}
31	*MMP9*	rs2274755	20:44,639,692	splice	0.138	0.194	5.4×10^{-11}
32	*C20orf85*	rs117739907	20:56,652,781	intergenic	0.063	0.079	7.8×10^{-18}
33	*SYN3*	rs5754227	22:33,105,817	intronic	0.124	0.781	2.0×10^{-27}
34	*SLC16A8/PICK1*	rs8135665	22:38,476,276	intronic	0.205	0.596	2.9×10^{-12}

Variants with fGWAS PPs >0.5 or the highest fGWAS PPs in the loci are listed in this table. Shown are reside/nearby genes, dbSNPIDs, positions, functional annotations, MAFs (unfolded), fGWAS PPs, and P-values.

Table S5: Candidate AMD loci identified by bfGWAS, accounting for gene-based annotations.

Locus	Reside gene	*dbSNPID*	Chr:Position	Anno	MAF	P-value	Regional-PP	bfGWAS PP	Effect-size
1	*PPIL3*	*rs7562391*	2:201,736,166	missense	0.127	4.8×10^{-7}	0.989	0.666	-0.061
2	*ZNRD1ASP*	*rs114318558*	6:29,966,787	downstream	0.175	2.3×10^{-7}	0.993	0.135	0.058
3	*CPN1*	*rs61751507*	10:101,829,514	missense	0.043	6.7×10^{-8}	0.994	0.598	-0.106
4	*ABHD2*	*rs6496562*	15:89,736,558	splice	0.417	8.4×10^{-8}	0.974	0.517	0.042
5	*LBP*	*rs2232613*	20:36,997,655	missense	0.073	4.3×10^{-7}	0.955	0.881	-0.079

Variants with the highest bfGWAS single variant PP in the candidate loci are listed in this table. Shown are reside genes, dbSNPIDs, positions, functional annotations, MAFs, P-values, Bayesian regional-PPs, and Bayesian PPs/effect-sizes.

Table S6: Candidate AMD loci identified by fGWAS, accounting for gene-based annotations.

Locus	Reside gene	dbSNPID	Chr:Position	Anno	MAF	P-value	Regional-PP	fGWAS PP	Effect-size
1	*PPIL3*	*rs7562391*	2:201,736,166	missense	0.127	4.8×10^{-7}	0.986	0.475	-0.061
2	*HLA-K*	*rs116803720*	6:29,889,989	upstream	0.691	9.3×10^{-10}	0.998	0.101	0.056
3	*CPN1*	*rs61733667*	10:101,802,262	coding-syn	0.036	1.0×10^{-7}	0.994	0.254	-0.118
4	*ABHD2*	*rs6496562*	15:89,736,558	splice	0.417	8.4×10^{-8}	0.978	0.405	0.042
5	*LBP*	*rs2232613*	20:36,997,655	missense	0.073	4.3×10^{-7}	0.973	0.796	-0.079

Variants with the highest fGWAS single variant PP in the candidate loci are listed in this table. Shown are reside genes, dbSNPIDs, positions, functional annotations, MAFs, P-values, fGWAS regional-PPs, fGWAS PPs, and Bayesian effect-sizes

Table S7: AMD risk variants by bfGWAS in the 34 known loci, accounting for summarized regulatory annotations.

Signal number	Reside/nearby gene	dbSNPID	Chr:Position	Anno	MAF	bfGWAS PP	Effect-size	P-value
1.1	*KCNT2*	rs144520124	1:196,371,908	DHS	0.005	1.000	-0.383	1.9×10^{-23}
1.2	*CFH*	rs74979069	1:196,588,463	intergenic	0.049	1.000	0.181	8.1×10^{-92}
1.3	*CFH*	rs1089033	1:196,666,793	intronic	0.412	1.000	-0.117	$< 9.0\times10^{-321}$
1.4	*CFH*	rs2133143	1:196,718,099	intergenic	0.165	0.736	-0.358	5.7×10^{-246}
1.5	*CFH*	esv2672010	1:196,733,401	others	0.157	1.000	-0.283	3.3×10^{-314}
1.6	*CFHR3*	rs188826801	1:196,762,123	intronic	0.014	0.993	0.176	1.2×10^{-39}
1.7	*CFH*	rs79251424	1:196,782,416	intergenic	0.030	0.998	0.144	2.1×10^{-6}
1.8	*RP4-608O15.3*	rs146093852	1:196,811,860	intergenic	0.277	0.994	-0.143	5.7×10^{-254}
2	*COL4A3*	rs11884770	2:228,086,920	intronic	0.731	0.213	0.050	5.6×10^{-9}
3	*ADAMTS9-AS2*	rs11914351	3:64,723,441	intronic	0.240	0.950	-0.064	8.7×10^{-7}
4	*COL8A1*	rs140647181	3:99,180,668	intergenic	0.019	0.575	0.221	5.4×10^{-13}
5	*CFI*	rs10033900	4:110,659,067	intergenic	0.506	0.994	-0.067	7.2×10^{-19}
6	*C9*	rs34882957	5:39,331,894	coding	0.012	0.982	0.278	4.0×10^{-9}
7	*PRLR/SPEF2*	rs114092250	5:35,494,448	intergenic	0.019	0.346	-0.172	2.5×10^{-9}
8.1	*C2/CFB*	rs4151667	6:31,914,024	coding	0.035	0.579	-0.284	1.3×10^{-44}
8.2	*SKIV2/NELFE*	rs115270436	6:31,928,306	coding	0.071	0.566	-0.321	2.8×10^{-99}
9	*VEGFA*	rs943080	6:43,826,627	DHS	0.518	0.678	0.063	2.0×10^{-16}
10	*LINC01004/KMT2E-AS1*	rs6950894	7:104,652,671	promoter	0.511	0.063	-0.047	9.8×10^{-10}
11	*PILRB*	rs7783159	7:100,017,454	coding	0.203	0.115	0.059	5.1×10^{-10}
12	*TNFRSF10A*	rs79037040	8:23,082,971	DHS	0.534	0.995	0.053	2.9×10^{-12}
13	*MIR6130/RORB*	rs10781180	9:76,615,662	intergenic	0.684	0.070	-0.052	3.0×10^{-10}
14	*TRPM3*	rs71507014	9:73,438,605	intronic	0.584	0.763	-0.046	3.2×10^{-9}
15	*TGFBR1*	rs401186	9:101,925,077	promoter	0.200	0.109	-0.063	2.5×10^{-11}
16	*ABCA1*	rs2740488	9:107,661,742	intronic	0.266	0.727	-0.053	1.7×10^{-9}
17	*ARHGAP21*	rs12357257	10:24,999,593	intronic	0.232	0.297	0.053	4.3×10^{-9}
18.1	*ARMS2*	rs7068411	10:124,202,878	intergenic	0.621	1.000	0.252	2.4×10^{-212}
18.2	*ARMS2*	rs7898343	10:124,212,887	promoter	0.083	0.868	-0.311	2.0×10^{-51}
18.3	*ARMS2*	rs10490923	10:124,214,251	coding	0.109	0.962	-0.272	1.7×10^{-53}
18.4	*ARMS2*	rs2736911	10:124,214,355	coding	0.137	0.781	-0.350	1.8×10^{-53}
18.5	*HTRA1*	rs2672601	10:124,220,023	promoter	0.136	0.524	-0.321	4.8×10^{-53}
18.6	*HTRA1*	rs74895474	10:124,230,397	intronic	0.094	1.000	-0.199	1.3×10^{-42}
18.7	*HTRA1*	rs12252027	10:124,234,988	intronic	0.099	1.000	-0.189	1.4×10^{-51}
18.8	*HTRA1*	rs2672589	10:124,234988	DHS	0.653	1.000	0.220	8.9×10^{-180}
19	*RDH5/CD63*	rs143673140	12:56,514,414	coding	0.009	0.001	-0.096	1.3×10^{-2}
20	*MAPKAPK5*	rs61941287	12:112,330,305	intronic	0.019	0.318	0.199	1.2×10^{-10}
21	*B3GALTL*	rs9564692	13:31,821,240	DHS	0.288	0.429	-0.056	3.2×10^{-11}
22	*RAD51B*	rs2842344	14:68,976,971	DHS	0.899	0.215	-0.082	3.7×10^{-7}
23	*ALDH1A2*	rs2414577	15:58,680,638	DHS	0.366	0.508	-0.067	1.5×10^{-9}
24	*CETP*	rs5883	16:57,007,353	promoter	0.060	0.415	0.085	1.4×10^{-20}

Signal number	Reside/nearby gene	dbSNPID	Chr:Position	Anno	MAF	bfGWAS PP	Effect-size	P-value
25	*CTRB2*	rs55993634	16:75,236,763	promoter	0.082	0.321	-0.104	4.6×10^{-5}
26	*POLDIP2/TNFAIP1*	rs13469	17:26,676,135	coding	0.524	0.280	0.044	5.2×10^{-9}
27	*NPLOC4/TSPAN10*	rs9894429	17:79,596,811	coding	0.441	0.261	-0.045	4.0×10^{-12}
28.1	*FUT6/NRTN*	rs17855739	19:5,831,840	coding	0.044	0.549	-0.159	1.5×10^{-16}
28.2	*C3/CTD-3128G10.7*	rs147859257	19:6,718,146	coding	0.008	1.000	0.501	4.3×10^{-31}
28.3	*C3/CTD-3128G10.7*	rs2230199	19:6,718,387	coding	0.764	0.999	-0.173	1.7×10^{-77}
29	*ABCA7*	rs3752241	19:1,053,524	coding	0.160	0.268	0.055	3.2×10^{-7}
30	*APOE(EXOC3L2/MARK4)*	rs429358	19:45,411,941	coding	0.118	1.000	-0.173	3.3×10^{-46}
31	*MMP9/RP11-465L10.10*	rs17577	20:44,643,111	coding	0.138	0.377	-0.072	6.8×10^{-11}
32	*RP13-379L11.1*	rs7266392	20:56,651,542	DHS	0.063	0.115	-0.134	9.2×10^{-18}
33	*SYN3*	rs5754227	22:33,105,817	intronic	0.124	0.524	-0.129	2.0×10^{-27}
34	*SLC16A8/BAIAP2L2*	rs77968014	22:38,478,666	coding	0.009	0.842	0.207	3.1×10^{-6}

Variants with Bayesian PPs >0.5 or the highest bfGWAS PPs in the loci are listed (horizontal lines separate loci). Shown are reside/nearby genes, dbSNPIDs, positions, functional annotations, MAFs (unfolded, corresponding to the direction of effect-sizes), Bayesian PPs/effect-sizes, and P-values.

Table S8: AMD risk variants by fGWAS in the 34 known loci, accounting for summarized regulatory annotations.

Signal number	Reside/nearby gene	dbSNPID	Chr:Position	Anno	MAF	fGWAS PP	P-value
1	*CFH*	rs1089033	1:196,666,793	Intronic	0.412	0.522	$< 9.0\times10^{-321}$
2	*COL4A3*	rs112103000	2:228,072,336	intronic	0.163	0.135	2.0×10^{-8}
3	*ADAMTS9-AS2*	rs6793431	3:64,729,510	intronic	0.891	0.001	6.4×10^{-7}
4	*Intergenic*	rs115407994	3:99,268,860	intergenic	0.018	0.367	9.4×10^{-13}
5	*CFI*	rs10033900	4:110,659,067	intergenic	0.506	0.996	7.2×10^{-19}
6	*C9*	rs34882957	5:39,331,894	coding	0.012	0.757	4.0×10^{-16}
7	*Intergenic*	rs114092250	5:35,494,448	intergenic	0.019	0.617	2.5×10^{-9}
8	*NELFE/SKIV2L*	rs116503776	6:31,930,462	intronic	0.120	0.789	2.1×10^{-114}
9	*Intergenic*	rs943080	6:43,826,627	DHS	0.518	0.557	2.0×10^{-16}
10	*KMT2E/SRPK2*	rs1142	7:104,756,326	UTR	0.357	0.215	1.5×10^{-10}
11	*ZCWPW1*	rs7783159	7:100,017,454	coding	0.203	0.047	5.1×10^{-10}
12	*TNFRSF10A*	rs79037040	8:23,082,971	DHS	0.534	0.995	2.9×10^{-12}
13	*Intergenic*	rs10781180	9:76,615,662	intergenic	0.683	0.067	3.0×10^{-10}
14	*TRPM3*	rs71507014	9:73,438,605	intronic	0.584	0.837	3.2×10^{-9}
15	*TGFBR1*	rs10760667	9:101,864,607	DHS	0.105	0.186	2.5×10^{-11}
16	*ABCA1*	rs2740488	9:107,661,742	intronic	0.266	0.667	1.7×10^{-9}
17	*ARHGAP21*	rs142336524	10:24,879,784	intronic	0.215	0.255	3.2×10^{-8}
18	*ATE1-AS1*	rs11594070	10:123,702,736	nc-transcript	0.334	0.003	1.7×10^{-1}
19	*RDH5/CD63*	rs3138136	12:56,117,570	intronic	0.098	0.001	3.9×10^{-4}
20	*MAPKAPK5*	rs61941287	12:112,330,305	nc-transcript	0.019	0.153	1.2×10^{-10}
21	*B3GALTL*	rs9564692	13:31,821,240	DHS	0.288	0.543	3.2×10^{-11}
22	*RAD51B*	rs11158728	14:68,762,205	DHS	0.641	0.040	1.2×10^{-11}
23	*ALDH1A2*	rs2414577	15:58,680,638	DHS	0.366	0.500	4.8×10^{-17}
24	*CETP*	rs7499892	16:57,006,590	intronic	0.169	0.182	5.3×10^{-21}
25	*BCAR1*	rs72802395	16:75,286,484	intronic	0.068	0.623	2.1×10^{-11}
26	*POLDIP2/NFAIP1*	rs13469	17:26,676,135	coding	0.523	0.134	5.1×10^{-12}
27	*NPLOC4*	rs8070929	17:79,530,993	intronic	0.378	0.176	1.1×10^{-12}
28	*C3*	rs2230199	19:6,718,387	coding	0.764	0.999	1.7×10^{-77}
29	*CNN2/ABCA7*	rs58369307	19:1,038,290	UTR	0.109	0.207	8.5×10^{-9}
30	*APOE/TOMM40*	rs429358	19:45,411,941	coding	0.118	1.000	3.3×10^{-46}
31	*MMP9*	rs17577	20:44,643,111	coding	0.138	0.131	6.8×10^{-11}
32	*RP13-379L11.1*	rs141945849	20:56,650,604	DHS	0.063	0.092	9.3×10^{-18}
33	*SYN3*	rs5754227	22:33,105,817	intronic	0.124	0.681	2.0×10^{-27}
34	*SLC16A8/PICK1*	rs8135665	22:38,476,276	intronic	0.205	0.607	2.9×10^{-12}

Variants with fGWAS PPs >0.5 or the highest fGWAS PPs in the loci or are listed (horizontal lines separate loci). Shown are reside/nearby genes, dbSNPIDs, positions, annotations, MAFs (unfolded, corresponding to the direction of effect-sizes), fGWAS PPs, and P-values.

Table S9: Candidate AMD loci identified by bfGWAS, accounting for summarized regulatory annotations.

Locus	Reside gene	*dbSNPID*	Chr:Position	Anno	MAF	P-value	Regional-PP	bfGWAS PP	Effect-size
1	*PPIL3*	*rs7562391*	2:201,736,166	coding	0.127	$\mathbf{4.8\times10^{-7}}$	0.967	0.475	-0.061
2	*ZNRD1-AS1*	*rs114357644*	6:29,924,728	intergenic	0.669	$\mathbf{2.3\times10^{-7}}$	0.999	0.609	0.051
3	*CPN1*	*rs61733667*	10:101,829,514	coding	0.036	$\mathbf{1.0\times10^{-7}}$	0.994	0.463	-0.118

Variants with the highest bfGWAS PP in the candidate loci are listed in this table. Shown are reside genes, dbSNPIDs, positions, functional annotations, MAFs, P-values, Bayesian regional-PPs, and Bayesian PPs/effect-sizes.

Table S10: Candidate AMD loci identified by fGWAS, accounting for summarized regulatory annotations.

Locus	Reside gene	dbSNPID	Chr:Position	Anno	MAF	P-value	Regional-PP	fGWAS PP	Effect-size
1	*PPIL3*	*rs7562391*	2:201,736,166	coding	0.127	$\mathbf{4.8\times10^{-7}}$	0.976	0.322	-0.061
2	*Intergenic*	*rs115754868*	6:29,884,646	intergenic	0.653	$\mathbf{9.6\times10^{-10}}$	0.998	0.101	0.053
3	*CPN1*	*rs61733667*	10:101,802,262	coding	0.036	$\mathbf{1.0\times10^{-7}}$	0.994	0.253	-0.118
4	*ABHD2*	*rs8042649*	15:89,740,469	UTR	0.417	$\mathbf{1.2\times10^{-7}}$	0.973	0.093	0.049

Variants with the highest fGWAS PP in the candidate loci are listed in this table. Shown are reside genes, dbSNPIDs, positions, functional annotations, MAFs, P-values, fGWAS regional-PPs, fGWAS PPs, and Bayesian effect-sizes.

Table S11: AMD risk variants by bfGWAS in the 34 known loci, accounting for chromatin states profiled with the epigenome of fetal thymus.

Signal number	Reside/nearby gene	dbSNPID	Chr:Position	Anno	MAF	bfGWAS PP	Effect-size	P-value
1.1	*KCNT2*	*rs144520124*	1:196,371,908	Quies	0.005	1.000	-0.389	$\mathbf{1.9\times10^{-23}}$
1.2	*KCNT2*	*rs10754198*	1:196,573,505	Quies	0.258	1.000	-0.078	$\mathbf{1.4\times10^{-228}}$
1.3	*Intergenic*	*rs74979069*	1:196,588,463	Quies	0.049	1.000	0.160	$\mathbf{8.1\times10^{-92}}$
1.4	*CFH*	*rs72734340*	1:196,681,376	Quies	0.037	1.000	-0.189	$\mathbf{1.1\times10^{-1}}$
1.5	*Intergenic*	*rs200467660*	1:196,721,770	Quies	0.161	1.000	-0.405	$\mathbf{1.1\times10^{-249}}$
1.6	*Intergenic*	*rs113632891*	1:196,731,186	Quies	0.155	1.000	-0.173	$\mathbf{2.8\times10^{-296}}$
1.7	*ZNF675*	*rs146093952*	1:196,811,860	Quies	0.277	1.000	-0.207	$\mathbf{2.2\times10^{-310}}$
1.8	*CFHR4*	*rs76258418*	1:196,815,863	Quies	0.130	1.000	-0.199	$\mathbf{2.7\times10^{-293}}$
2	*COL4A3*	*rs112103000*	2:228,072,336	Quies	0.064	0.072	0.064	$\mathbf{2.0\times10^{-8}}$
3.1	*ADAMTS9-AS2*	*rs57305229*	3:64,720,574	Quies	0.304	0.572	-0.057	$\mathbf{2.3\times10^{-5}}$
3.2	*ADAMTS9-AS2*	*rs11914351*	3:64,723,441	Quies	0.240	0.968	-0.064	$\mathbf{8.7\times10^{-7}}$
4	*Intergenic*	*rs140647181*	3:99,180,668	Quies	0.019	0.703	0.222	$\mathbf{5.3\times10^{-13}}$
5	*CFI*	*rs10033900*	4:110,659,067	Quies	0.506	0.999	-0.067	$\mathbf{7.2\times10^{-19}}$
6	*C9*	*rs62358361*	5:39,327,888	Quies	0.012	0.551	0.271	$\mathbf{3.1\times10^{-16}}$
7	*Intergenic*	*rs114092250*	5:35,494,448	Quies	0.019	0.213	-0.171	$\mathbf{2.5\times10^{-9}}$
8.1	*SKIV2L*	*rs116503776*	6:31,930,462	Tx	0.120	1.000	-0.307	$\mathbf{2.1\times10^{-114}}$
8.2	*STK19/C4A*	*rs144629244*	6:31,946,792	Enh	0.014	0.536	0.435	$\mathbf{4.4\times10^{-7}}$
8.3	*PBX2/AGER/GPSM3*	*rs114254831*	6:32,155,581	EnhG	0.271	0.693	0.080	$\mathbf{8.1\times10^{-13}}$
9	*Intergenic*	*rs943080*	6:43,826,627	Quies	0.518	0.422	0.063	$\mathbf{2.0\times10^{-16}}$
10	*KMT2E/SRPK2*	*rs1142*	7:104,756,326	Tx	0.357	0.197	0.051	$\mathbf{1.5\times10^{-10}}$
11	*NYAP1*	*rs67040465*	7:100,083,078	ReprPCWk	0.200	0.040	0.059	$\mathbf{5.7\times10^{-10}}$
12	*TNFRSF10A*	*rs79037040*	8:23,082,971	BivFlnk	0.534	0.967	0.053	$\mathbf{2.9\times10^{-12}}$
13	*Intergenic*	*rs10781180*	9:76,615,662	Quies	0.684	0.090	-0.052	$\mathbf{3.0\times10^{-10}}$
14	*TRPM3*	*rs71507014*	9:73,438,605	Quies	0.585	0.819	-0.046	$\mathbf{3.2\times10^{-9}}$
15	*TGFBR1*	*rs10819635*	9:10,819,635	TxWk	0.186	0.084	-0.066	$\mathbf{2.5\times10^{-11}}$
16	*ABCA1*	*rs2740488*	9:107,661,742	TxWk	0.266	0.759	-0.053	$\mathbf{1.7\times10^{-9}}$
17	*ARHGAP21*	*rs12357257*	10:24,999,593	Quies	0.232	0.308	0.053	$\mathbf{4.3\times10^{-9}}$
18.1	*Intergenic*	*rs7068411*	10:124,202,878	Quies	0.621	1.000	0.198	$\mathbf{2.4\times10^{-212}}$
18.2	*HTRA1*	*rs2672595*	10:124,227,288	ReprePCWk	0.213	0.844	-0.466	$\mathbf{8.7\times10^{-111}}$
18.3	*HTRA1*	*rs74895474*	10:124,230,397	ReprePCWk	0.094	0.578	-0.181	$\mathbf{1.3\times10^{-42}}$
18.4	*HTRA1*	*rs4752699*	10:124,234,320	ReprePCWk	0.128	1.000	-0.292	$\mathbf{2.1\times10^{-51}}$
18.5	*HTRA1*	*rs2672589*	10:124,234,988	ReprePCWk	0.653	1.000	0.274	$\mathbf{8.9\times10^{-180}}$
19	*CDK2/PMEL*	*rs2069389*	12:56,359,642	Enh	0.044	0.001	0.042	$\mathbf{5.3\times10^{-2}}$
20	*CUX2*	*rs142641895*	12:111,786,202	Het	0.019	0.635	0.249	$\mathbf{1.6\times10^{-9}}$
21	*B3GALTL*	*rs9564692*	13:31,821,240	Quies	0.288	0.411	-0.056	$\mathbf{3.2\times10^{-11}}$
22	*RAD51B*	*rs2842339*	14:68,986,999	TxWk	0.899	0.206	-0.082	$\mathbf{3.1\times10^{-7}}$
23	*ALDH1A2*	*rs2414577*	15:58,680,638	Quies	0.366	0.525	-0.067	$\mathbf{4.8\times10^{-17}}$
24	*CETP*	*rs11076175*	16:57,006,378	TxWk	0.67	0.203	-0.072	$\mathbf{5.0\times10^{-21}}$

Signal number	Reside/nearby gene	dbSNPID	Chr:Position	Anno	MAF	bfGWAS PP	Effect-size	P-value
25	*CTRB2*	*rs72802342*	16:75,234,872	Enh	0.074	0.478	-0.114	$\mathbf{2.8\times10^{-13}}$
26	*SARM1/SLC46A1*	*rs4795433*	17:26,716,821	ReprPCWk	0.524	0.138	0.045	$\mathbf{1.6\times10^{-9}}$
27	*NPLOC4*	*rs8070929*	17:79,530,993	Tx	0.378	0.226	0.058	$\mathbf{1.1\times10^{-12}}$
28.1	*FUT6*	*rs12019136*	19:5,835,677	Quies	0.042	0.639	-0.160	$\mathbf{3.7\times10^{-17}}$
28.2	*C3*	*rs147859257*	19:6,718,146	Het	0.008	1.000	0.504	$\mathbf{4.3\times10^{-31}}$
28.3	*C3*	*rs2230199*	19:6,718,387	Het	0.764	0.996	-0.172	$\mathbf{1.7\times10^{-77}}$
29	*CNN2/ABCA7*	*rs3087680*	19:1,038,289	TxFlnk	0.109	0.208	0.072	$\mathbf{8.6\times10^{-9}}$
30	*APOE/TOMM40*	*rs429358*	19:45,411,941	ReprPCWk	0.118	1.000	-0.186	$\mathbf{3.3\times10^{-46}}$
31	*MMP9*	*rs142450006*	20:44,614,991	ReprPCWk	0.132	0.251	-0.079	$\mathbf{1.4\times10^{-11}}$
32	*Intergenic*	*rs140611615*	20:56,653,111	Quies	0.062	0.080	-0.135	$\mathbf{8.2\times10^{-18}}$
33	*SYN3*	*rs5754227*	22:33,105,817	Quies	0.124	0.896	-0.128	2.0×10^{-27}
34	*SLC16A8/PICK1/ BAIAP2L2*	*rs8135665*	22:38,476,276	ReprPC	0.206	0.624	0.066	2.9×10^{-12}

Variants with Bayesian PPs >0.5 or the highest bfGWAS PPs in the loci are listed in this table. Shown are reside/nearby genes, dbSNPIDs, positions, annotations, MAFs (unfolded, corresponding to the direction of effect-sizes), P-values, and Bayesian PPs/effect-sizes.

Table S12: AMD risk variants by fGWAS in the 34 known loci, accounting for chromatin states profiled with the epigenome of fetal thymus.

Signal number	Reside/Nearby Gene	dbSNPID	Chr:Position	Anno	MAF	fGWAS PP	P-value
1	*CFH*	rs1089033	1:196,666,793	Quies	0.412	1.000	$< 9.0\times10^{-321}$
2	*COL4A3*	rs11884770	2:228,086,920	Quies	0.731	0.731	5.7×10^{-9}
3	*ADAMTS9-AS2*	rs66793786	3:64,707,880	Quies	0.243	0.050	2.0×10^{-7}
4	*COL8A1*	rs140647181	3:99,180,668	Quies	0.019	0.307	5.4×10^{-13}
5	*CFI*	rs10033900	4:110,659,067	Quies	0.506	0.994	7.2×10^{-19}
6	*C9*	rs62358361	5:39,327,888	Quies	0.012	0.559	3.1×10^{-16}
7	*PRLR/SPEF2*	rs114092250	5:35,494,448	Quies	0.019	0.468	2.5×10^{-9}
8	*NELFE/SKIV2L*	rs116503776	6:31,930,462	Tx	0.120	0.967	2.1×10^{-114}
9	*VEGFA*	rs943080	6:43,826,627	Quies	0.518	0.437	2.0×10^{-16}
10	*KMT2E/SRPK2*	rs1142	7:104,756,326	Tx	0.357	0.141	1.5×10^{-10}
11	*ZKSCAN1*	rs2406255	7:100,053,690	EnhG	0.200	0.026	5.9×10^{-10}
12	*TNFRSF10A*	rs79037040	8:23,082,971	BivFlnk	0.534	0.998	2.9×10^{-12}
13	*Intergenic*	rs10781180	9:76,615,662	Quies	0.684	0.068	3.0×10^{-10}
14	*TRPM3*	rs71507014	9:73,438,605	Quies	0.584	0.776	3.2×10^{-9}
15	*TGFBR1*	rs6478972	9:101,869,278	Enh	0.200	0.103	3.5×10^{-11}
16	*ABCA1*	rs2740488	9:107,661,742	TxWk	0.266	0.746	1.7×10^{-9}
17	*ARHGAP21*	rs12357257	10:24,999,593	Quies	0.232	0.269	4.3×10^{-9}
18	*ARMS2*	rs2672599	10:124,211,875	Quies	0.641	1.000	2.7×10^{-263}
19	*RDH5/CD63*	rs3138136	12:56,117,570	EnhG	0.099	0.001	3.9×10^{-4}
20	*MAPKAPK5*	rs61941287	12:112,330,305	Tx	0.019	0.205	1.2×10^{-10}
21	*B3GALTL*	rs9564692	13:31,821,240	Quies	0.288	0.388	3.2×10^{-11}
22	*RAD51B*	rs11158728	14:68,762,205	Enh	0.640	0.066	1.0×10^{-11}
23	*ALDH1A2*	rs2414577	15:58,680,638	Quies	0.366	0.495	4.8×10^{-17}
24	*CETP*	rs5817082	16:56,997,349	TxWk	0.248	0.254	1.7×10^{-21}
25	*CTRB2*	rs72802342	16:75,234,872	Enh	0.073	0.656	2.8×10^{-13}
26	*TNFAIP1/POLDIP2*	rs733914	17:26,671,196	EnhG	0.526	0.156	3.5×10^{-9}
27	*NPLOC4*	rs8070929	17:79,530,993	Tx	0.378	0.221	1.1×10^{-12}
28	*C3*	rs2230199	19:6,718,387	Het	0.764	0.992	1.7×10^{-77}
29	*CNN2/ABCA7*	rs58369307	19:1,038,290	TxFlnk	0.109	0.369	8.5×10^{-9}
30	*APOE/TOMM40*	rs429358	19:45,411,941	ReprPCWk	0.118	1.000	3.3×10^{-46}
31	*MMP9*	rs1888235	20:44,623,967	Enh	0.133	0.281	1.4×10^{-11}
32	*C20orf85*	rs117739907	20:56,652,781	Quies	0.062	0.079	7.8×10^{-18}
33	*SYN3*	rs5754227	22:33,105,817	Quies	0.124	0.791	2.0×10^{-27}
34	*SLC16A8/PICK1*	rs8135665	22:38,476,276	ReprPC	0.205	0.773	2.9×10^{-12}

Variants with either the highest fGWAS PP per locus or fGWAS PP > 0.5 are listed (horizontal lines separate loci). Shown are reside/nearby genes, dbSNPIDs, positions, functional annotations, MAFs (unfolded, corresponding to the direction of effect-sizes), fGWAS PPs, and P-values.

Table S13: Candidate AMD loci identified by bfGWAS, accounting for chromatin states profiled with the epigenome of fetal thymus.

Locus	Reside gene	*dbSNPID*	Chr:Position	Anno	MAF	P-value	Regional-PP	bfGWAS PP	Effect-size
1	*HLA-W*	*rs114357644*	6:29,924,728	TxWk	0.669	2.3×10^{-7}	0.988	0.877	0.051
2	*CPN1*	*rs111563092*	10:101,808,993	ReprPCWk	0.045	7.2×10^{-8}	0.998	0.171	-0.106

Variants with the highest bfGWAS PPs in the candidate loci are listed in this table. Shown are reside genes, dbSNPIDs, positions, functional annotations, MAFs, P-values, Bayesian regional-PPs, and Bayesian PPs/effect-sizes.

Table S14: Candidate AMD loci identified by fGWAS, accounting for chromatin states profiled with the epigenome of fetal thymus.

Locus	Reside gene	dbSNPID	Chr:Position	Anno	MAF	P-value	Regional-PP	fGWAS PP	Effect-size
1	*PPIL3*	*rs7562391*	2:201,736,166	Tx	0.127	6.5×10^{-8}	0.969	0.088	-0.061
2	*Intergenic*	*rs140766203*	6:29,883,869	Quies	0.652	8.5×10^{-10}	0.998	0.044	0.053
3	*CPN1*	*rs113582392*	10:101,804,258	Enh	0.045	1.4×10^{-8}	0.993	0.154	-0.106
4	*ABHD2*	*rs4932480*	15:89,723,858	EnhG	0.501	7.2×10^{-8}	0.971	0.138	-0.043

Variants with the highest fGWAS PPs in the candidate loci are listed in this table. Shown are reside genes, dbSNPIDs, positions, functional annotations, MAFs, P-values, fGWAS regional-PPs, fGWAS PPs, and Bayesian effect-sizes.

Table S15: Haplotype analysis in locus C2/CFB/SKIV2L.

Region	Haplotype			Haplotype Frequency (%)		P-value	OR (95% CI)
	SKIV2L intronic (*rs116503776*)	*CFB* missense (*rs4151667*)	*CFB* missense (*rs115270436*)	Cases	Controls		
C2/CFB/SKIV2L	1	1	1	1.5×10^{-3}	4.2×10^{-3}	8.9×10^{-11}	0.364 (0.265, 0.501)
	1	0	1	0.046	0.085	1.5×10^{-86}	0.522 (0.490, 0.557)
	1	1	0	0.023	0.041	5.0×10^{-36}	0.561 (0.513, 0.613)
	0	0	1	8.9×10^{-4}	1.5×10^{-3}	0.024	0.586 (0.375, 0.917)
	1	0	0	0.018	0.017	0.092	1.102 (0.983, 1.236)
	0	0	0	0.909	0.850	-	Reference Haplotype
	0	1	0	6.1×10^{-5}	2.8×10^{-5}	0.306	1.840 (0.243, 13.938)

Considered the haplotype consisting with the top significant intronic variant found by single variant test P-values (*rs116503776* with p-value=2.1×10^{-114}), the top two significant missense variants (in the $\pm$20KB region around *rs116503776*) found by bfGWAS (*rs4151667* with Bayesian PP=0.903, *rs115270436* with Bayesian PP= 0.638).

Table S16: Model comparison.

Region (*C2/CFB/SKIV2L)*	*SKIV2L* intronic (*rs116503776*) & *PBX2* intronic (*rs114254831*)	*CFB* missense (*rs4151667*) & *SKIV2L* missense (*rs115270436*)	Differences (col2-col3)
Akaike information criterion (AIC)	95857.36	95752.63	104.73
Bayesian information criterion (BIC)	95891.1	95786.36	104.74
Log Likelihood	-47924.68	-47872.31	-52.37

Compared the linear regression model with the top two independent significant variants (*rs116503776*, *rs114254831*) found by conditional analysis, versus the linear regression model with the top two significant variants (*rs4151667*, *rs115270436*) found by bfGWAS accounting for gene-based annotations.

Supplemental References

[1] Wellcome Trust Case Control Consortium. Genome-wide association study of 14,000 cases of seven common diseases and 3,000 shared controls. *Nature*, 447(7145):661–678, 06 2007.

[2] A. P. Dempster, N. M. Laird, and D. B. Rubin. Maximum likelihood from incomplete data via the em algorithm. *Journal of the Royal Statistical Society. Series B (Methodological)*, 39(1):pp. 1–38, 1977.

[3] Edgar C Fieller. Some problems in interval estimation. *Journal of the Royal Statistical Society. Series B (Methodological)*, pages 175–185, 1954.

[4] Andrew Gelman and Donald B. Rubin. Inference from iterative simulation using multiple sequences. *Statistical Science*, 7(4):pp. 457–472, 1992.

[5] Edward I. George and Robert E. McCulloch. Variable selection via gibbs sampling. *Journal of the American Statistical Association*, 88(423):881–889, 1993.

[6] Yongtao Guan and Matthew Stephens. Bayesian variable selection regression for genome-wide association studies and other large-scale problems. *Ann. Appl. Stat.*, 5(3):1780–1815, 09 2011.

[7] Xiang Zhou, Peter Carbonetto, and Matthew Stephens. Polygenic modeling with bayesian sparse linear mixed models. *PLoS Genet*, 9(2):e1003264, 02 2013.